The Astronomical Journal, 166:232 (59pp), 2023 December https://doi.org/10.3847/1538-3881/acfda8


# Validating AU Microscopii d with Transit Timing Variations

Justin M. Wittrock[1], Peter P. Plavchan[1], Bryson L. Cale[2,3], Thomas Barclay[4,5], Mathis R. Ludwig[6], Richard P. Schwarz[7], Djamel Mékarnia[8], Amaury H. M. J. Triaud[9], Lyu Abe[8], Olga Suarez[8], Tristan Guillot[8], Dennis M. Conti[10], Karen A. Collins[7], Ian A. Waite[11], John F. Kielkopf[12], Kevin I. Collins[1], Stefan Dreizler[6], Mohammed El Mufti[1], Dax L. Feliz[13], Eric Gaidos[14], Claire S. Geneser[15], Keith D. Horne[16], Stephen R. Kane[17], Patrick J. Lowrance[18], Eder Martioli[19,20], Don J. Radford[21], Michael A. Reefe[22], Veronica Roccatagliata[23,24,25], Avi Shporer[26], Keivan G. Stassun[27], Christopher Stockdale[28], Thiam-Guan Tan[29,30], Angelle M. Tanner[15], and Laura D. Vega[5,31,32]

[1] Department of Physics & Astronomy, George Mason University, 4400 University Drive MS 3F3, Fairfax, VA 22030, USA; jwittroc@gmu.edu
[2] NASA JPL, 4800 Oak Grove Drive, Pasadena, CA 91109, USA
[3] IPAC, 770 South Wilson Avenue, Pasadena, CA 91125, USA
[4] University of Maryland, Baltimore County, 1000 Hilltop Circle, Baltimore, MD 21250, USA
[5] NASA Goddard Space Flight Center, 8800 Greenbelt Road, Greenbelt, MD 20771, USA
[6] Institut für Astrophysik, Georg-August-Universität, Friedrich-Hund-Platz 1, D-37077 Göttingen, Germany
[7] Center for Astrophysics | Harvard & Smithsonian, 60 Garden Street, Cambridge, MA 02138, USA
[8] Université Côte dAzur, Observatoire de la Côte dAzur, CNRS, Laboratoire Lagrange, Bd de lObservatoire, CS 34229, F-06304 Nice cedex 4, France
[9] School of Physics & Astronomy, University of Birmingham, Edgbaston, Birmingham, B15 2TT, UK
[10] American Association of Variable Star Observers, 185 Alewife Brooke Parkway, Suite 410, Cambridge, MA 02138 USA
[11] Centre for Astrophysics, University of Southern Queensland, Toowoomba, QLD, 4350, Australia
[12] Department of Physics and Astronomy, University of Louisville, Louisville, KY 40292, USA
[13] Department of Astrophysics, American Museum of Natural History, New York, NY 10024, USA
[14] Department of Earth Sciences, University of Hawai'i at Mānoa, 1680 East-West Road, Honolulu, HI 96822, USA
[15] Mississippi State University, 75 B.S. Hood Road, Mississippi State, MS 39762, USA
[16] SUPA Physics and Astronomy, University of St. Andrews, Fife, KY16 9SS, UK
[17] University of California, Riverside, 900 University Ave., Riverside, CA 92521, USA
[18] IPAC, Caajacfda8t13=^texttx);lifornia Institute of Technology, MC 314-6, 1200 E. California Boulevard, Pasadena, California 91125, USA
[19] Laboratório Nacional de Astrofísica, Rua Estados Unidos 154, Itajubá, MG 37504-364, Brazil
[20] Sorbonne Université, CNRS, UMR 7095, Institut d'Astrophysique de Paris, 98 bis bd Arago, F-75014 Paris, France
[21] Brierfield Observatory, Bowral, NSW, Australia
[22] Kavli Institute for Astrophysics and Space Research, Massachusetts Institute of Technology, 77 Massachusetts Avenue, Cambridge, MA 02139, USA
[23] INAF-Osservatorio Astrofisico di Arcetri, Largo E. Fermi 5, I-50125 Firenze, Italy
[24] INFN, Sezione di Pisa, Largo Bruno Pontecorvo 3, I-56127 Pisa, Italy
[25] Department of Physics "E. Fermi,"University of Pisa, Largo Bruno Pontecorvo 3, I-56127 Pisa, Italy
[26] Department of Physics and Kavli Institute for Astrophysics and Space Research, Massachusetts Institute of Technology, Cambridge, MA 02139, USA
[27] Department of Physics & Astronomy, Vanderbilt University, 6301 Stevenson Center Lane, Nashville, TN 37235, USA
[28] Hazelwood Observatory, Hazelwood South, VIC, Australia
[29] Perth Exoplanet Survey Telescope, Perth, WA, Australia
[30] Curtin Institute of Radio Astronomy, Curtin University, Bentley, WA 6102, Australia
[31] Department of Astronomy, University of Maryland, College Park, MD 20742, USA
[32] Center for Research and Exploration in Space Science & Technology, NASA/GSFC, Greenbelt, MD 20771, USA
*Received 2023 February 9; revised 2023 September 15; accepted 2023 September 25; published 2023 November 8*

## Abstract

AU Mic is a young (22 Myr), nearby exoplanetary system that exhibits excess transit timing variations (TTVs) that cannot be accounted for by the two known transiting planets nor stellar activity. We present the statistical "validation" of the tentative planet AU Mic d (even though there are examples of "confirmed" planets with ambiguous orbital periods). We add 18 new transits and nine midpoint times in an updated TTV analysis to prior work. We perform the joint modeling of transit light curves using `EXOFASTv2` and extract the transit midpoint times. Next, we construct an $O-C$ diagram and use `Exo-Striker` to model the TTVs. We generate TTV log-likelihood periodograms to explore possible solutions for d's period, then follow those up with detailed TTV and radial velocity Markov Chain Monte Carlo modeling and stability tests. We find several candidate periods for AU Mic d, all of which are near resonances with AU Mic b and c of varying order. Based on our model comparisons, the most-favored orbital period of AU Mic d is $12.73596 \pm 0.00793$ days ($T_{C,\mathrm{d}} = 2458340.55781 \pm 0.11641$ BJD), which puts the three planets near 4:6:9 mean-motion resonance. The mass for d is $1.053 \pm 0.511\ M_{\oplus}$, making this planet Earth-like in mass. If confirmed, AU Mic d would be the first known Earth-mass planet orbiting a young star and would provide a valuable opportunity in probing a young terrestrial planet's atmosphere. Additional TTV observations of the AU Mic system are needed to further constrain the planetary masses, search for possible transits of AU Mic d, and detect possible additional planets beyond AU Mic c.

*Unified Astronomy Thesaurus concepts:* Exoplanet astronomy (486); Exoplanet dynamics (490); Exoplanet systems (484); Exoplanets (498)

## 1. Introduction

AU Microscopii (TOI-2221, TIC 441420236, HD 197481, GJ 803) is a fundamental system proven to be quite viable for study of planetary formation and orbital dynamics of young systems given its youthfulness ($22 \pm 3$ Myr; Mamajek & Bell 2014), proximity (9.71 pc; Gaia Collaboration et al. 2021), and relative brightness ($m_V = 8.81$ mag). It is highly active (Butler et al. 1981; Kundu et al. 1987; Cully et al. 1993; Tsikoudi & Kellett 2000; Feinstein et al. 2022; Gilbert et al. 2022) and reported to have the largest number of flare events among the Kepler and Transiting Exoplanet Survey Satellite (TESS) targets to date (Ilin & Poppenhaeger 2022). Ilin & Poppenhaeger (2022) examined TESS data for any flares caused by star-to-planet interaction (SPI) between AU Mic b and the host star; they did not find any and concluded that most flares were attributed to stellar activity, but they have not ruled this phenomenon out yet. The aforementioned heightened stellar activity of AU Mic had made it a challenging target for radial velocity (RV) and transit observations (Addison et al. 2021; Cale et al. 2021; Gilbert et al. 2022; Wittrock et al. 2022; Zicher et al. 2022).

AU Mic hosts two transiting planets (Plavchan et al. 2020; Martioli et al. 2021; Gilbert et al. 2022) and a large dust disk (Fajardo-Acosta et al. 2000; Zuckerman 2001; Song et al. 2002; Kalas et al. 2004; Liu et al. 2004; Plavchan et al. 2005; Strubbe & Chiang 2006; MacGregor et al. 2013; Grady et al. 2020; Arnold et al. 2022; Olofsson et al. 2022; Vizgan et al. 2022). Gallenne et al. (2022) searched for additional companions in the inner-disk region (0.4–2.4 au) with high-angular-resolution observations through the Very Large Telescope (VLT)/SPHERE and with combined data from VLT/NACO, Very Large Telescope Interferometer (VLTI)/PIONIER, and VLTI/GRAVITY, but did not find any brighter than $K_s \approx 11.2$ mag, which in turn caps the upper planetary mass limit at $12.3 \pm 0.5$ $M_J$. Szabó et al. (2021, 2022) probed the AU Mic system with the CHaracterising ExOPlanet Satellite (CHEOPS) and did a joint TESS + CHEOPS transit timing variation (TTV) analysis, which found the timing of the transits during summer of 2022 to be 30–85 minutes later than predicted using the linear ephemeris available at the time. Wittrock et al. (2022) did a TTV and photodynamical analysis of the AU Mic systems and detected a TTV excess that cannot be accounted for with the presence of both planets b and c and the stellar activities of AU Mic; thus, a nontransiting hypothetical planet, d, between AU Mic b and c was proposed. This would have made AU Mic among the few systems that have a nontransiting planet between its adjacent transiting planets; other systems include HD 3167 d (Christiansen et al. 2017), Kepler-20 g (Buchhave et al. 2016), Kepler-411 e (Sun et al. 2019), and TOI-431 c (Osborn et al. 2021). Kane et al. (2022) explored the orbital dynamics of the AU Mic system by injecting the hypothetical planet d; they found that it lies at the very edge of instability, and that d's eccentricity will vary between 0.0 and 0.3 even on short timescales.

This paper is a continuation of the work done in Wittrock et al. (2022), with an emphasis now placed on validating the tentative planet AU Mic d through the TTV method. In Section 2, we highlight the new light curves in addition to the old data sets we include for TTV analyses. Next, we summarize the steps taken in modeling the observed transits using the `EXOFASTv2` package (Eastman et al. 2019) in Section 3. Section 4 presents our modeling of the extracted TTVs using the `Exo-Striker` package (Trifonov 2019) and presents a novel technique, called a TTV log-likelihood periodogram, which searches for parameters that maximize the log-likelihood. In Section 5, we perform the RV vetting of our TTV analysis to check for consistency between the RV results and those of the TTV analysis. We discuss the results in Section 6, and present our conclusion in Section 7.

## 2. Data from Observations

We incorporated a total of 54 data sets from four years of AU Mic's photometric and Rossiter–McLaughlin (R-M) observations with various facilities, of which 45 are of AU Mic b and nine are of AU Mic c (Tables 1 and 2). The following transits had been presented in the previous works: the R-M observations (Martioli et al. 2020; Palle et al. 2020), the TESS and one of the Spitzer observations (Plavchan et al. 2020; Martioli et al. 2021; Gilbert et al. 2022), the CHEOPS observations (Szabó et al. 2021, 2022), and the Brierfield, the Las Cumbres Observatory (LCO) South African Astronomical Observatory (SAAO) and Siding Spring Observatory (SSO) prior to 2021, the PEST, and two of the Spitzer observations (Wittrock et al. 2022). This paper introduces 18 new and unpublished observations from the Antarctic Search for Transiting ExoPlanets (ASTEP), the Las Cumbres Observatory Global Telescope (LCOGT) network, and the Mount Kent Observatory (MKO) CDK700 and adds nine midpoint times from CHEOPS observations. Therefore, this section will describe only the new observations that were not included in Wittrock et al. (2022).

### 2.1. CHaracterising ExOPlanet Satellite Photometry

CHaracterising ExOPlanet Satellite Photometry (CHEOPS) is a space-based telescope whose mission is to search for transits of known exoplanets and recover their radii more accurately, which will then place constraints on atmospheric and interior modeling and formation processes (Rando et al. 2020; Benz et al. 2021). Szabó et al. (2021, 2022) observed seven transits for AU Mic b and two transits for AU Mic c. The CHEOPS light curves have been processed and modeled separately, as described in Szabó et al. (2021, 2022), and this paper only incorporates the transit midpoint times from those works.

### 2.2. Ground-based Photometry

All of the ground-based observations listed in Table 1 have been coordinated through the TESS Follow-up Observing Program (TFOP) Working Group (WG).[33] Along with the ones mentioned in Wittrock et al. (2022), we added 13 new follow-up photometric transit observations, including one from ASTEP, four from the LCO Cerro Tololo Interamerican Observatory (CTIO) 1.0 m, three from LCO SAAO 1.0 m, four from LCO SSO 1.0 m, and one from LCO Teide Observatory (TO) 1.0 m. These light curves are available on ExoFOP-TESS[34] (Akeson et al. 2013). The follow-up observation schedules were conducted with the online version of the `TAPIR` package (Jensen 2013). `AstroImageJ` (`AIJ`; Collins et al. 2017) had been utilized to process the ground-based light curves and then create a subset table containing only BJD_TDB, normalized detrended flux, flux uncertainty, and

[33] https://tess.mit.edu/followup

[34] https://exofop.ipac.caltech.edu/tess

**Table 1**
List of AU Mic's Photometric and R-M Observation Data Incorporated for Transit and TTV Analyses

| Planet | Telescope | Date (UT) | Filter | Exposure Time (s) | No. of Images | Obs. Dur. (min) | Transit Coverage | References |
|---|---|---|---|---|---|---|---|---|
| b | ASTEP 0.4 m | 2021-07-09 | $R_c$ | 9 | 636 | 377 | Full | New |
| | | 2021-07-26 | $R_c$ | 9 | 724 | 407 | Full | |
| | | 2021-08-12 | $R_c$ | 9 | 801 | 550 | Full | |
| c | ASTEP 0.4 m | 2021-07-21 | $R_c$ | 9 | 1294 | 752 | Full | New |
| | | 2021-08-09 | $R_c$ | 9 | 951 | 560 | Full | |
| b | Brierfield 0.36 m | 2020-08-13 | $I$ | 16 | 398 | 379 | Full | 1 |
| b | CFHT (SPIRou) | 2019-06-17 | 955–2515 nm | 122.6 | 116 | 302.8 | egress | 2 |
| b | CHEOPS | 2020-07-10 | CHEOPS | 15 | 7 194 | 938.1 | Full | 3 |
| | | 2020-08-21 | CHEOPS | 15 | 8844 | 658.3 | Full | |
| | | 2020-09-24 | CHEOPS | 3 | 12,222 | 1066.1 | Full | |
| | | 2021-07-26 | CHEOPS | 3 | 9366 | 666.9 | Full | 4 |
| | | 2021-08-12 | CHEOPS | 3 | 11,746 | 687.3 | Full | |
| | | 2021-08-29 | CHEOPS | 3 | 9338 | 687.3 | Full | |
| | | 2021-09-06 | CHEOPS | 3 | 9002 | 687.3 | Full | |
| c | CHEOPS | 2021-08-09 | CHEOPS | 3 | 14,406 | 878.5 | Full | 4 |
| | | 2021-08-28 | CHEOPS | 3 | 12,698 | 865.8 | Full | |
| b | IRTF (iSHELL) | 2019-06-17 | 2.18–2.47 nm | 120 | 47 | 105.2 | Egress | 2 |
| b | LCO CTIO 1.0 m | 2021-06-14 | Pan-STARRS $z_s$ | 15 | 452 | 342 | Full | New |
| | | 2021-07-01 | Pan-STARRS $z_s$ | 15 | 440 | 340 | Full | |
| | | 2021-08-04 | Pan-STARRS $z_s$ | 15 | 362 | 274 | Egress | |
| c | LCO CTIO 1.0 m | 2021-10-04 | Pan-STARRS $z_s$ | 15 | 412 | 311 | Ingress | New |
| b | LCO SAAO 1.0 m | 2020-05-20 | Pan-STARRS $Y$ | 35 | 99 | 262 | Egress | 1 |
| | | 2020-05-20 | Pan-STARRS $z_s$ | 15 | 333 | 266 | Egress | |
| | | 2020-06-06 | Pan-STARRS $z_s$ | 15 | 266 | 218 | Egress | |
| | | 2020-06-23 | Pan-STARRS $z_s$ | 15 | 223 | 183 | Egress | |
| | | 2020-09-07 | Pan-STARRS $z_s$ | 15 | 211 | 172 | Ingress | |
| | | 2021-07-18 | Pan-STARRS $z_s$ | 15 | 259 | 212 | Ingress | New |
| | | 2021-08-03 | Pan-STARRS $z_s$ | 15 | 317 | 252 | Ingress | |
| | | 2021-09-23 | Pan-STARRS $z_s$ | 15 | 456 | 344 | Full | |
| b and c | LCO SAAO 1.0 m | 2020-10-11 | Pan-STARRS $z_s$ | 15 | 311 | 266 | Ingress and egress | 1 and new |
| b | LCO SSO 1.0 m | 2020-04-25 | Pan-STARRS $Y$ | 35 | 40 | 104 | Egress | 1 |
| | | 2020-04-25 | Pan-STARRS $z_s$ | 15 | 212 | 172 | Egress | |
| | | 2020-08-13 | Pan-STARRS $z_s$ | 15 | 379 | 312 | Full | |
| | | 2020-09-16 | Pan-STARRS $z_s$ | 15 | 408 | 340 | Full | |
| | | 2020-10-03 | Pan-STARRS $z_s$ | 15 | 248 | 219 | Egress | |
| | | 2021-06-22 | Pan-STARRS $z_s$ | 15 | 351 | 281 | Full | New |
| | | 2021-08-12 | Pan-STARRS $z_s$ | 15 | 406 | 343 | Full | |
| | | 2021-08-29 | Pan-STARRS $z_s$ | 15 | 448 | 340 | Full | |
| | | 2021-09-15 | Pan-STARRS $z_s$ | 15 | 295 | 277 | Egress | |
| b | LCO TO 1.0 m | 2021-09-23 | Pan-STARRS $z_s$ | 15 | 300 | 231 | Egress | New |
| c | MKO CDK700 0.7 m | 2021-08-28 | $r'$ | 16 | 74 | 87 | Egress | New |
| b | PEST 0.30 m | 2020-07-10 | $V$ | 15 | 1 143 | 556 | Full | 1 |
| b | Spitzer (IRAC) | 2019-02-10 | 4.5 $\mu$m | 0.08 | 3020 | 475.7 | Full | 1 |
| | | 2019-02-27 | 4.5 $\mu$m | 0.08 | 3377 | 475.7 | Egress | |
| | | 2019-09-09 | 4.5 $\mu$m | 0.08 | 6002 | 990.9 | Full | |
| b | TESS[b] | 2018-07-26 | TESS | 120 | 329 | 718.0 | Full | 5 |
| | | 2018-08-12 | TESS | 120 | 296 | 708.0 | Full | |
| | | 2020-07-10 | TESS | 20 | 2132 | 719.7 | Full | |

**Table 1**
(Continued)

| Planet | Telescope | Date (UT) | Filter | Exposure Time (s) | No. of Images | Obs. Dur. (min) | Transit Coverage | References |
|---|---|---|---|---|---|---|---|---|
| | | 2020-07-19 | TESS | 20 | 2137 | 719.7 | Full | |
| | | 2020-07-27 | TESS | 20 | 2120 | 719.7 | Full | |
| c | TESS[b] | 2018-08-11 | TESS | 120 | 342 | 718.0 | Full | 5 |
| | | 2020-07-09 | TESS | 20 | 2138 | 719.7 | Full | |
| | | 2020-07-28 | TESS | 20 | 2133 | 719.7 | Full | |
| b | VLT (ESPRESSO) | 2019-08-07 | 378.2–788.7 nm | 200 | 88 | 359 | Full | 6 |

**Notes.** All ground-based photometric observations listed here were organized via the TESS Follow-up Observing Program Working Group (TFOPWG).[a]
[a] https://tess.mit.edu/followup.
[b] ∼12 hr snippets of the ∼27 days duration TESS Cycles 1 and 3 light curves were extracted for our analysis, centered approximately on each transit.
**References.** (1) Wittrock et al. (2022); (2) Martioli et al. (2020); (3) Szabó et al. (2021); (4) Szabó et al. (2022); (5) Gilbert et al. (2022); (6) Palle et al. (2020).

**Table 2**
List of Facilities Utilized for Photometric and Rossiter–McLaughlin Follow-up Observations of AU Mic

| Telescope | Instrument | Location | Aperture (m) | Pixel Scale (arcsec) | Resolution (pixels) | FOV (arcmin) | References |
|---|---|---|---|---|---|---|---|
| ASTEP 400 | FLI Proline 16800E | Concordia Research Station, Antarctica | 0.4 | 0.93 | 4096 × 4096 | 63.5 × 63.5 | 1 |
| Brierfield | Moravian 16803 | Bowral, New South Wales | 0.36 | 0.732 | 4 096 × 4 096 | 50.0 × 50.0 | 2 |
| CFHT | SPIRou | Maunakea, Hawai'i | 3.58 | ... | ... | ... | 3 |
| CHEOPS | ... | ... | 0.32 | 1.11 | 1024 × 1024 | 19 × 19 | 4 |
| IRTF | iSHELL | Maunakea, Hawai'i | 3.2 | ... | ... | ... | 5 |
| LCO CTIO | Sinistro | Cerro Tololo, Chile | 1.0 | 0.389 | 4096 × 4096 | 26.5 × 26.5 | 6 |
| LCO SAAO | Sinistro | Sutherland, South Africa | 1.0 | 0.389 | 4096 × 4096 | 26.5 × 26.5 | 6 |
| LCO SSO | Sinistro | Mount Woorut, New South Wales | 1.0 | 0.389 | 4096 × 4096 | 26.5 × 26.5 | 6 |
| LCO TO | Sinistro | Mount Teide, Tenerife, Canary Islands | 1.0 | 0.389 | 4096 × 4096 | 26.5 × 26.5 | 6 |
| MKO CDK700 | U16 | Mount Kent, Queensland | 0.7 | 0.401 | 4096 × 4096 | 27.4 × 27.4 | ... |
| PEST | SBIG ST-8XME | Perth, Western Australia | 0.3048 | 1.23 | 1 530 × 1 020 | 31 × 21 | 7 |
| Spitzer | IRAC | ... | 0.85 | 1.22 | 256 × 256 | 5.2 × 5.2 | 8 |
| VLT | ESPRESSO | Cerro Paranal, Chile | 8.2 | ... | ... | ... | 9 |

**References.** (1) https://astep.oca.eu; (2) https://www.brierfieldobservatory.com; (3) https://www.cfht.hawaii.edu; (4) https://cheops.unibe.ch; (5) http://irtfweb.ifa.hawaii.edu; (6) https://lco.global/observatory; (7) http://pestobservatory.com; (8) https://www.spitzer.caltech.edu; (9) https://www.eso.org/public/teles-instr/paranal-observatory/vlt.

detrending parameter columns from the ground-based light curves (e.g., airmass, position centroid, FWHM, etc.). We use these detrending parameter columns for EXOFASTv2 modeling and extraction of midpoint times to assess the impact of systematic trends in the ground-based light curves on the modeled transit midpoint time posterior distributions (Section 3). The choice of detrending parameters were modified for some ground transit observations from Wittrock et al. (2022) to improve signal rms and minimize the uncertainty in the timing of the transits; see Table 3 for a complete list of detrending parameters applied to each transit observation for this paper.

#### *2.2.1. Antarctic Search for Transiting ExoPlanets (FLI Proline 16800E) Photometry*

ASTEP 400, part of the Antarctic Search for Transiting ExoPlanets (ASTEP) program and located at the Concordia Research Station, Antarctica, is a 0.4 m telescope that has been utilized for transiting exoplanet searches (Guillot et al. 2015; Mékarnia et al. 2016). The data collected with ASTEP 400 were processed on site with an IDL-based aperture photometry pipeline (Abe et al. 2013; Mékarnia et al. 2016). Although five AU Mic transit observations were made with ASTEP 400, the photometric conditions during four of those nights were of suboptimal quality, so only the first transit observation of AU Mic b is included in this paper.

#### *2.2.2. Las Cumbres Observatory Global Telescope (Sinistro) Photometry*

The Las Cumbres Observatory Global Telescope (LCOGT; Brown et al. 2013) network partipated in collecting the transits of the AU Mic systems through four different 1.0 m LCO Ritchey–Chretien Cassegrain telescopes equipped with Sinistro;[35] Pan-STARRS $z_s$ was used with an exposure time of 15 s for all new LCO observations.

The third night from LCO CTIO was impacted by poor sky conditions. The third transit observation from LCO SAAO was affected by intermittent clouds. Additionally, the 2020 October 11 night from LCO SAAO fortuitously observed the egress of planet c while intending to observe the transit of planet b; this transit was not included in the previous analysis of Wittrock et al. (2022) but is now included in this work. The first night from LCO SSO was impacted by poor sky conditions and tracking. All LCOGT light curves have been reduced and detrended with AIJ, then a subset table generated from each light curve.

#### *2.2.3. Mount Kent Observatory CDK700 (U16) Photometry*

The light curve from the Mount Kent Observatory CDK700 has been reduced and detrended with AIJ, then a subset table generated from it. However, this observation was found to have missed AU Mic c's predicted transit calculated by the EXOFASTv2 package. Since we are employing the reject-flatmodel option to improve the convergence of our transit models, this set is dropped from the analysis (see Section 3 regarding the use of rejectflatmodel).

## 3. EXOFASTv2 Transit Modeling

We model the 33 photometric transits of AU Mic b and five photometric transits of AU Mic c using the EXOFASTv2 package (Eastman et al. 2013, 2019); CHEOPS and R-M observations are not included in this transit modeling step. EXOFASTv2 utilizes the Markov chain Monte Carlo (MCMC) technique to estimate the posterior probabilities and determine the statistical significance of our detections and the confidence intervals in their corresponding transit midpoint times. Since EXOFASTv2 is written in IDL, it uses the differential evolution MCMC algorithm (Ter Braak 2006) instead of emcee (Foreman-Mackey et al. 2013) for sampling purposes (Eastman et al. 2013). The detrending parameters flare (Spitzer), sky (Spitzer and PEST), Sky/Pixel_T1 (LCOGT), and SKY (ASTEP) are treated as additive, while the remaining detrending parameters are treated as multiplicative. See Table 3

[35] https://lco.global/observatory

**Table 3**
Detrending Parameters Incorporated into EXOFASTv2 Modeling of AU Mic b Transits

| Telescope | Date (UT) | Filter | Detrending Parameter(s) | Note |
|---|---|---|---|---|
| TESS | 2018-07-26 | TESS | ... | a |
| TESS | 2018-08-11 | TESS | ... | a |
| TESS | 2018-08-12 | TESS | ... | a |
| Spitzer | 2019-02-10 | 4.5 $\mu$m | $x$, $y$, noise/pixel, FWHM_x, FWHM_y, sky, linear, quadratic | b |
| Spitzer | 2019-02-27 | 4.5 $\mu$m | $x$, $y$, noise/pixel, FWHM_x, FWHM_y, sky, linear, quadratic, flare | b |
| Spitzer | 2019-09-09 | 4.5 $\mu$m | $x$, $y$, noise/pixel, FWHM_x, FWHM_y, sky, linear, quadratic, Gaussian | b |
| LCO SSO | 2020-04-25 | $z'$ | AIRMASS | c |
| LCO SSO | 2020-04-25 | $y$ | AIRMASS | c |
| LCO SAAO | 2020-05-20 | $z'$ | AIRMASS | c |
| LCO SAAO | 2020-05-20 | $y$ | AIRMASS | c |
| LCO SAAO | 2020-06-06 | $z'$ | AIRMASS | c |
| LCO SAAO | 2020-06-23 | $z'$ | AIRMASS, Width_T1 | c |
| TESS | 2020-07-09 | TESS | ... | a |
| TESS | 2020-07-10 | TESS | ... | a |
| PEST | 2020-07-10 | $V$ | comp_flux, dist_center, fwhm, airmass, sky | d |
| TESS | 2020-07-19 | TESS | ... | a |
| TESS | 2020-07-27 | TESS | ... | a |
| TESS | 2020-07-28 | TESS | ... | a |
| Brierfield | 2020-08-13 | $I$ | Meridian_Flip, tot_C_cnts, X(FITS)_T1, Y(FITS)_T1 | c |
| LCO SSO | 2020-08-13 | $z'$ | AIRMASS, Width_T1 | c |
| LCO SAAO | 2020-09-07 | $z'$ | Sky/Pixel_T1, Width_T1 | c |
| LCO SSO | 2020-09-16 | $z'$ | AIRMASS, Width_T1 | c |
| LCO SSO | 2020-10-03 | $z'$ | Sky/Pixel_T1, Width_T1 | c |
| LCO SAAO | 2020-10-11 | $z'$ | AIRMASS | c |
| LCO CTIO | 2021-06-14 | $z'$ | tot_C_cnts, Sky/Pixel_T1, Width_T1 | c |
| LCO SSO | 2021-06-22 | $z'$ | tot_C_cnts, Y(FITS)_T1, Width_T1 | c |
| LCO CTIO | 2021-07-01 | $z'$ | tot_C_cnts, Sky/Pixel_T1, Width_T1 | c |
| ASTEP | 2021-07-09 | $R$ | SKY | e |
| LCO SAAO | 2021-07-18 | $z'$ | AIRMASS, Sky/Pixel_T1 | c |
| LCO SAAO | 2021-08-03 | $z'$ | X(FITS)_T1, Y(FITS)_T1, Sky/Pixel_T1 | c |
| LCO CTIO | 2021-08-04 | $z'$ | AIRMASS | c |
| LCO SSO | 2021-08-12 | $z'$ | Y(FITS)_T1, Sky/Pixel_T1, Width_T1 | c |
| LCO SSO | 2021-08-29 | $z'$ | tot_C_cnts, X(FITS)_T1, Width_T1 | c |
| LCO SSO | 2021-09-15 | $z'$ | AIRMASS, X(FITS)_T1, Y(FITS)_T1 | c |
| LCO SAAO | 2021-09-23 | $z'$ | Sky/Pixel_T1, Width_T1 | c |
| LCO TO | 2021-09-23 | $z'$ | tot_C_cnts, Width_T1 | c |
| LCO CTIO | 2021-10-04 | $z'$ | AIRMASS, X(FITS)_T1, Width_T1 | c |

**Notes.** The flare (Spitzer), sky (Spitzer and PEST), Sky/Pixel_T1 (LCOGT), and SKY (ASTEP) were implemented as additives; the remaining detrending parameters were implemented as multiplicative. See Section 2 for details on detrending parameters used for each observation. Since both Pan-STARRS $Y$ and Pan-STARRS $z_s$ are not available among the filters in EXOFASTv2, $y$ and $z'$ (Sloan $z$) were used as respective approximate substitutes. (a) See Gilbert et al. (2022) for details on the detrending parameters applied to TESS data. (b) See Wittrock et al. (2022) for details on the detrending parameters applied to Spitzer data. (c) Detrending parameters generated from AIJ (Collins et al. 2017). (d) Detrending parameters generated from the PEST pipeline (http://pestobservatory.com/the-pest-pipeline). (e) Detrending parameters generated from IDL-based aperture photometry pipeline (Abe et al. 2013; Mékarnia et al. 2016).

for a full list of nights included for EXOFASTv2 analysis and their corresponding detrending parameters. Since both Pan-STARRS $Y$ and Pan-STARRS $z_s$ are not available among the filters in EXOFASTv2, $y$ and $z'$ (Sloan $z$) were used as respective approximate substitutes.

We use MIST for evolutionary models (Choi et al. 2016; Dotter 2016) and have EXOFASTv2 ignore the Claret and Bloemen limb-darkening tables (Claret & Bloemen 2011) since AU Mic is a low-mass red dwarf. Table 4 provides a list of priors for EXOFASTv2. The logarithmic version of stellar mass and orbital period were used because they are the fitted priors in EXOFASTv2. The purpose of TTVs and depth offset priors are to place constraints on the variation of transit timing and depth of all light curves; any transit depth variability was not explored for this paper. We set MAXSTEPS = 7500 and NTHIN = 25 and include the rejectflatmodel option for all light curves with NTEMPS = 8 to aid in faster convergence. The reason for allowing the rejectflatmodel option to become active for this work is that both AU Mic b and c are confirmed transiting planets with well-established orbital periods, so we "reject" any flat models to help narrow the vast range of possible outcomes. After EXOFASTv2 completes the transit modeling, it generates the transit models (Figure 1), median posteriors (Tables 5, 6, 7, and 8), and midpoint times (Table 11).

## 4. Exo-Striker Transit Timing Variation Modeling

In this section, we present our $O-C$ diagram from EXOFASTv2, the super-period of AU Mic b's TTVs, and the TTV dynamical modeling with Exo-Striker. We explore three different scenarios: a system with two planets, b and c; a system with three planets, where planet d is interior to b; and a system with three planets, where planet d is between b and c.

**Table 4**
Stellar, Planetary, and Transit Priors for EXOFASTv2 Modeling

| Prior | Unit | Input | | References |
|---|---|---|---|---|
| | | AU Mic b | AU Mic c | |
| $\log_{10}\left(\frac{M_\star}{M_\odot}\right)$ | ... | $\mathcal{N}(-0.301, 0.026)$ | | 1 |
| $R_\star$ | $R_\odot$ | $\mathcal{N}(0.75, 0.03)$ | | 2 |
| $T_{\mathrm{eff}}$ | K | $\mathcal{N}(3700, 100)$ | | 3 |
| Age | Gyr | $\mathcal{N}(0.022, 0.003)$ | | 4 |
| $T_C$ | BJD_TDB | $\mathcal{N}(2458330.39080, 0.00058)$ | $\mathcal{N}(2458342.2239, 0.0019)$ | 5 |
| $\log_{10}\left(\frac{\mathrm{Period}}{\mathrm{days}}\right)$ | ... | $\mathcal{N}(0.92752436, 0.00000031)$ | $\mathcal{N}(1.2755182, 0.0000012)$ | 5 |
| $R_p/R_\star$ | ... | $\mathcal{N}(0.0512, 0.0020)$ | $\mathcal{N}(0.0340, 0.0034)$ | 5 |
| TTV offset | days | $\mathcal{U}(-0.02, 0.02)$ | | ... |
| Depth offset | ... | $\mathcal{U}(-0.01, 0.01)$ | | ... |

**Notes.** $\mathcal{N}$ denotes the Gaussian priors, and $\mathcal{U}$ denotes the uniform priors. TTVs and depth offsets are arbitrary and applied as constraints to all transits. The logarithmic version of stellar mass and orbital period were used because they are the fitted priors in EXOFASTv2. The equivalent evolutionary point (EEP) was set to 1 but is allowed to float freely, so it is not included in the prior table above.

**References.** (1) Plavchan et al. (2020); (2) White et al. (2019); (3) Plavchan et al. (2009); (4) Mamajek & Bell (2014); (5) Gilbert et al. (2022)

Additionally, we develop a novel technique, a TTV log-likelihood periodogram, which aids us in exploring the TTV parameters that maximize the log-likelihood.

### 4.1. O−C *Diagram and Transit Timing Variation Super-period*

In the previous section, we ran the EXOFASTv2 package to model the transits and generate the observed midpoint times (Table 11). CHEOPS and R-M data were not included in transit modeling, but CHEOPS midpoint times from Szabó et al. (2021, 2022) and R-M midpoints times from Martioli et al. (2020) and Palle et al. (2020) are now added to the list of midpoint times generated from EXOFASTv2. We calculate the expected midpoint times using the planets' EXOFASTv2-generated periods and $T_C$. Then, we use both the calculated and the observed midpoint times to create the $O-C$ diagram of both AU Mic b and c (Figure 2).

Relative to the space-based transit midpoint times, most ground-based photometric transits have larger timing uncertainties and some larger scatter. Some of the notable outliers in transit midpoint time of AU Mic b (regardless of timing uncertainty) include ESPRESSO, PEST 0.3 m, Brierfield 0.36 m, ASTEP 0.4 m, and at least one each of LCO CTIO, SAAO, and SSO 1.0 m. Many of AU Mic b's transits observed in 2021 are considerably later (∼20 minutes) than those observed from 2020 given the previously measured ephemerides.

AU Mic b's TTVs appear to have a quasi-sinusoidal pattern. This indicates that there is potentially a "super-period" embedded in the TTV observations. To model the super-period, we construct a sinusoidal model that includes a linear trend to account for the apparent drift in the TTVs:

$$y(t) = A\sin(Bt + C) + Dt + E, \tag{1}$$

where $t$ is the time since the first transit of b, and $A$, $B$, $C$, $D$, and $E$ are the unknown coefficients. The coefficients are optimized using the scipy.optimize.curve_fit[36] (Table 9), and we use Equation (1) to model the super-period onto AU Mic b's $O-C$ diagram (Figure 3).

[36] https://docs.scipy.org/doc/scipy/reference/generated/scipy.optimize.curve_fit.html

We can use that super-period to estimate the period of AU Mic d using Equation (5) from Lithwick et al. (2012):

$$P^j \equiv \frac{1}{|j/P' - (j-1)/P|}, \tag{2}$$

where $j$ is an integer that represents the $j{:}j-1$ mean-motion orbital resonant (MMR) chain, $P$ is the orbital period of the inner planet, $P'$ is the orbital period of the outer planet, and $P^j$ is the super-period of the TTVs. Since the 3:2 period ratio is the most common pairing for the MMR (Fabrycky et al. 2014), we assume $j = 3$ and will not consider other $j$ values for this problem. From the coefficient $B$, we obtain the super-period $P^3 = 1186.44931 \pm 153.24946$ days. From Equation (2), we end up with the estimated periods $P_{\mathrm{d}} = 5.62927 \pm 0.00177$ days or $5.65482 \pm 0.00178$ days (assuming AU Mic d is orbiting interior to AU Mic b), and $P_{\mathrm{d}} = 12.65156 \pm 0.00594$ days or $12.73779 \pm 0.00603$ days (assuming AU Mic d is orbiting between AU Mic b and c); the absolute value brackets in the denominator of Equation (2) allow us to have two potential solutions for both the inner d and middle d scenarios. Additionally, we note a statistically significant ($3.2\sigma$) nonzero linear drift of $0.03052 \pm 0.00964$ min day$^{-1}$ in the TTVs of AU Mic b.

This approach, in using AU Mic b's TTV super-period, is meant to provide a starting point for estimating the orbital period of AU Mic d that could drive the observed excess TTVs of AU Mic b as reported by Wittrock et al. (2022). Additionally, numerous compact systems have planets in near-MMR chains—e.g., HD 158259 (Hara et al. 2020), TRAPPIST-1 (Gillon et al. 2016, 2017; Luger et al. 2017), V1298 Tau (David et al. 2019a), and several Kepler systems (Lissauer et al. 2011; Fabrycky et al. 2014)—and most Kepler systems with measured TTVs have planets in near-MMR chains (Lithwick et al. 2012; also see Steffen et al. 2013 for example), so it is not unreasonable or unwarranted to assume that AU Mic d might be near-MMR pairing with b and with c.

Wittrock et al. (2022) generated the massless no-TTV two-planet model with Exo-Striker as a control test on the presence and statistical significance of TTVs, but it also serves as

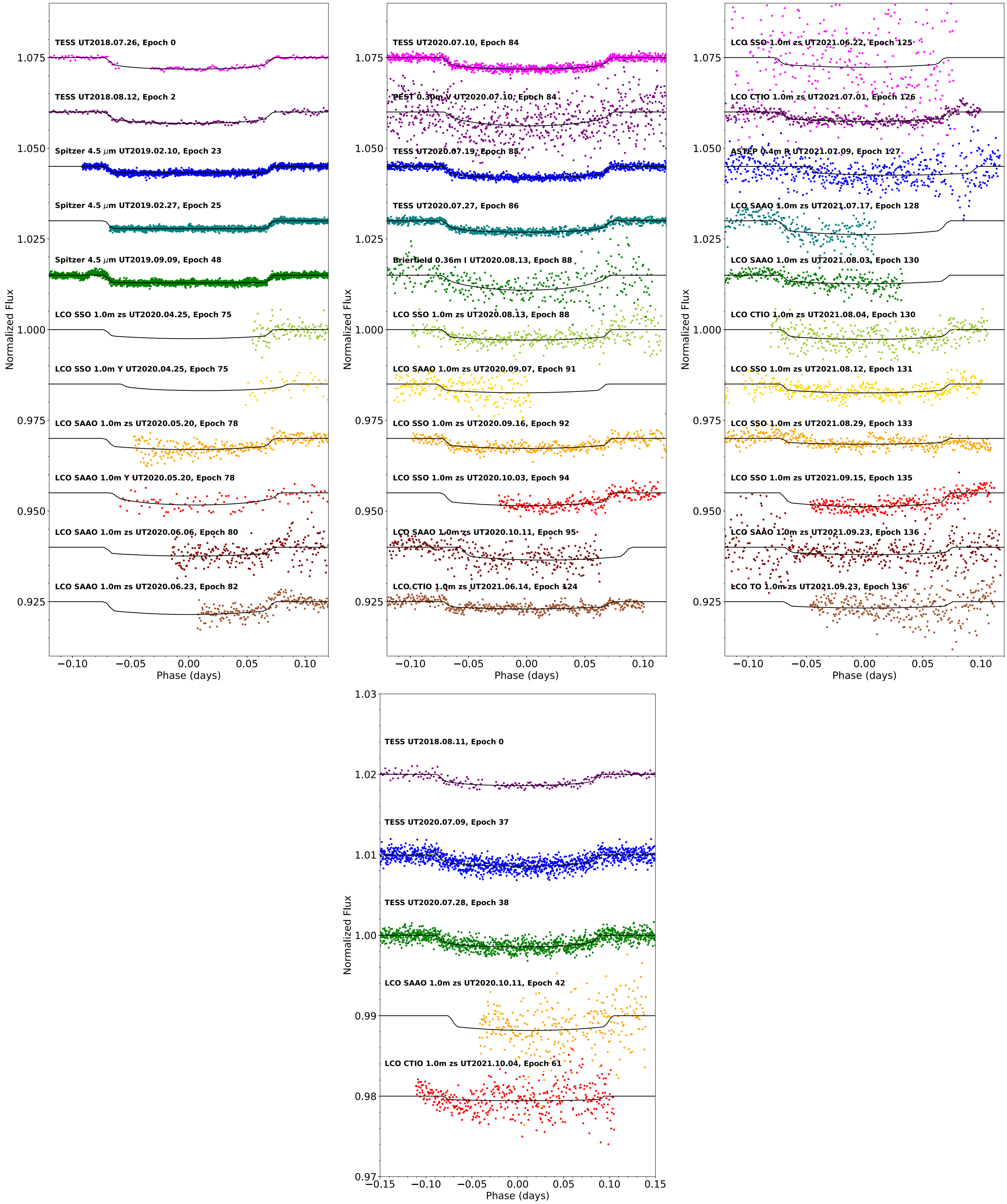


**Figure 1.** Comparison between ground-based + Spitzer + TESS transits (multicolors) and EXOFASTv2's best-fit model (black) for AU Mic b (first three columns in the top row) and c (last column in the bottom row). Each transit is labeled with the name of telescope, the date of observation in UT, and the epoch, which refers to the number of transits since the first transit of b and c, respectively.

**Table 5**
EXOFASTv2-generated Median Values and 68% Confidence Interval for AU Mic System

| Posterior | Description | Unit | Output | |
|---|---|---|---|---|
| | | | AU Mic b | AU Mic c |
| $M_\star$ | Stellar mass | $M_\odot$ | $0.510^{+0.028}_{-0.027}$ | |
| $R_\star$ | Stellar radius | $R_\odot$ | $0.744^{+0.023}_{-0.021}$ | |
| $L_\star$ | Stellar luminosity | $L_\odot$ | $0.0916^{+0.011}_{-0.0098}$ | |
| $\rho_\star$ | Stellar density | g cm$^{-3}$ | $1.75^{+0.14}_{-0.16}$ | |
| $\log g$ | Surface gravity | $\log_{10}$(g cm$^{-3}$) | $4.404^{+0.026}_{-0.031}$ | |
| $T_{\rm eff}$ | Effective temperature | K | $3678^{+90}_{-88}$ | |
| [Fe/H] | Metallicity | dex | $0.23^{+0.24}_{-0.30}$ | |
| $[\rm Fe/H]_0$ | Initial metallicity[a] | dex | $0.17^{+0.22}_{-0.28}$ | |
| Age | ... | Gyr | $0.0201^{+0.0025}_{-0.0024}$ | |
| EEP | Equal evolutionary phase[b] | ... | $162.0 \pm 2.9$ | |
| $P_{\rm orb}$ | Orbital period | days | $8.4630177^{+0.0000052}_{-0.0000050}$ | $18.858970^{+0.000051}_{-0.000052}$ |
| $M_p$ | Planetary mass[c] | $M_J$ | $0.053^{+0.019}_{-0.012}$ | $0.0247^{+0.010}_{-0.0065}$ |
| $R_p$ | Planetary radius | $R_J$ | $0.353 \pm 0.013$ | $0.225 \pm 0.022$ |
| $T_C$ | Time of conjunction[d] | BJD_TDB | $2458330.39168 \pm 0.00053$ | $2458342.2240^{+0.0019}_{-0.0018}$ |
| $T_T$ | Time of minimum projected separation[e] | BJD_TDB | $2458330.39169 \pm 0.00053$ | $2458342.2240^{+0.0019}_{-0.0018}$ |
| $T_0$ | Optimal conjunction time[f] | BJD_TDB | $2458525.04109^{+0.00052}_{-0.00051}$ | $2458342.2240^{+0.0019}_{-0.0018}$ |
| $a$ | Semimajor axis | au | $0.0649 \pm 0.0012$ | $0.1108 \pm 0.0020$ |
| $e$ | Eccentricity | ... | $0.081^{+0.17}_{-0.058}$ | $0.101^{+0.11}_{-0.066}$ |
| $i$ | Inclination | deg | $89.57^{+0.28}_{-0.31}$ | $89.43^{+0.35}_{-0.23}$ |
| $\omega$ | Argument of periastron | deg | $-202^{+44}_{-120}$ | $115^{+66}_{-95}$ |
| $T_{\rm eq}$ | Equilibrium temperature[g] | K | $600^{+17}_{-16}$ | $459^{+13}_{-12}$ |
| $\tau_{\rm circ}$ | Tidal circularization timescale | Gyr | $161 \pm 76$ | $22800^{+15000}_{-9500}$ |
| $K$ | RV semi-amplitude[c] | m s$^{-1}$ | $8.4^{+3.0}_{-1.9}$ | $2.99^{+1.2}_{-0.78}$ |
| $R_p/R_\star$ | ... | ... | $0.0488 \pm 0.0010$ | $0.0311 \pm 0.0028$ |
| $a/R_\star$ | ... | ... | $18.79^{+0.50}_{-0.59}$ | $32.05^{+0.86}_{-1.0}$ |
| $\delta$ | Transit depth $(R_{\rm p}/R_\star)^2$ | ... | $0.002379^{+0.000100}_{-0.000099}$ | $0.00097^{+0.00018}_{-0.00017}$ |
| $\delta_I$ | Transit depth in $I$ | ... | $0.0039^{+0.0025}_{-0.0011}$ | $0.00156^{+0.00099}_{-0.00047}$ |
| $\delta_R$ | Transit depth in $R$ | ... | $0.0039^{+0.0031}_{-0.0012}$ | $0.00154^{+0.0012}_{-0.00049}$ |
| $\delta_{z'}$ | Transit depth in $z'$ | ... | $0.00310 \pm 0.00023$ | $0.00123^{+0.00025}_{-0.00022}$ |
| $\delta_{4.5\mu{\rm m}}$ | Transit depth in 4.5 $\mu$m | ... | $0.00239 \pm 0.00010$ | $0.00097^{+0.00019}_{-0.00017}$ |
| $\delta_{\rm TESS}$ | Transit depth in TESS | ... | $0.00308 \pm 0.00017$ | $0.00123^{+0.00024}_{-0.00022}$ |
| $\delta_V$ | Transit depth in $V$ | ... | $0.00344^{+0.0012}_{-0.00057}$ | $0.00133^{+0.00057}_{-0.00033}$ |
| $\delta_y$ | Transit depth in $y$ | ... | $0.0038^{+0.0027}_{-0.0010}$ | $0.00151^{+0.0011}_{-0.00043}$ |
| $\tau$ | Ingress/egress transit duration | days | $0.00691^{+0.00028}_{-0.00020}$ | $0.00589^{+0.00086}_{-0.00069}$ |
| $T_{14}$ | Total transit duration | days | $0.14553^{+0.00031}_{-0.00028}$ | $0.1765 \pm 0.0012$ |
| $T_{\rm FWHM}$ | FWHM transit duration | days | $0.13859 \pm 0.00019$ | $0.17053^{+0.00098}_{-0.00097}$ |
| $b$ | Transit impact parameter | ... | $0.134^{+0.096}_{-0.089}$ | $0.30^{+0.13}_{-0.19}$ |
| $b_S$ | Eclipse impact parameter | ... | $0.136^{+0.095}_{-0.090}$ | $0.32^{+0.11}_{-0.19}$ |
| $\tau_S$ | Ingress/egress eclipse duration | days | $0.00711^{+0.00052}_{-0.00054}$ | $0.00631^{+0.00076}_{-0.00072}$ |
| $T_{S,14}$ | Total eclipse duration | days | $0.1486^{+0.0099}_{-0.010}$ | $0.186^{+0.018}_{-0.012}$ |
| $T_{S,\rm FWHM}$ | FWHM eclipse duration | days | $0.1415^{+0.0095}_{-0.0097}$ | $0.180^{+0.018}_{-0.011}$ |
| $\delta_{S,2.5\mu{\rm m}}$ | Blackbody eclipse depth at 2.5 $\mu$m | ppm | $0.62^{+0.15}_{-0.13}$ | $0.0134^{+0.0055}_{-0.0040}$ |
| $\delta_{S,5.0\mu{\rm m}}$ | Blackbody eclipse depth at 5.0 $\mu$m | ppm | $23.6^{+2.8}_{-2.5}$ | $2.19^{+0.56}_{-0.46}$ |
| $\delta_{S,7.5\mu{\rm m}}$ | Blackbody eclipse depth at 7.5 $\mu$m | ppm | $69.6^{+5.6}_{-5.2}$ | $10.4^{+2.3}_{-2.0}$ |
| $\rho_p$ | Planetary density[c] | g cm$^{-3}$ | $1.48^{+0.52}_{-0.34}$ | $2.70^{+1.0}_{-0.67}$ |
| $\log g_p$ | Surface gravity[c] | ... | $3.02^{+0.13}_{-0.11}$ | $3.08^{+0.13}_{-0.11}$ |
| $\Theta$ | Safronov number | ... | $0.0380^{+0.013}_{-0.0085}$ | $0.047^{+0.017}_{-0.011}$ |
| $\langle F \rangle$ | Incident flux | $10^9$ erg s$^{-1}$ cm$^{-2}$ | $0.0288^{+0.0034}_{-0.0033}$ | $0.0099^{+0.0012}_{-0.0011}$ |
| $T_P$ | Time of periastron | BJD_TDB | $2458322.77^{+0.83}_{-2.3}$ | $2458324.0^{+2.9}_{-3.7}$ |
| $T_S$ | Time of eclipse | BJD_TDB | $2458334.56^{+0.52}_{-0.93}$ | $2458351.6^{+1.5}_{-1.6}$ |
| $T_A$ | Time of ascending node | BJD_TDB | $2458328.28^{+0.29}_{-0.47}$ | $2458337.67^{+0.81}_{-0.75}$ |
| $T_D$ | Time of descending node | BJD_TDB | $2458332.42^{+0.26}_{-0.44}$ | $2458346.73^{+0.71}_{-0.83}$ |
| $V_c/V_e$ | [i] | ... | $0.980^{+0.022}_{-0.033}$ | $0.962^{+0.037}_{-0.044}$ |
| $\sqrt{\left(1-\frac{R_p}{R_\star}\right)^2-b^2}$ | Transit chord | ... | $1.0401^{+0.0074}_{-0.017}$ | $0.985^{+0.039}_{-0.050}$ |
| sign | [j] | ... | $0.51^{+0.41}_{-0.26}$ | $0.51^{+0.39}_{-0.27}$ |
| $e\cos\omega$ | ... | ... | $-0.011^{+0.097}_{-0.17}$ | $-0.00^{+0.12}_{-0.13}$ |

**Table 5**
(Continued)

| Posterior | Description | Unit | Output | |
|---|---|---|---|---|
| | | | AU Mic b | AU Mic c |
| e sin $\omega$ | ... | ... | $0.010^{+0.033}_{-0.036}$ | $0.030^{+0.047}_{-0.037}$ |
| $M_p \sin i$ | Minimum mass[c] | $M_J$ | $0.053^{+0.019}_{-0.012}$ | $0.0247^{+0.010}_{-0.0065}$ |
| $M_p/M_\star$ | Mass ratio[c] | ... | $0.000099^{+0.000036}_{-0.000023}$ | $0.000046^{+0.000019}_{-0.000012}$ |
| $d/R_\star$ | Separation at mid-transit | ... | $18.19^{+0.96}_{-1.3}$ | $30.5^{+1.8}_{-2.0}$ |
| $P_T$ | A priori nongrazing transit probability | ... | $0.0523^{+0.0042}_{-0.0026}$ | $0.0317^{+0.0023}_{-0.0018}$ |
| $P_{T,G}$ | A priori transit probability | ... | $0.0577^{+0.0046}_{-0.0029}$ | $0.0338^{+0.0024}_{-0.0019}$ |
| $P_S$ | A priori nongrazing eclipse probability | ... | $0.05024^{+0.0045}_{-0.00099}$ | $0.0297^{+0.0021}_{-0.0014}$ |
| $P_{S,G}$ | A priori eclipse probability | ... | $0.0554^{+0.0050}_{-0.0011}$ | $0.0316^{+0.0023}_{-0.0015}$ |
| $u_{1,I}$ | Linear limb-darkening coefficient in $I$ | ... | $0.80^{+0.47}_{-0.48}$ | |
| $u_{1,R}$ | Linear limb-darkening coefficient in $R$ | ... | $0.80^{+0.53}_{-0.56}$ | |
| $u_{1,z'}$ | Linear limb-darkening coefficient in $z'$ | ... | $0.477^{+0.094}_{-0.10}$ | |
| $u_{1,4.5\mu m}$ | Linear limb-darkening coefficient in 4.5 $\mu$m | ... | $0.0076^{+0.012}_{-0.0057}$ | |
| $u_{1,\mathrm{TESS}}$ | Linear limb-darkening coefficient in TESS | ... | $0.467^{+0.057}_{-0.058}$ | |
| $u_{1,V}$ | Linear limb-darkening coefficient in $V$ | ... | $0.63^{+0.46}_{-0.42}$ | |
| $u_{1,y}$ | Linear limb-darkening coefficient in $y$ | ... | $0.76^{+0.52}_{-0.47}$ | |
| $u_{2,I}$ | Quadratic limb-darkening coefficient in $I$ | ... | $-0.10^{+0.49}_{-0.40}$ | |
| $u_{2,R}$ | Quadratic limb-darkening coefficient in $R$ | ... | $-0.13^{+0.41}_{-0.40}$ | |
| $u_{2,z'}$ | Quadratic limb-darkening coefficient in $z'$ | ... | $-0.174^{+0.12}_{-0.078}$ | |
| $u_{2,4.5\mu m}$ | Quadratic limb-darkening coefficient in 4.5 $\mu$m | ... | $0.067 \pm 0.038$ | |
| $u_{2,\mathrm{TESS}}$ | Quadratic limb-darkening coefficient in TESS | ... | $0.186^{+0.092}_{-0.091}$ | |
| $u_{2,V}$ | Quadratic limb-darkening coefficient in $V$ | ... | $0.15^{+0.45}_{-0.47}$ | |
| $u_{2,y}$ | Quadratic limb-darkening coefficient in $y$ | ... | $-0.08^{+0.47}_{-0.41}$ | |

**Notes.** See Table 3 in Eastman et al. (2019) for a detailed description of all parameters. Since both Pan-STARRS $Y$ and Pan-STARRS $z_s$ are not available among the filters in `EXOFASTv2`, $y$ and $z'$ (Sloan $z$) were used as respective approximate substitutes. Additionally, the Claret and Bloemen limb-darkening tables (Claret & Bloemen 2011) default option has been disabled since AU Mic is a low-mass red dwarf.
[a] The metallicity of the star at birth.
[b] Corresponds to static points in a star's evolutionary history. See Section 2 in Dotter (2016).
[c] Uses measured radius and estimated mass from Chen & Kipping (2017).
[d] Time of conjunction is commonly reported as the "transit time."
[e] Time of minimum projected separation is a more correct "transit time."
[f] Optimal time of conjunction minimizes the covariance between $T_C$ and period.
[g] Assumes no albedo and perfect redistribution.
[h] Depends on the tidal $Q$ factor.
[i] The velocity at $T_C$ of an assumed circular orbit divided by the velocity of the modeled eccentric orbit.
[j] The sign of the solution to the quadratic mapping from $V_c/V_e$ to $e$.

a useful snapshot on whether AU Mic b's TTVs are behaving linearly over time. The massless planets' $O-C$ diagram (Figure 5 from Wittrock et al. 2022) and the statistical comparison between the massless two-planet model and the non-massless two-planet model—e.g., reduced chi-square $\chi^2_{\mathrm{red}} = 8.7 \times 10^8$ versus 38, respectively, and log-likelihood $\ln \mathcal{L} = -6.1 \times 10^9$ versus $-75$, respectively (Wittrock et al. 2022)—show very clear indications that a linear trend does not fit very well with AU Mic b's observed TTVs.

In the meanwhile, given the relatively sparse observations of AU Mic c, we cannot draw any meaningful interpretation of what c's TTV super-period could be. Thus, the potential super-period in AU Mic c's observed TTVs is not explored in this paper.

### 4.2. `Exo-Striker` Dynamical Modeling Preparations and Processes

The $O-C$ diagram from Wittrock et al. (2022) displayed the apparent deviation of the TTVs from a linear ephemeris; this was believed to be attributed to the yet-to-be-confirmed planet AU Mic d even after accounting for the impacts from stellar activity, such as flaring and spot crossings. With the new data from Section 2 added to this work, we model the TTVs of AU Mic b and c using the `Exo-Striker` package (Trifonov 2019), with our focus now on validating AU Mic d. `Exo-Striker` is capable of applying MCMC via `emcee` (Foreman-Mackey et al. 2013) to determine the statistical significance of our TTV measurements and the confidence in their corresponding dynamical model posteriors.

For our `Exo-Striker` modeling, we incorporate the priors for the host star and the planets from Table 10 and the midpoint time priors from Table 11. `Exo-Striker` uses only the `Simplex` algorithm for any TTV models. We use the `N-body` algorithm for all model fittings and MCMC runs, and we set the dynamical model time steps to 0.01 days. For our model fittings, we use the following `scipy` minimizer algorithms: the truncated Newton algorithm[37] as a primary minimizer and the

[37] https://docs.scipy.org/doc/scipy/reference/optimize.minimize-tnc.html

**Table 6**
EXOFASTv2-generated Median Values and 68% Confidence Interval for Follow-up Observations of AU Mic Transits (Part I)

| Planet | Telescope | Date (UT) | Filter | $\sigma^2$ (Added Variance) | TTV[a] (days) | $T\delta V$[b] | $F_0$[c] |
|---|---|---|---|---|---|---|---|
| b | TESS | 2018-07-26 | TESS | $0.000000010^{+0.000000012}_{-0.000000011}$ | $-0.00242^{+0.00065}_{-0.00066}$ | $0.0020 \pm 0.0011$ | $0.999994 \pm 0.000030$ |
| c | TESS | 2018-08-11 | TESS | $0.000000006^{+0.000000012}_{-0.000000010}$ | $-0.0007 \pm 0.0020$ | $0.0030 \pm 0.0029$ | $0.999992 \pm 0.000030$ |
| b | TESS | 2018-08-12 | TESS | $0.000000003^{+0.000000017}_{-0.000000015}$ | $-0.00063 \pm 0.00075$ | $0.0021 \pm 0.0011$ | $1.000012 \pm 0.000039$ |
| b | Spitzer | 2019-02-10 | 4.5 $\mu$m | $0.0000000700^{+0.0000000056}_{-0.0000000054}$ | $0.00336^{+0.00053}_{-0.00054}$ | $-0.0063 \pm 0.0012$ | $1.000028^{+0.000034}_{-0.000033}$ |
| b | Spitzer | 2019-02-27 | 4.5 $\mu$m | $0.0000000384^{+0.0000000043}_{-0.0000000041}$ | $0.00413^{+0.00052}_{-0.00054}$ | $-0.0024 \pm 0.0011$ | $1.000312 \pm 0.000027$ |
| b | Spitzer | 2019-09-09 | 4.5 $\mu$m | $0.0000001237^{+0.0000000061}_{-0.0000000058}$ | $0.00082^{+0.00054}_{-0.00055}$ | $-0.0025 \pm 0.0012$ | $0.999765 \pm 0.000027$ |
| b | LCO SSO | 2020-04-25 | $z'$ | $0.00000275^{+0.00000033}_{-0.00000029}$ | $-0.0047^{+0.0016}_{-0.0014}$ | $-0.0033^{+0.0054}_{-0.0044}$ | $0.99999 \pm 0.00014$ |
| b | LCO SSO | 2020-04-25 | $y$ | $0.00000066^{+0.0000013}_{-0.00000093}$ | $0.003 \pm 0.010$ | $0.0005^{+0.0065}_{-0.0070}$ | $1.00009^{+0.00048}_{-0.00044}$ |
| b | LCO SAAO | 2020-05-20 | $z'$ | $0.00000188^{+0.00000017}_{-0.00000016}$ | $-0.0048^{+0.0018}_{-0.0016}$ | $0.0040^{+0.0023}_{-0.0024}$ | $1.00034 \pm 0.00017$ |
| b | LCO SAAO | 2020-05-20 | $y$ | $0.00000141^{+0.00000054}_{-0.00000043}$ | $0.0088^{+0.0065}_{-0.0041}$ | $0.0005^{+0.0051}_{-0.0053}$ | $0.99984^{+0.00038}_{-0.00037}$ |
| b | LCO SAAO | 2020-06-06 | $z'$ | $0.00000673^{+0.00000069}_{-0.00000062}$ | $-0.0079 \pm 0.0032$ | $0.0000^{+0.0053}_{-0.0055}$ | $0.99995^{+0.00035}_{-0.00034}$ |
| b | LCO SAAO | 2020-06-23 | $z'$ | $0.00000189^{+0.00000024}_{-0.00000021}$ | $-0.0019 \pm 0.0014$ | $0.0075^{+0.0018}_{-0.0029}$ | $0.99982^{+0.00016}_{-0.00019}$ |
| c | TESS | 2020-07-09 | TESS | $-0.000000003^{+0.000000016}_{-0.000000015}$ | $-0.0011^{+0.0029}_{-0.0026}$ | $0.0034 \pm 0.0029$ | $1.000009 \pm 0.000024$ |
| b | TESS | 2020-07-10 | TESS | $0.000000005^{+0.000000014}_{-0.000000013}$ | $-0.00393^{+0.00063}_{-0.00067}$ | $0.0020 \pm 0.0011$ | $1.000002 \pm 0.000021$ |
| b | PEST | 2020-07-10 | $V$ | $0.0000163^{+0.0000013}_{-0.0000012}$ | $-0.0116^{+0.0033}_{-0.0034}$ | $0.00879^{+0.00090}_{-0.0020}$ | $0.99931^{+0.00020}_{-0.00021}$ |
| b | TESS | 2020-07-19 | TESS | $-0.000000005^{+0.000000012}_{-0.000000011}$ | $-0.00326^{+0.00064}_{-0.00066}$ | $0.0020 \pm 0.0011$ | $0.999998 \pm 0.000020$ |
| b | TESS | 2020-07-27 | TESS | $-0.000000001^{+0.000000012}_{-0.000000011}$ | $-0.00217^{+0.00063}_{-0.00066}$ | $0.0019^{+0.0011}_{-0.0010}$ | $0.999994 \pm 0.000020$ |
| c | TESS | 2020-07-28 | TESS | $0.000000010^{+0.000000014}_{-0.000000013}$ | $0.0008^{+0.0029}_{-0.0026}$ | $0.0033 \pm 0.0029$ | $1.000004 \pm 0.000022$ |
| b | Brierfield | 2020-08-13 | $I$ | $0.0000171^{+0.0000015}_{-0.0000013}$ | $0.0074^{+0.0039}_{-0.0030}$ | $0.0047^{+0.0035}_{-0.0051}$ | $0.99996^{+0.00031}_{-0.00034}$ |
| b | LCO SSO | 2020-08-13 | $z'$ | $0.00000406^{+0.00000035}_{-0.00000032}$ | $-0.0035^{+0.0018}_{-0.0021}$ | $0.0013^{+0.0034}_{-0.0035}$ | $1.00003^{+0.00026}_{-0.00025}$ |
| b | LCO SAAO | 2020-09-07 | $z'$ | $0.00000688^{+0.00000077}_{-0.00000067}$ | $0.0060^{+0.0090}_{-0.0072}$ | $-0.0038^{+0.0049}_{-0.0040}$ | $0.99972^{+0.00043}_{-0.00034}$ |
| b | LCO SSO | 2020-09-16 | $z'$ | $0.000001191^{+0.00000011}_{-0.000000100}$ | $-0.00314^{+0.00093}_{-0.00097}$ | $-0.0009 \pm 0.0021$ | $1.00000 \pm 0.00013$ |
| b | LCO SSO | 2020-10-03 | $z'$ | $0.00000125^{+0.00000016}_{-0.00000014}$ | $-0.0013 \pm 0.0011$ | $0.0071^{+0.0017}_{-0.0021}$ | $1.00225^{+0.00016}_{-0.00017}$ |
| b and c | LCO SAAO | 2020-10-11 | $z'$ | $0.00000613^{+0.00000063}_{-0.00000056}$ | $-0.002^{+0.017}_{-0.013}$ | $0.0044^{+0.0031}_{-0.0036}$ | $1.00301^{+0.00045}_{-0.00048}$ |
| b | LCO CTIO | 2021-06-14 | $z'$ | $0.000000740^{+0.000000075}_{-0.000000068}$ | $0.01230^{+0.00099}_{-0.0010}$ | $-0.0076^{+0.0018}_{-0.0015}$ | $1.000026^{+0.000092}_{-0.000086}$ |
| b | LCO SSO | 2021-06-22 | $z'$ | $0.0001177^{+0.000010}_{-0.0000095}$ | $-0.0086^{+0.013}_{-0.0070}$ | $-0.0012^{+0.0070}_{-0.0060}$ | $0.99832^{+0.00076}_{-0.00074}$ |
| b | LCO CTIO | 2021-07-01 | $z'$ | $0.000000980^{+0.000000089}_{-0.000000082}$ | $0.0139^{+0.0011}_{-0.0010}$ | $0.0009 \pm 0.0019$ | $1.00003^{+0.00012}_{-0.00011}$ |
| b | ASTEP | 2021-07-09 | $R$ | $0.00001316^{+0.00000087}_{-0.00000081}$ | $-0.0130^{+0.020}_{-0.0045}$ | $-0.0050^{+0.0036}_{-0.0030}$ | $0.99998^{+0.00021}_{-0.00020}$ |
| b | LCO SAAO | 2021-07-17 | $z'$ | $0.00000535^{+0.00000054}_{-0.00000049}$ | $0.0131^{+0.0022}_{-0.0018}$ | $0.0087^{+0.0010}_{-0.0020}$ | $0.99904^{+0.00020}_{-0.00021}$ |
| b | LCO SAAO | 2021-08-03 | $z'$ | $0.00000215^{+0.00000022}_{-0.00000020}$ | $0.0179^{+0.0014}_{-0.0018}$ | $-0.0039^{+0.0045}_{-0.0039}$ | $0.99990^{+0.00028}_{-0.00023}$ |
| b | LCO CTIO | 2021-08-04 | $z'$ | $0.00000574^{+0.00000047}_{-0.00000043}$ | $0.0078^{+0.0024}_{-0.0030}$ | $0.0017^{+0.0030}_{-0.0031}$ | $1.00031 \pm 0.00026$ |
| b | LCO SSO | 2021-08-12 | $z'$ | $0.00000264^{+0.00000024}_{-0.00000022}$ | $0.0132^{+0.0015}_{-0.0016}$ | $-0.0029^{+0.0032}_{-0.0033}$ | $0.99992^{+0.00021}_{-0.00020}$ |
| b | LCO SSO | 2021-08-29 | $z'$ | $0.00000197^{+0.00000016}_{-0.00000015}$ | $0.01952^{+0.00036}_{-0.00072}$ | $-0.00973^{+0.00042}_{-0.00020}$ | $0.999574^{+0.000088}_{-0.000087}$ |
| b | LCO SSO | 2021-09-15 | $z'$ | $0.00000194^{+0.00000020}_{-0.00000018}$ | $0.01954^{+0.00034}_{-0.00069}$ | $0.00914^{+0.00063}_{-0.0012}$ | $0.99952 \pm 0.00015$ |
| b | LCO SAAO | 2021-09-23 | $z'$ | $0.0000181^{+0.0000014}_{-0.0000013}$ | $0.0124^{+0.0030}_{-0.011}$ | $-0.0040^{+0.0044}_{-0.0038}$ | $1.00029^{+0.00031}_{-0.00029}$ |
| b | LCO TO | 2021-09-23 | $z'$ | $0.0000106^{+0.0000012}_{-0.0000010}$ | $0.0169^{+0.0022}_{-0.0035}$ | $0.0001^{+0.0061}_{-0.0064}$ | $0.99959^{+0.00053}_{-0.00048}$ |
| c | LCO CTIO | 2021-10-04 | $z'$ | $0.00000273^{+0.00000022}_{-0.00000020}$ | $-0.0105^{+0.015}_{-0.0066}$ | $-0.0077^{+0.0031}_{-0.0017}$ | $1.00047^{+0.00018}_{-0.00015}$ |

**Notes.** See Table 3 in Eastman et al. (2019) for a detailed description of all parameters. Since both Pan-STARRS $Y$ and Pan-STARRS $z_s$ are not available among the filters in EXOFASTv2, $y$ and $z'$ (Sloan $z$) were used as respective approximate substitutes.
[a] Transit timing variation.
[b] Transit depth variation.
[c] Baseline flux.

Nelder–Mead algorithm[38] as a secondary minimizer, with the configurations of both minimizers set at default, including one consecutive integration and 5000 integration steps. We manually fit the model to the data using the previously mentioned minimizer algorithms, then each time we find a possible best-fit model, we proceed to perform MCMC computations by adopting MCMC parameters as best $\ln \mathcal{L}$ and with 1000 burn-in steps, 10,000 main steps for the two-planet dynamical models and 8 000 main steps for the three-planet dynamical models, and 196 walkers for the two-planet dynamical models and 441 walkers for the three-planet dynamical models. The three aforementioned scenarios are explored and presented in the following sections.

### 4.3. Two-planet Dynamical Modeling

We explored a best-fit scenario for a two-planet model for the purpose of obtaining the statistical significance of TTVs and comparing the results with those of the three-planet models. We share our maximum-likelihood two-planet model with its MCMC $O-C$ diagram (Figure 4), posteriors (Table 12), and MCMC corner plot (Figure 5). The $O-C$ diagram from Figure 4 does exhibit the super-period that was obvious in Figure 3. However, the planets' inferred masses are very small ($K < 0.07$ m s$^{-1}$) and their eccentricities relatively large ($e > 0.2$), neither of which are in agreement with those

[38] https://docs.scipy.org/doc/scipy/reference/optimize.minimize-neldermead.html

**Table 7**
EXOFASTv2-generated Median Values and 68% Confidence Interval for Follow-up Observations of AU Mic b (Part II)

| Planet | Telescope | Date (UT) | Filter | $C_0$[a] | $C_1$[a] | $M_0$[b] | $M_1$[b] | $M_2$[b] |
|---|---|---|---|---|---|---|---|---|
| b | TESS | 2018-07-26 | TESS | ... | ... | ... | ... | ... |
| c | TESS | 2018-08-11 | TESS | ... | ... | ... | ... | ... |
| b | TESS | 2018-08-12 | TESS | ... | ... | ... | ... | ... |
| b | Spitzer | 2019-02-10 | 4.5 $\mu$m | $-0.000148 \pm 0.000046$ | ... | $-0.00097 \pm 0.00036$ | $-0.0105 \pm 0.0014$ | $0.0121 \pm 0.0014$ |
| b | Spitzer | 2019-02-27 | 4.5 $\mu$m | $-0.000271 \pm 0.000046$ | $0.000077 \pm 0.000031$ | $0.00021^{+0.00040}_{-0.00041}$ | $0.00037 \pm 0.00044$ | $-0.00208^{+0.00092}_{-0.00089}$ |
| b | Spitzer | 2019-09-09 | 4.5 $\mu$m | $-0.00051 \pm 0.00014$ | ... | $-0.00129 \pm 0.00032$ | $0.00280 \pm 0.00027$ | $0.0020 \pm 0.0017$ |
| b | LCO SSO | 2020-04-25 | $z'$ | ... | ... | $-0.00009^{+0.00038}_{-0.00035}$ | ... | ... |
| b | LCO SSO | 2020-04-25 | $y$ | ... | ... | $-0.00005^{+0.0010}_{-0.00099}$ | ... | ... |
| b | LCO SAAO | 2020-05-20 | $z'$ | ... | ... | $0.00104 \pm 0.00031$ | ... | ... |
| b | LCO SAAO | 2020-05-20 | $y$ | ... | ... | $-0.00034^{+0.00070}_{-0.00073}$ | ... | ... |
| b | LCO SAAO | 2020-06-06 | $z'$ | ... | ... | $0.00000^{+0.00070}_{-0.00065}$ | ... | ... |
| b | LCO SAAO | 2020-06-23 | $z'$ | ... | ... | $-0.00032^{+0.00049}_{-0.00052}$ | $-0.00007^{+0.00056}_{-0.00055}$ | ... |
| c | TESS | 2020-07-09 | TESS | ... | ... | ... | ... | ... |
| b | TESS | 2020-07-10 | TESS | ... | ... | ... | ... | ... |
| b | PEST | 2020-07-10 | $V$ | $-0.0043 \pm 0.0025$ | ... | $0.00017^{+0.00076}_{-0.00074}$ | $0.00026 \pm 0.00080$ | $0.0007^{+0.0012}_{-0.0011}$ |
| b | TESS | 2020-07-19 | TESS | ... | ... | ... | ... | ... |
| b | TESS | 2020-07-27 | TESS | ... | ... | ... | ... | ... |
| c | TESS | 2020-07-28 | TESS | ... | ... | ... | ... | ... |
| b | Brierfield | 2020-08-13 | $I$ | ... | ... | $0.0036 \pm 0.0055$ | $-0.0021 \pm 0.0018$ | $0.0032^{+0.0050}_{-0.0051}$ |
| b | LCO SSO | 2020-08-13 | $z'$ | ... | ... | $-0.00003 \pm 0.00039$ | $0.00001^{+0.00027}_{-0.00026}$ | ... |
| b | LCO SAAO | 2020-09-07 | $z'$ | $-0.00021 \pm 0.00060$ | ... | $-0.00056^{+0.00097}_{-0.00089}$ | ... | ... |
| b | LCO SSO | 2020-09-16 | $z'$ | ... | ... | $0.00002 \pm 0.00035$ | $0.00001^{+0.00032}_{-0.00033}$ | ... |
| b | LCO SSO | 2020-10-03 | $z'$ | $-0.00153 \pm 0.00019$ | ... | $-0.00134 \pm 0.00026$ | ... | ... |
| b and c | LCO SAAO | 2020-10-11 | $z'$ | ... | ... | $0.00073^{+0.00082}_{-0.0012}$ | ... | ... |
| b | LCO CTIO | 2021-06-14 | $z'$ | $-0.00003 \pm 0.00017$ | ... | $0.00002 \pm 0.00037$ | $-0.00001 \pm 0.00022$ | ... |
| b | LCO SSO | 2021-06-22 | $z'$ | ... | ... | $0.0014^{+0.0020}_{-0.0019}$ | $0.0016 \pm 0.0016$ | $-0.0006^{+0.0021}_{-0.0022}$ |
| b | LCO CTIO | 2021-07-01 | $z'$ | $-0.00004 \pm 0.00018$ | ... | $0.00002 \pm 0.00049$ | $0.00001 \pm 0.00017$ | ... |
| b | ASTEP | 2021-07-09 | $R$ | $-0.00001 \pm 0.00044$ | ... | ... | ... | ... |
| b | LCO SAAO | 2021-07-17 | $z'$ | $-0.00088^{+0.00065}_{-0.00067}$ | ... | $-0.00100^{+0.00068}_{-0.00067}$ | ... | ... |
| b | LCO SAAO | 2021-08-03 | $z'$ | $-0.00002^{+0.00048}_{-0.00043}$ | ... | $-0.00033^{+0.00057}_{-0.00056}$ | $0.00004 \pm 0.00035$ | ... |
| b | LCO CTIO | 2021-08-04 | $z'$ | ... | ... | $-0.00022^{+0.00046}_{-0.00045}$ | ... | ... |
| b | LCO SSO | 2021-08-12 | $z'$ | $0.00032^{+0.00056}_{-0.00057}$ | ... | $-0.00000 \pm 0.00023$ | $-0.00020^{+0.00030}_{-0.00029}$ | ... |
| b | LCO SSO | 2021-08-29 | $z'$ | ... | ... | $-0.00301 \pm 0.00050$ | $0.00131 \pm 0.00022$ | $-0.00131 \pm 0.00048$ |
| b | LCO SSO | 2021-09-15 | $z'$ | ... | ... | $0.00081 \pm 0.00033$ | $-0.00047 \pm 0.00047$ | $-0.00001^{+0.00037}_{-0.00038}$ |
| b | LCO SAAO | 2021-09-23 | $z'$ | $-0.00038^{+0.00061}_{-0.00066}$ | ... | $0.00095^{+0.00077}_{-0.00080}$ | ... | ... |
| b | LCO TO | 2021-09-23 | $z'$ | ... | ... | $0.00052^{+0.00059}_{-0.00060}$ | $0.00002^{+0.00071}_{-0.00074}$ | ... |
| c | LCO CTIO | 2021-10-04 | $z'$ | ... | ... | $-0.00054^{+0.00070}_{-0.00071}$ | $0.00009 \pm 0.00065$ | $-0.00070^{+0.00062}_{-0.00064}$ |

**Notes.** See Table 3 in Eastman et al. (2019) for a detailed description of all parameters. Since both Pan-STARRS $Y$ and Pan-STARRS $z_s$ are not available among the filters in EXOFASTv2, $y$ and $z'$ (Sloan $z$) were used as respective approximate substitutes. Additionally, the detrending parameters flare (Spitzer), sky (Spitzer and PEST), Sky/Pixel_T1 (LCOGT), and SKY (ASTEP) were set as additive while the remaining detrending parameters were set as multiplicative.

[a] Additive detrending coefficient.

[b] Multiplicative detrending coefficient.

**Table 8**

EXOFASTv2-generated Median Values and 68% Confidence Interval for Follow-up Observations of AU Mic b (Part III)

| Planet | Telescope | Date (UT) | Filter | $M_3$[a] | $M_4$[a] | $M_5$[a] | $M_6$[a] | $M_7$[a] |
|---|---|---|---|---|---|---|---|---|
| b | TESS | 2018-07-26 | TESS | ... | ... | ... | ... | ... |
| c | TESS | 2018-08-11 | TESS | ... | ... | ... | ... | ... |
| b | TESS | 2018-08-12 | TESS | ... | ... | ... | ... | ... |
| b | Spitzer | 2019-02-10 | 4.5 $\mu$m | -0.00618 $\pm$ 0.00092 | 0.00376 $\pm$ 0.00064 | -0.000281 $\pm$ 0.000045 | $-0.000316^{+0.000062}_{-0.000061}$ | ... |
| b | Spitzer | 2019-02-27 | 4.5 $\mu$m | $0.00226^{+0.00088}_{-0.00090}$ | $0.00061^{+0.00071}_{-0.00072}$ | 0.00065 $\pm$ 0.00022 | -0.00065 $\pm$ 0.00024 | ... |
| b | Spitzer | 2019-09-09 | 4.5 $\mu$m | -0.00183 $\pm$ 0.00091 | -0.0039 $\pm$ 0.0013 | $0.000004^{+0.000031}_{-0.000032}$ | $-0.000486^{+0.000095}_{-0.000094}$ | $-0.000761^{+0.000088}_{-0.000086}$ |
| b | LCO SSO | 2020-04-25 | $z'$ | ... | ... | ... | ... | ... |
| b | LCO SSO | 2020-04-25 | $y$ | ... | ... | ... | ... | ... |
| b | LCO SAAO | 2020-05-20 | $z'$ | ... | ... | ... | ... | ... |
| b | LCO SAAO | 2020-05-20 | $y$ | ... | ... | ... | ... | ... |
| b | LCO SAAO | 2020-06-06 | $z'$ | ... | ... | ... | ... | ... |
| b | LCO SAAO | 2020-06-23 | $z'$ | ... | ... | ... | ... | ... |
| c | TESS | 2020-07-09 | TESS | ... | ... | ... | ... | ... |
| b | TESS | 2020-07-10 | TESS | ... | ... | ... | ... | ... |
| b | PEST | 2020-07-10 | $V$ | 0.0013 $\pm$ 0.0014 | ... | ... | ... | ... |
| b | TESS | 2020-07-19 | TESS | ... | ... | ... | ... | ... |
| b | TESS | 2020-07-27 | TESS | ... | ... | ... | ... | ... |
| c | TESS | 2020-07-28 | TESS | ... | ... | ... | ... | ... |
| b | Brierfield | 2020-08-13 | $I$ | 0.0013 $\pm$ 0.0024 | ... | ... | ... | ... |
| b | LCO SSO | 2020-08-13 | $z'$ | ... | ... | ... | ... | ... |
| b | LCO SAAO | 2020-09-07 | $z'$ | ... | ... | ... | ... | ... |
| b | LCO SSO | 2020-09-16 | $z'$ | ... | ... | ... | ... | ... |
| b | LCO SSO | 2020-10-03 | $z'$ | ... | ... | ... | ... | ... |
| b and c | LCO SAAO | 2020-10-11 | $z'$ | ... | ... | ... | ... | ... |
| b | LCO CTIO | 2021-06-14 | $z'$ | ... | ... | ... | ... | ... |
| b | LCO SSO | 2021-06-22 | $z'$ | ... | ... | ... | ... | ... |
| b | LCO CTIO | 2021-07-01 | $z'$ | ... | ... | ... | ... | ... |
| b | ASTEP | 2021-07-09 | $R$ | ... | ... | ... | ... | ... |
| b | LCO SAAO | 2021-07-17 | $z'$ | ... | ... | ... | ... | ... |
| b | LCO SAAO | 2021-08-03 | $z'$ | ... | ... | ... | ... | ... |
| b | LCO CTIO | 2021-08-04 | $z'$ | ... | ... | ... | ... | ... |
| b | LCO SSO | 2021-08-12 | $z'$ | ... | ... | ... | ... | ... |
| b | LCO SSO | 2021-08-29 | $z'$ | ... | ... | ... | ... | ... |
| b | LCO SSO | 2021-09-15 | $z'$ | ... | ... | ... | ... | ... |
| b | LCO SAAO | 2021-09-23 | $z'$ | ... | ... | ... | ... | ... |
| b | LCO TO | 2021-09-23 | $z'$ | ... | ... | ... | ... | ... |
| c | LCO CTIO | 2021-10-04 | $z'$ | ... | ... | ... | ... | ... |

**Notes.** See Table 3 in Eastman et al. (2019) for a detailed description of all parameters. Since both Pan-STARRS $Y$ and Pan-STARRS $z_s$ are not available among the filters in EXOFASTv2, $y$ and $z'$ (Sloan $z$) were used as respective approximate substitutes. Additionally, the detrending parameters flare (Spitzer), sky (Spitzer and PEST), Sky/Pixel_T1 (LCOGT), and SKY (ASTEP) were set as additive while the remaining detrending parameters were set as multiplicative.

[a] Multiplicative detrending coefficient.

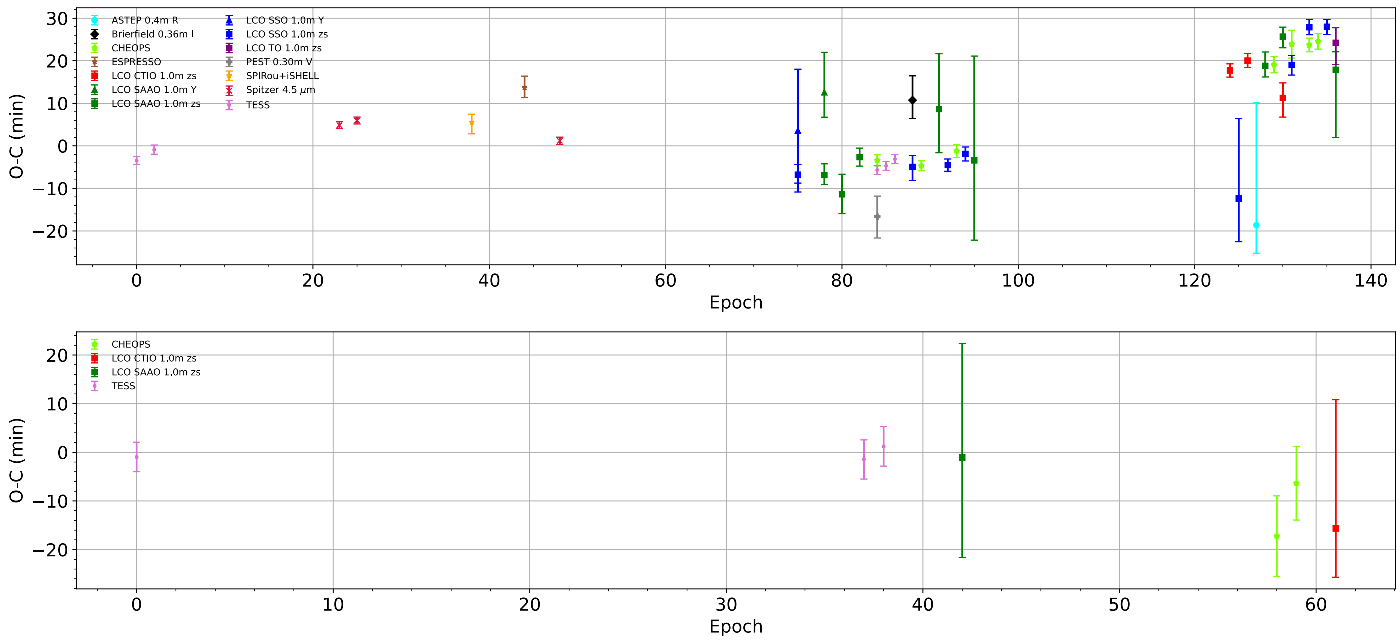


**Figure 2.** $O-C$ diagrams of AU Mic b (top) and AU Mic c (bottom), using the EXOFASTv2-generated measured midpoint times (Table 11) and the calculated expected midpoint times for all transit data sets from Table 1. The planets' period and $T_C$ from EXOFASTv2 posteriors were used for the calculation of expected midpoint times. The epoch refers to the number of transits since the first transit of b and c, respectively.

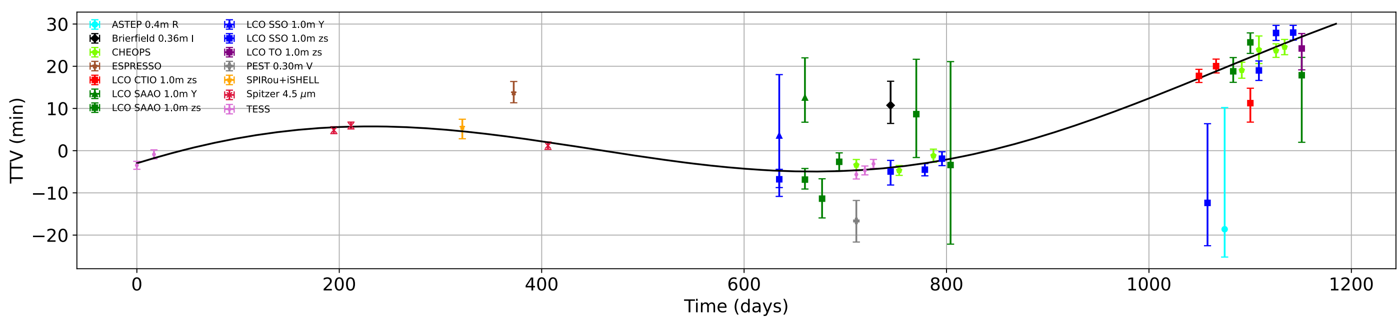


**Figure 3.** $O-C$ diagram of AU Mic b with the super-period model overlaid (black). The super-period model was generated using the coefficients from Table 9 and Equation (1), and the $O-C$ diagram was generated using the EXOFASTv2-generated measured midpoint times (Table 11) and the calculated expected midpoint times for all transit data sets from Table 1. The planet's period and $T_C$ from EXOFASTv2 posteriors were used for the calculation of expected midpoint times. The time is with respect to the first transit of b.

**Table 9**
Coefficients from Equation (1) as Part of Modeling the Super-period of AU Mic b's TTVs (Figure 3)

| Coefficient | Unit | Output |
|---|---|---|
| $A$ | min | 13.46394 ± 3.06443 |
| $B$ | day$^{-1}$ | 0.00504 ± 0.00070 |
| $C$ | ... | 0.87455 ± 0.28102 |
| $D$ | min day$^{-1}$ | 0.03052 ± 0.00964 |
| $E$ | min | -13.31819 ± 4.52818 |

**Notes.** The coefficients were solved using the scipy.optimize.curve_fit[a].
[a] https://docs.scipy.org/doc/scipy/reference/generated/scipy.optimize.curve_fit.html.

from RV literature (e.g., Cale et al. 2021; Donati et al. 2023). Moreover, the angular momentum deficit (AMD; Laskar 1997, 2000; Laskar & Petit 2017) criteria built within the Exo-Striker package indicated that this model is unstable. We followed this up by testing its stability over 20 Myr with the $N$-body simulator rebound (Rein & Liu 2012; Rein & Spiegel 2015).

Since this model's inferred masses are very small, we performed two stability tests (Figure 6): one with the planets' original $K$'s from Table 12, and another with the planets' $K$'s from Cale et al.'s (2021) RV models. At first glance, the original $K$'s case appears to be dynamically stable, but the planets' already highly eccentric orbits become increasingly eccentric over time, and both planets' orbits become increasingly misaligned with the system, which would cause both planets to quickly lose their transiting status. The RV $K$'s case exhibits signs of chaos in the AU Mic system, with both planets undergoing orbital migrations, with planet c demonstrating greater wobbles in its orbital path. Also, both planets' eccentricities oscillate rapidly between 0 and 1, and their highly fluctuating inclinations would frequently put both transiting planets in nontransiting configurations. Given that both planets' observed orbital periods are very consistent and with very small timing uncertainties (Martioli et al. 2020; Plavchan et al. 2020; Cale et al. 2021; Gilbert et al. 2022;

**Table 10**
AU Mic's Stellar and Planetary Priors for `Exo-Striker` Best-fit and MCMC Modeling

| Prior | Unit | Input | | |
|---|---|---|---|---|
| | | AU Mic b | AU Mic c | AU Mic d |
| Mass | $M_\odot$ | | $\mathcal{N}(0.510, 0.028)$ | |
| Radius | $R_\odot$ | | $\mathcal{N}(0.744, 0.023)$ | |
| Luminosity | $L_\odot$ | | $\mathcal{N}(0.0916, 0.011)$ | |
| $T_{\rm eff}$ | K | | $\mathcal{N}(3678, 90)$ | |
| $v \sin i$ | km s$^{-1}$ | | $\mathcal{N}(8.7, 0.2)$ | |
| $K$ | m s$^{-1}$ | $\mathcal{U}(0.0, 10000.0)$ | $\mathcal{U}(0.0, 10000.0)$ | $\mathcal{U}(0.0, 10000.0)$ |
| $P_{\rm orb}$ | day | $\mathcal{N}(8.463, 0.001)$ | $\mathcal{N}(18.859, 0.001)$ | $\mathcal{U}(0.0, 100000.0)$ |
| $e$ | ... | $\mathcal{U}(0.000, 0.999)$ | $\mathcal{U}(0.000, 0.999)$ | $\mathcal{U}(0.000, 0.999)$ |
| $\omega$ | deg | $\mathcal{U}(0.0, 360.0)$ | $\mathcal{U}(0.0, 360.0)$ | $\mathcal{U}(0.0, 360.0)$ |
| $M_0$ | deg | $\mathcal{U}(0.0, 360.0)$ | $\mathcal{U}(0.0, 360.0)$ | $\mathcal{U}(0.0, 360.0)$ |
| $i$ | deg | $\mathcal{N}(89.57, 0.31)$ | $\mathcal{N}(89.43, 0.35)$ | $\mathcal{U}(0.0, 180.0)$ |
| $\Omega$ | deg | $\mathcal{U}(0.0, 360.0)$ | $\mathcal{U}(0.0, 360.0)$ | $\mathcal{U}(0.0, 360.0)$ |

**Notes.** The stellar, orbital period, and inclination priors are taken from `EXOFASTv2` posteriors. AU Mic d's priors apply to three-planet modeling only. $M_0 \equiv$ mean anomaly, and $\Omega \equiv$ longitude of ascending node.

Wittrock et al. 2022; Donati et al. 2023), that the RV models from Cale et al. (2021) and Donati et al. (2023) place both planets' orbits at much lower eccentricities, and that there have not been any known cases in which either planet "misses" its transit due to being outside the line of sight between the observers and the host star, this two-planet high-eccentricity configuration appears to be nonphysical and highly implausible.

We then turned to an alternative two-planet model with lower eccentricities. We present our low-eccentricity maximum-likelihood two-planet model with its MCMC $O-C$ diagram (Figure 7), posteriors (Table 13), and MCMC corner plot (Figure 8). This time, the AMD criteria indicated that this two-planet low-eccentricity model is stable. However, the inclinations from Table 13 suggest that the planets are misaligned, which contradicts the observed transits of both AU Mic b and c and the inclinations from transit and TTV literature (e.g., Martioli et al. 2021; Gilbert et al. 2022; Wittrock et al. 2022). Additionally, the $O-C$ diagram from Figure 7 does not exhibit the super-period that was very distinctive in the $O-C$ diagram from Figure 3, resulting in the model not converging very well with many observed TTVs, including those from the R-M observations, CHEOPS, and some TESS. Thus, both the two-planet diagram and the statistics information from Table 13 (e.g., $\chi^2_{\rm red,b} = 75.69$ and $\chi^2_{\rm red,c} = 454.17$) clearly show that the model is of a poor fit, suggesting that we need a third planet to account for the observed TTV excess, a conclusion also reached in Wittrock et al. (2022), but now much more obvious by eye with the additional season of 2021 transit observations.

### 4.4. Three-planet Dynamical Modeling

The two-planet high-eccentricity case's high orbital eccentricities and very low inferred masses from Table 12 put this configuration in strong disagreement with the RV models from Cale et al. (2021) and Donati et al. (2023), and this orbital configuration exhibits potential instability (Figure 6), with both planets' eccentricities and inclinations undergoing significant fluctuations; these issues suggest that the two-planet high-eccentricity case does not provide a good fit for a two-planet model. The two-planet low-eccentricity case has both transiting planets being misaligned based on the inclinations from Table 13, and Figure 7 and the relatively high $\chi^2_{\rm red}$ and corrected Akaike information criterion (AIC$_c$; Sugiura 1978; Hurvich & Tsai 1989; Cavanaugh 1997) from Table 13 (e.g., $\chi^2_{\rm red,b} = 75.69$, $\chi^2_{\rm red,c} = 454.17$, and AIC$_c = 1967.84$) demonstrate that the two-planet low-eccentricity model is inadequate in describing the observed TTVs; as such, we consider a three-planet model.

Both Cale et al. (2021) and Wittrock et al. (2022) probed the AU Mic system with RVs and TTVs, respectively, and modeled a tentative planet AU Mic d between the known planets AU Mic b and c with an orbital period of 12.742 and 13.466 days, respectively, the former of which would put the three planets near a 4:6:9 MMR chain. Since no additional transits have been identified for AU Mic, it was proposed that a third planet might be nontransiting. A nontransiting planet between two transiting planets is unusual but not unprecedented: HD 3167 d (Christiansen et al. 2017), Kepler-20 g (Buchhave et al. 2016), Kepler-411 e (Sun et al. 2019), and TOI-431 c (Osborn et al. 2021) are among the confirmed nontransiting planets orbiting between their adjacent transiting planets. We explore two possible scenarios for the three-planet modeling: AU Mic d orbiting interior to AU Mic b, and AU Mic d orbiting between AU Mic b and c. We first investigate the interior orbit case.

#### 4.4.1. Planet d Interior to b

As the 2:3 orbital resonance pair is the most common pairing for mature, compact multiplanet systems (Fabrycky et al. 2014), and since near-resonances are necessary to produce the observed detectable TTVs, we explored the possibility that $P_{\rm d} = 5.629$ days and modeled the best-fit three-planet configuration using that period as a starting point (Figure 9 and Table 14). The $O-C$ diagram from Figure 9 now displays a super-period in AU Mic b's TTVs, and the statistics from Table 14 (e.g., $\chi^2_{\rm red,b} = 5.21$, $\chi^2_{\rm red,c} = 31.23$, and AIC$_c = -343.02$) demonstrate that the three-planet model has significantly better fitting than both of the two-planet models.

Next, we constructed TTV log-likelihood periodograms using the optimization functions from the `Exo-Striker` library to probe a range of possible orbital periods for AU Mic d using the parameters from Table 14 as the starting point; we generated a set of 4801 orbital periods between 3.5 and 6.5 days corresponding to a step size of 0.0005 days. Since the `Exo-Striker` modeling did not significantly deviate from its initial value during the periodogram run, we adjusted d's initial inclination prior to each run to brute force a broader exploration of this model parameter. We performed two TTV periodograms with different initial inclinations $i_{\rm d} = (85°, 90°)$, respectively (Figure 10). From those runs, we came across six most favored inner d periods based on their respective log-likelihoods: 5.08 days ($\ln \mathcal{L} = 208.22$ and 208.84), 5.39 days ($\ln \mathcal{L} = 209.99$ and 209.80), 5.64 days ($\ln \mathcal{L} = 209.65$ and 209.62), 5.86 days ($\ln \mathcal{L} = 214.36$ and 214.33), 6.20 days ($\ln \mathcal{L} = 209.95$ and 208.43), and 6.47 days ($\ln \mathcal{L} = 207.76$ and 211.40).

We perform best-fit modeling and MCMC calculations for each of those best inner d cases and plotted the $O-C$ diagrams

**Table 11**
AU Mic Planets' Midpoint Time Priors for Exo-Striker Models

| Planet | Telescope | Transit N | Date (UT) | Band | $T_0$ (BJD) |
|---|---|---|---|---|---|
| b | TESS | 1 | 2018-07-26 | TESS | 2458330.38927 ± 0.00039 |
| | TESS | 3 | 2018-08-12 | TESS | 2458347.31710 ± 0.00053 |
| | Spitzer | 24 | 2019-02-10 | 4.5 $\mu$m | 2458525.04446 ± 0.00016 |
| | Spitzer | 26 | 2019-02-27 | 4.5 $\mu$m | 2458541.97126 ± 0.00014 |
| | SPIRou + iSHELL | 39 | 2019-06-17 | [a] | 2458651.99020 ± 0.00180 |
| | ESPRESSO | 45 | 2019-08-07 | 378.2–788.7 nm | 2458702.77397 ± 0.00178 |
| | Spitzer | 49 | 2019-09-09 | 4.5 $\mu$m | 2458736.61735 ± 0.00014 |
| | LCO SSO | 76 | 2020-04-25 | Pan-STARRS $Y$ | 2458965.11330 ± 0.00150 |
| | LCO SSO | 76 | 2020-04-25 | Pan-STARRS $z_s$ | 2458965.12050 ± 0.01000 |
| | LCO SAAO | 79 | 2020-05-20 | Pan-STARRS $z_s$ | 2458990.50230 ± 0.00170 |
| | LCO SAAO | 79 | 2020-05-20 | Pan-STARRS $Y$ | 2458990.51580 ± 0.00650 |
| | LCO SAAO | 81 | 2020-06-06 | Pan-STARRS $z_s$ | 2459007.42520 ± 0.00320 |
| | LCO SAAO | 83 | 2020-06-23 | Pan-STARRS $z_s$ | 2459024.35730 ± 0.00130 |
| | TESS | 85 | 2020-07-10 | TESS | 2459041.28124 ± 0.00026 |
| | PEST | 85 | 2020-07-10 | $V$ | 2459041.27360 ± 0.00340 |
| | CHEOPS | 85 | 2020-07-10 | CHEOPS | 2459041.28280 ± 0.00060 |
| | TESS | 86 | 2020-07-19 | TESS | 2459049.74493 ± 0.00024 |
| | TESS | 87 | 2020-07-27 | TESS | 2459058.20903 ± 0.00024 |
| | Brierfield | 89 | 2020-08-13 | $I$ | 2459075.14470 ± 0.00390 |
| | LCO SSO | 89 | 2020-08-13 | Pan-STARRS $z_s$ | 2459075.13380 ± 0.00210 |
| | CHEOPS | 90 | 2020-08-21 | CHEOPS | 2459083.59700 ± 0.00040 |
| | LCO SAAO | 92 | 2020-09-07 | Pan-STARRS $z_s$ | 2459100.53230 ± 0.00900 |
| | LCO SSO | 93 | 2020-09-16 | Pan-STARRS $z_s$ | 2459108.98618 ± 0.00072 |
| | CHEOPS | 94 | 2020-09-24 | CHEOPS | 2459117.45150 ± 0.00080 |
| | LCO SSO | 95 | 2020-10-03 | Pan-STARRS $z_s$ | 2459125.91403 ± 0.00090 |
| | LCO SAAO | 96 | 2020-10-11 | Pan-STARRS $z_s$ | 2459134.37600 ± 0.01700 |
| | LCO CTIO | 125 | 2021-06-14 | Pan-STARRS $z_s$ | 2459379.81818 ± 0.00069 |
| | LCO SSO | 126 | 2021-06-22 | Pan-STARRS $z_s$ | 2459388.26030 ± 0.01300 |
| | LCO CTIO | 127 | 2021-07-01 | Pan-STARRS $z_s$ | 2459396.74582 ± 0.00079 |
| | ASTEP | 128 | 2021-07-09 | $R$ | 2459405.18200 ± 0.02000 |
| | LCO SAAO | 129 | 2021-07-17 | Pan-STARRS $z_s$ | 2459413.67100 ± 0.00210 |
| | CHEOPS | 130 | 2021-07-26 | CHEOPS | 2459422.13420 ± 0.00100 |
| | LCO SAAO | 131 | 2021-08-03 | Pan-STARRS $z_s$ | 2459430.60180 ± 0.00160 |
| | LCO CTIO | 131 | 2021-08-04 | Pan-STARRS $z_s$ | 2459430.59180 ± 0.00300 |
| | LCO SSO | 132 | 2021-08-12 | Pan-STARRS $z_s$ | 2459439.06020 ± 0.00140 |
| | CHEOPS | 132 | 2021-08-12 | CHEOPS | 2459439.06360 ± 0.00210 |
| | LCO SSO | 134 | 2021-08-29 | Pan-STARRS $z_s$ | 2459455.99240 ± 0.00089 |
| | CHEOPS | 134 | 2021-08-29 | CHEOPS | 2459455.98950 ± 0.00070 |
| | CHEOPS | 135 | 2021-09-06 | CHEOPS | 2459464.45310 ± 0.00090 |
| | LCO SSO | 136 | 2021-09-15 | Pan-STARRS $z_s$ | 2459472.91850 ± 0.00088 |
| | LCO SAAO | 137 | 2021-09-23 | Pan-STARRS $z_s$ | 2459481.37450 ± 0.01100 |
| | LCO TO | 137 | 2021-09-23 | Pan-STARRS $z_s$ | 2459481.37890 ± 0.00340 |
| c | TESS | 1 | 2018-08-11 | TESS | 2458342.22333 ± 0.00093 |
| | TESS | 38 | 2020-07-09 | TESS | 2459040.00487 ± 0.00072 |
| | TESS | 39 | 2020-07-28 | TESS | 2459058.86571 ± 0.00066 |
| | LCO SAAO | 43 | 2020-10-11 | Pan-STARRS $z_s$ | 2459134.30000 ± 0.01600 |
| | CHEOPS | 59 | 2021-08-09 | CHEOPS | 2459436.03230 ± 0.00450 |
| | CHEOPS | 60 | 2021-08-28 | CHEOPS | 2459454.89880 ± 0.00380 |
| | LCO CTIO | 62 | 2021-10-04 | Pan-STARRS $z_s$ | 2459492.61030 ± 0.01800 |

**Notes.** These midpoint times, with the exception of those from CHEOPS (Szabó et al. 2021, 2022) and R-M observations (Martioli et al. 2020; Palle et al. 2020), were generated from EXOFASTv2 transit modeling.
[a] 955–2515 nm (SPIRou) and 2.18–2.47 nm (iSHELL).

(Figures A1 and A2), the output parameters (Tables A1, A2, A3, A4, A5, and A6), and the corner plots (Figures A4, A5, A6, A7, A8, and A9). For all inner d cases, the three-planet models reproduces the TTV super-period of AU Mic b in $O-C$ diagrams. The statistics criteria (e.g., $\chi^2_{\rm red}$ and AIC$_c$ values from Tables A1 through A6 versus those from Tables 12 and 13) indicate that these inner d cases are strongly favored over the two-planet cases. Notably, only $P_{\rm d} = 5.64$ days has AU Mic d being coplanar with the AU Mic system based on its inclination; the 5.86 and 6.47 days cases have the planet being moderately misaligned with the system, and the 5.08, 5.39, and 6.20 days cases have the planet being highly misaligned with the system.

The AMD criteria in Exo-Striker suggest that all inner d cases are unstable, so we investigate this further. We tested the stability of these three-planet cases over 2 Myr with the $N$-body simulator rebound and found that all of those configurations are stable (Figure A13). However, the 5.39 days case has all

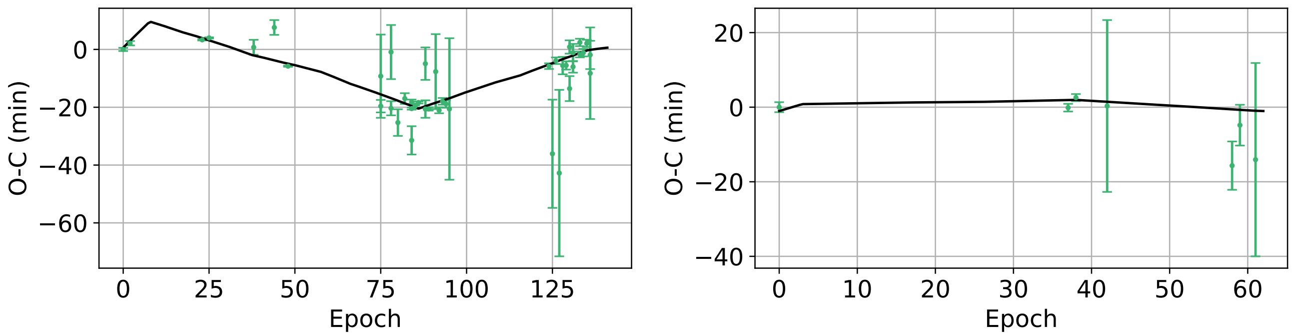


**Figure 4.** $O-C$ diagrams of AU Mic b (left) and AU Mic c (right), with comparison between TTVs (green) and `Exo-Striker`-generated MCMC models (black) for a two-planet high-eccentricity configuration.

**Table 12**
`Exo-Striker`-generated Best-fit and MCMC Modeling Parameters for Two-planet High-eccentricity Configuration

| Parameter | Unit | Best Fit | | MCMC | |
|---|---|---|---|---|---|
| | | AU Mic b | AU Mic c | AU Mic b | AU Mic c |
| $K$ | m s$^{-1}$ | 0.00543 | 0.05368 | 0.00385 ± 0.00114 | 0.06702 ± 0.01389 |
| $P_{orb}$ | day | 8.46302 | 18.85898 | 8.46401 ± 0.00097 | 18.85941 ± 0.00060 |
| $e$ | ... | 0.22188 | 0.51009 | 0.21098 ± 0.00952 | 0.51720 ± 0.00786 |
| $\omega$ | deg | 172.51565 | 150.13429 | 173.20702 ± 0.76278 | 149.73899 ± 0.35421 |
| $M_0$ | deg | 251.90049 | 13.83210 | 252.49015 ± 0.71508 | 13.42102 ± 0.35754 |
| $i$ | deg | 88.94778 | 86.96414 | 89.00381 ± 0.16286 | 88.15442 ± 1.22945 |
| $\Omega$ | deg | 154.51121 | 0.65309 | 155.13328 ± 0.77348 | 1.28668 ± 0.76259 |
| $\chi^2$ | ... | 182.65010 | 8.66743 | 187.17573 | 11.10833 |
| $\chi^2_{red}$ | ... | 6.37725 | 38.26351 | 6.60947 | 39.65681 |
| $\ln \mathcal{L}$ | ... | 176.17820 | | 176.09710 | |
| BIC | ... | -297.87092 | | -297.70872 | |
| AIC$_c$ | ... | -312.00346 | | -311.84126 | |

**Note.** The $K$'s listed here are unconstrained, but see Section 6 for discussion regarding the planets' low $K$'s generated by `Exo-Striker`.

three planets' orbits fluctuate toward high-eccentricity configuration, and these planets, especially AU Mic b and d, become highly misaligned for much of the 2 Myr timeline. The 5.86 days case's misalignment issue appears more pronounced, with all three planets becoming quickly misaligned with the system. Although the 5.64 days case has AU Mic d initially being coplanar, `rebound` has it become misaligned periodically. Lastly, the 6.47 days case has the planets exhibiting the most consistent coplanarity among the inner d cases.

#### *4.4.2. Planet d between b and c*

We repeat the steps described in the previous section for the middle d scenario. Based on AU Mic b's TTV super-period and assuming the near-2:3 orbital resonance pair between b and d, we explored the possibility that $P_d = 12.738$ days. Using this orbital period as a starting point, we obtained an initial best-fit model for the three-planet configuration (Figure 11 and Table 15). The $O-C$ diagram from Figure 11 also displays the super-period in AU Mic b's TTVs, and the statistics from Table 15 (e.g., $\chi^2_{red,b} = 5.92$, $\chi^2_{red,c} = 35.53$, and AIC$_c = -330.97$) demonstrate that this three-planet model yields a significantly better fit than the two-planet models.

Next, we utilize the TTV periodogram to probe a range of possible orbital periods for AU Mic d using the parameters from Table 15 as the starting point; we generated a set of 8001 orbital periods between 11 and 15 days with 0.0005 days interval in between. We adjusted d's initial inclination prior to each run and did two runs with different initial inclinations $i_d = (80°, 90°)$, respectively (Figure 12). From those runs, we came across four most favored periods based on their log-likelihood: 11.9 days ($\ln \mathcal{L} = 208.16$) and 14.1 days ($\ln \mathcal{L} = 201.45$) from the initial $i_d = 80°$ case, and 12.6 days ($\ln \mathcal{L} = 209.21$ and 205.70) and 12.7 days ($\ln \mathcal{L} = 211.25$ and 209.79) from both respective inclination cases.

We perform best-fit modeling and MCMC calculations for each of those four best middle d cases and generated the $O-C$ diagrams (Figures 14 and A3), the output parameters (Tables 18, A7, A8, and A9), and the corner plots (Figures 15, A10, A11, and A12). For all of those four cases, the three-planet models adequately account for the TTV super-period of AU Mic b in the $O-C$ diagrams, and the statistics criteria (e.g., $\chi^2_{red}$ and AIC$_c$ values from Tables 18 and A7 through A9 versus those from Tables 12 and 13) indicate that all three-planet middle d cases are strongly favored over the two-planet case. Curiously, planet d's inclination varies considerably among these four cases. For instance, the 12.6 and 12.7 days cases have planet d being relatively coplanar with the AU Mic system, while the 11.9 and 14.1 days cases have it being highly misaligned.

The AMD criteria in `Exo-Striker` suggest that these three-planet cases might be unstable. As before, we utilized `rebound` to test the stability of the three-planet cases; through this package, we found that each of these three-planet configurations is stable (Figures 16 and A13). Among the middle d cases, both the 12.6 and 12.7 days cases are the most consistent in maintaining the coplanarity of the planets.

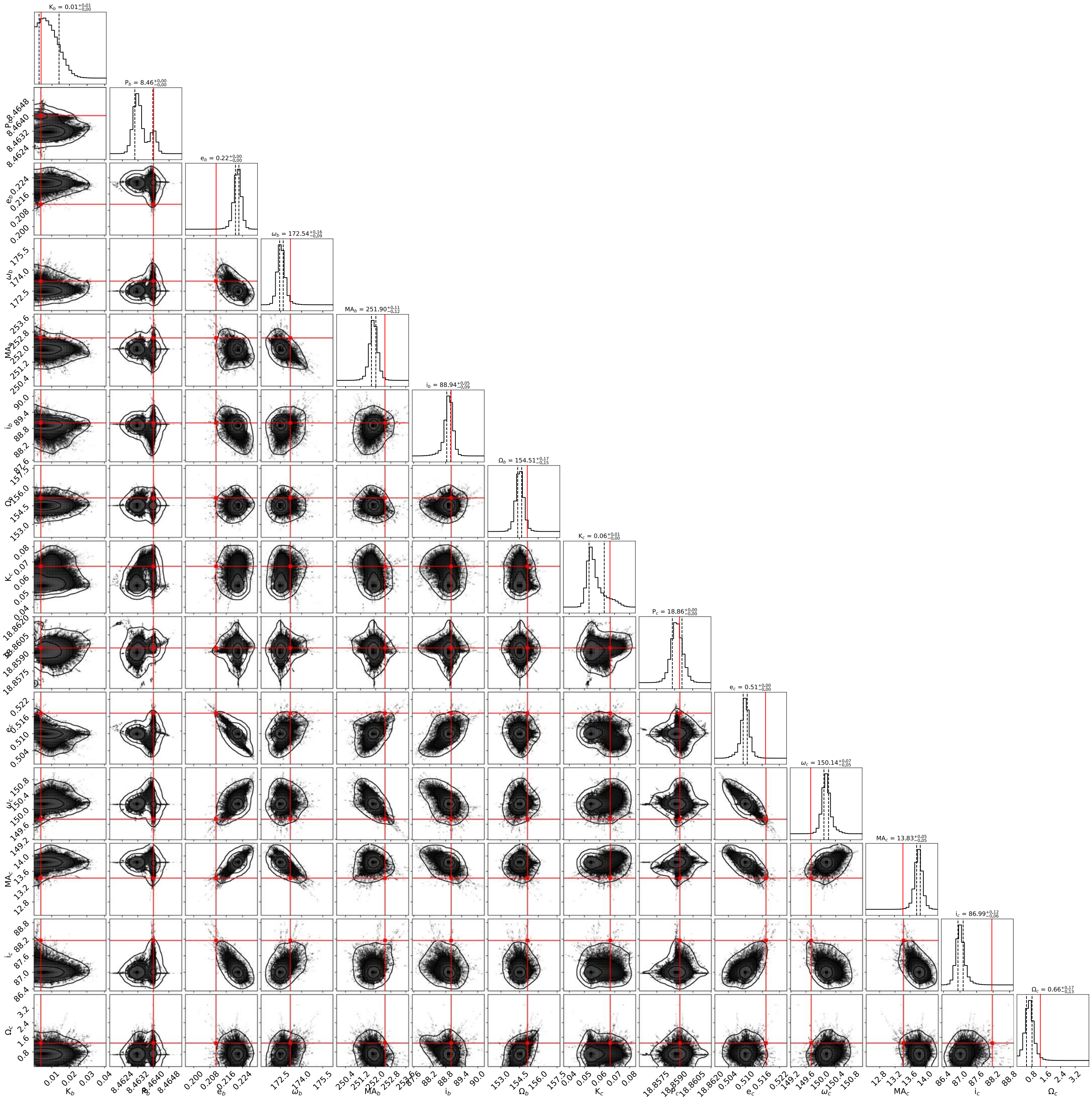

**Figure 5.** Corner plot of AU Mic b and c's orbital parameters from `Exo-Striker` MCMC analysis for a two-planet high-eccentricity configuration.

### *4.5. Transit Timing Variation Model Comparisons*

We perform a model comparison among both the two-planet and three-planet cases, as seen in Table 16. Based on the TTV model information criterion, the $P_\mathrm{d} = 12.7$ days configuration is the most favored overall, and the $P_\mathrm{d} = 6.47$ days configuration is the most favored among the inner d cases, followed closely by the 6.20 days and 5.86 days cases. All other configurations are not as well favored based on their corresponding Bayesian information criterion ($\Delta$BIC; Schwarz 1978; Wit et al. 2012) and $\Delta \mathrm{AIC}_c$, but they are not statistically ruled out. The two-planet cases' $\Delta$BIC and $\Delta \mathrm{AIC}_c$ are much larger, so both two-planet models can be rejected.

Next, we checked the robustness of the results by including only the high-precision TTVs, namely the TESS + Spitzer + SPIRou + CHEOPS joint modeling, and by performing the best-fit modeling and MCMC calculations, then we did a model comparison of the results (Table 17). This time, the 14.1 days case is the most favored overall, followed closely by the 12.7 days case; the 5.39 days case is the most favored among the inner d cases; and all other cases are disfavored but not statistically ruled out. Again, the two-planet cases are

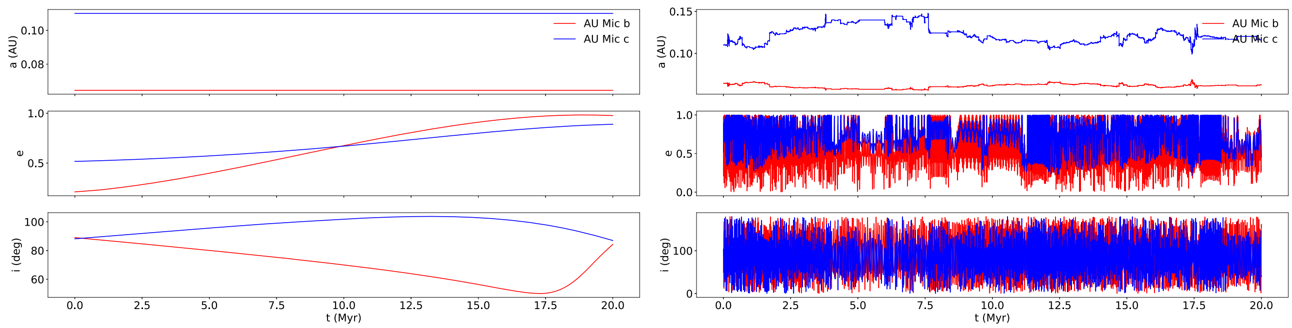


**Figure 6.** rebound models of the stability of the AU Mic system on a timescale of 20 Myr for a two-planet high-eccentricity configuration with original $K$'s from Table 12 (left) and with $K$'s from Cale et al. (2021) RV models (right), due to the original $K$'s being very small ($<$0.07 m s$^{-1}$). While the original $K$'s case appears to be stable, both planets' orbits become increasingly eccentric over time, and both planets would quickly become nontransiting due to their increasing orbital misalignment. The RV $K$'s case exhibits signs of chaos in the AU Mic system, with the planets undergoing orbital migrations but no orbital crossing, their eccentricities being extremely erratic throughout, rapidly oscillating between 0 and 1, and their highly fluctuating inclinations frequently placing both transiting planets in nontransiting configurations.

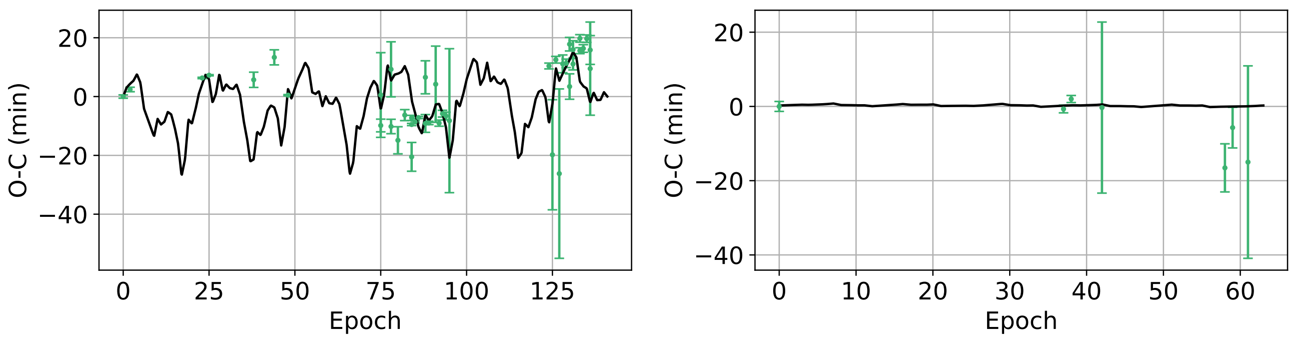


**Figure 7.** $O-C$ diagrams of AU Mic b (left) and AU Mic c (right), with comparison between TTVs (green) and Exo-Striker-generated MCMC models (black) for a two-planet low-eccentricity configuration.

**Table 13**
Exo-Striker-generated Best-fit and MCMC Modeling Parameters for Two-planet Low-eccentricity Configuration

| Parameter | Unit | Best Fit | | MCMC | |
|---|---|---|---|---|---|
| | | AU Mic b | AU Mic c | AU Mic b | AU Mic c |
| $K$ | m s$^{-1}$ | 2.25722 | 7.65452 | 0.42086 ± 0.13722 | 27.70929 ± 1.41812 |
| $P_{\rm orb}$ | day | 8.46265 | 18.86039 | 8.46026 ± 0.00011 | 18.85925 ± 0.00009 |
| $e$ | ... | 0.00000 | 0.00000 | 0.00723 ± 0.00510 | 0.12867 ± 0.00279 |
| $\omega$ | deg | 89.92745 | 229.20188 | 0.74540 ± 0.24389 | 212.29306 ± 0.04038 |
| $M_0$ | deg | 0.00049 | 354.88367 | 90.08325 ± 10.09994 | 359.95202 ± 0.75854 |
| $i$ | deg | 89.56579 | 89.43523 | 92.68980 ± 0.30871 | 85.98426 ± 0.23709 |
| $\Omega$ | deg | 0.00814 | 0.00004 | 160.82677 ± 82.66571 | 141.76084 ± 81.43847 |
| $\chi^2$ | ... | 4151.71376 | 11.59895 | 2259.05984 | 11.77892 |
| $\chi^2_{\rm red}$ | ... | 138.77709 | 832.66254 | 75.69463 | 454.16775 |
| $\ln \mathcal{L}$ | ... | -1808.30801 | | -963.74485 | |
| BIC | ... | 3671.10150 | | 1981.97518 | |
| AIC$_c$ | ... | 3656.96896 | | 1967.84264 | |

**Note.** The $K$'s listed here are unconstrained, but see Section 6 for discussion regarding planet b's low $K$'s generated by Exo-Striker.

statistically ruled out due to their significantly high ΔBIC and ΔAIC$_c$.

Taking into consideration both model comparisons, the 12.7 days, 14.1 days, 5.39 days, and 6.20 days cases are consistently favored while the 12.6 days, 11.9 days, 5.64 days, 5.08 days, and both two-planet cases are consistently disfavored relative to the other cases. The 5.86 and 6.47 days cases are inconsistent, with both being more relatively favored in the all-TTVs model comparison and much less so in the high-precision TTVs model comparison.

We did not explore randomly removing individual TTVs to evaluate the robustness of these results and the dependence of our results on particular TTV measurements. Our data set is notably heterogeneous, and some of the earlier observations, particularly the Spitzer transit times, are critical in determining the super-period because they sparsely fill in the TTV curve.

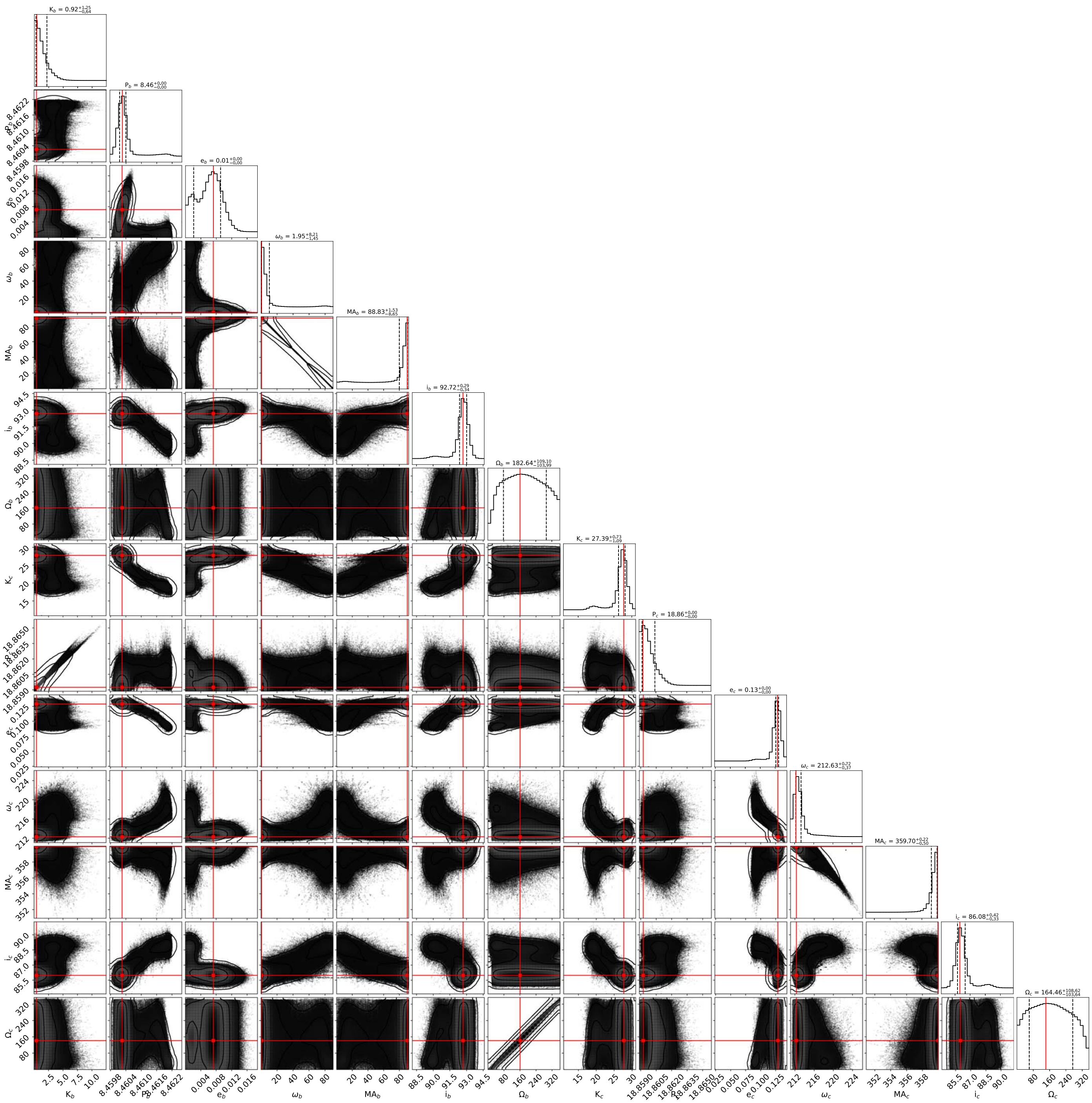

**Figure 8.** Corner plot of AU Mic b and c's orbital parameters from `Exo-Striker` MCMC analysis for a two-planet low-eccentricity configuration.

Thus, as would expected, our results are highly dependent on these space-based timing measurements. Conversely, for the 2021 season, we have much denser transit timing sampling, and thus our results will be less impacted by the removal of those data sets.

### *4.6. Stability Analysis of the Ten Cases*

With both two-planet cases statistically ruled out and therefore excluded (Tables 16 and 17), we proceeded to test the dynamical stability of the aforementioned ten three-planet configurations by utilizing the `SPOCK` packages `FeatureClassifier` and `NbodyRegressor` (Tamayo et al. 2020). The `FeatureClassifier`, hereafter referred to as `SPOCK`, is a trained model estimating the stability probability after $10^9$ orbits of the innermost planet (for AU Mic d in the inner d scenario, 13.9 Myr for 5.08 days, 14.8 Myr for 5.39 days, 15.4 Myr for 5.64 days, 16.0 Myr for 5.86 days, 17.0 Myr for 6.20 days, and 17.7 Myr for 6.47 days; for AU Mic b in the middle d scenario, 23.2 Myr, which is comparable to the age of the system). Subsequently, we weight the parameters by their stability probability to sort out or give weaker weight to unstable systems that would likely have already destroyed themselves over time.

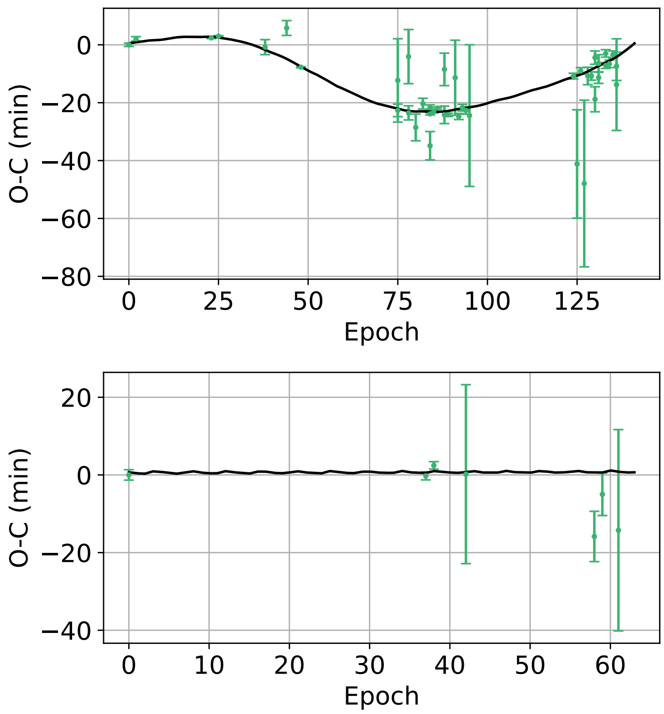


**Figure 9.** Initial three-planet (with d interior to b) best-fit $O-C$ diagrams of AU Mic b (top) and AU Mic c (bottom), with comparison between TTVs (green) and `Exo-Striker`-generated MCMC models (black).

**Table 14**
`Exo-Striker`-generated Initial Three-planet (with d Interior to b) Best-fit Modeling Parameters

| Parameter | Unit | AU Mic b | AU Mic c | AU Mic d |
|---|---|---|---|---|
| $K$ | m s$^{-1}$ | 5.03491 | 0.51952 | 0.34401 |
| $P_{\rm orb}$ | day | 8.46334 | 18.86226 | 5.63749 |
| $e$ | ... | 0.00000 | 0.00459 | 0.00019 |
| $\omega$ | deg | 98.48619 | 223.69811 | 167.66115 |
| $M_0$ | deg | 351.49848 | 0.00066 | 239.37339 |
| $i$ | deg | 89.57446 | 89.43918 | 87.32379 |
| $\Omega$ | deg | 30.38207 | 31.22049 | 9.19867 |
| $\chi^2$ | ... | 113.87171 | 11.06507 | ... |
| $\chi^2_{\rm red}$ | ... | 5.20570 | 31.23419 | ... |
| $\ln \mathcal{L}$ | ... | | 209.62069 | |
| BIC | ... | | -337.51315 | |
| AIC$_c$ | ... | | -343.01916 | |

**Note.** The $K$'s listed here are unconstrained, but see Section 6 for discussion regarding the planets' low $K$'s generated by `Exo-Striker`.

The `NbodyRegressor`, hereafter referred to as `Nbody`, performs an `Nbody` simulation and checks a system for stability after an arbitrarily chosen number of orbits of the innermost planet. Due to the high numerical cost of an `Nbody` simulation over a large number of orbits, we chose a simulation period of $2 \times 10^5$ orbits for this part of the analysis (for AU Mic d in the inner d scenario, 2.78 kyr for 5.08 days, 2.95 kyr for 5.39 days, 3.09 kyr for 5.64 days, 3.21 kyr for 5.86 days, 3.40 kyr for 6.20 days, and 3.54 kyr for 6.47 days; for AU Mic b in the middle d scenario, 4.63 kyr). We utilized `Nbody` for two purposes: To notice any deviations that may arise between `SPOCK` and `Nbody` results, and to validate the results from `SPOCK`. `SPOCK` was trained with planetary configurations showing mutual inclinations $\lesssim 10°$. Since higher values for the

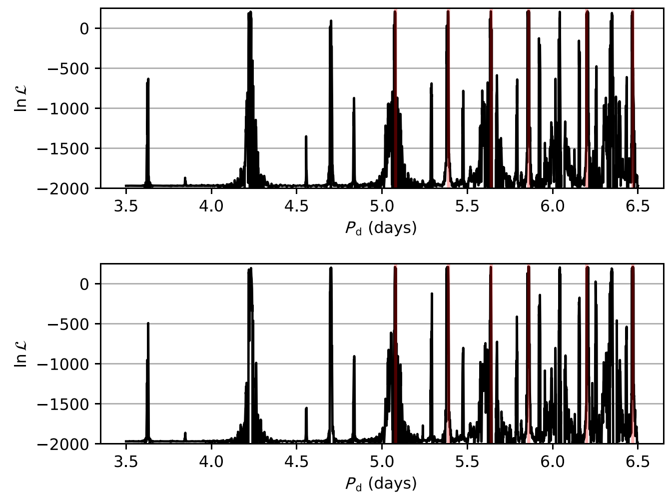


**Figure 10.** TTV log-likelihood periodograms of AU Mic d's orbital period using the parameters from Table 14 as the starting point and initial inclinations $i_d = 85°$ (top) and 90° (bottom). We obtained the six most favored inner d periods based on their log-likelihood: 5.08 days ($\ln \mathcal{L} = 208.22$ and 208.84), 5.39 days ($\ln \mathcal{L} = 209.99$ and 209.80), 5.64 days ($\ln \mathcal{L} = 209.65$ and 209.62), 5.86 days ($\ln \mathcal{L} = 214.36$ and 214.33), 6.20 days ($\ln \mathcal{L} = 209.95$ and 208.43), and 6.47 days ($\ln \mathcal{L} = 207.76$ and 211.40) from both respective inclination cases. The red lines denote those periods corresponding to best-fitting peaks in the periodograms.

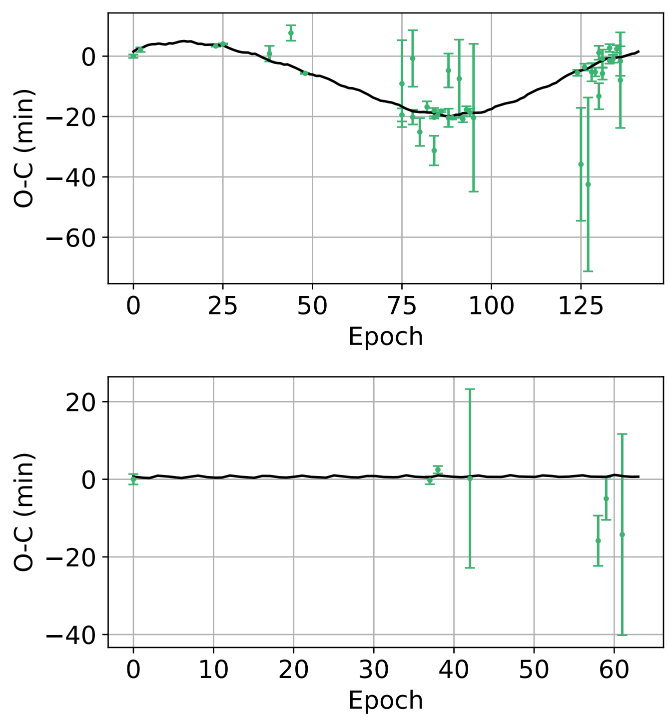


**Figure 11.** Initial three-planet (with d between b and c) best-fit $O-C$ diagrams of AU Mic b (top) and AU Mic c (bottom), with comparison between TTVs (green) and `Exo-Striker`-generated MCMC models (black).

mutual inclinations can be found for the cases of 5.08 days, 5.39 days, 6.20 days, and 14.1 days, we considered it useful to use additional analysis methods for comparison. At this point, however, it is important to note that differences and similarities between the results of `SPOCK` and `Nbody` can only serve as an indication and not a proof of `SPOCK`'s reliability, since the time period after which a system is tested for stability differs significantly. A system that becomes unstable after $10^6$ orbits

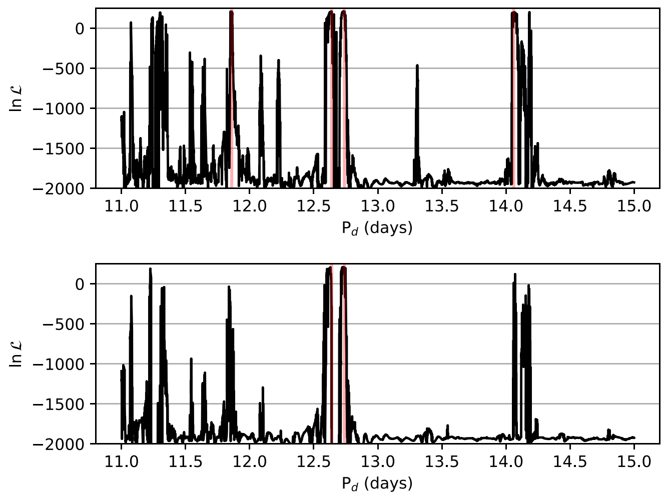


**Figure 12.** TTV periodograms of AU Mic d's orbital period using the parameters from Table 15 as the starting point and initial inclinations $i_d = 80°$ (top) and 90° (bottom). We obtained the four most favored periods based on their log-likelihood: 11.9 days ($\ln \mathcal{L} = 208.16$) and 14.1 days ($\ln \mathcal{L} = 201.45$) from the initial $i_d = 80°$ case, and 12.6 days ($\ln \mathcal{L} = 209.21$ and 205.70) and 12.7 days ($\ln \mathcal{L} = 211.25$ and 209.79) from both respective inclination cases. The red lines denote those days corresponding to best-fitting peaks in the periodograms.

**Table 15**
Exo-Striker-generated Initial Three-planet (with d Between b and c) Best-fit Modeling Parameters

| Parameter | Unit | Best Fit | | |
|---|---|---|---|---|
| | | AU Mic b | AU Mic c | AU Mic d |
| $K$ | m s$^{-1}$ | 4.85810 | 1.49734 | 0.16823 |
| $P_{\rm orb}$ | day | 8.46325 | 18.86214 | 12.73040 |
| $e$ | ... | 0.00704 | 0.00136 | 0.00283 |
| $\omega$ | deg | 89.95582 | 223.96004 | 166.18027 |
| $M_0$ | deg | 0.00002 | 0.00018 | 0.00017 |
| $i$ | deg | 89.39532 | 89.41147 | 81.08949 |
| $\Omega$ | deg | 0.00002 | 0.00000 | 0.00000 |
| $\chi^2$ | ... | 131.05680 | 11.06507 | ... |
| $\chi^2_{\rm red}$ | ... | 5.92174 | 35.53047 | ... |
| $\ln \mathcal{L}$ | ... | | 203.59374 | |
| BIC | ... | | -325.45925 | |
| AIC$_c$ | ... | | −330.96526 | |

**Note.** The $K$'s listed here are unconstrained, but see Section 6 for discussion regarding the planets' low $K$'s generated by Exo-Striker.

will be classified as stable by Nbody in our case, although SPOCK will probably assign a low probability of stability to the system. Nevertheless, we think it is useful to use Nbody as a comparison to notice significant differences and to look at the stability of the system over different timescales.

We also utilized MEGNO (mean exponential growth factor of nearby orbits; Cincotta & Simó 2000; Cincotta et al. 2003), which is a fast indicator for chaotic orbits, for our orbital simulations. MEGNO can be used similarly to SPOCK to estimate the orbital stability of planetary systems, as done by Tamayo et al. (2020), although it is pointed out that a direct comparison is only possible to a limited extent (see Section 1. D. in Tamayo et al. 2020). Since SPOCK uses MEGNO as one of ten features for internal analysis, we consider a comparison of results useful in this case as well. However, also in this case it is important to emphasize that discrepancies between SPOCK and MEGNO can only be an indication of inconsistencies of the SPOCK results, since orbital stability and regularity of orbits cannot be used synonymously.

We incorporated the stellar parameters from Table 10 and the planetary parameters from Exo-Striker-generated posteriors (Tables 18 and A1 thru A9). We generated 20,000 random configurations for each of the 10 cases, drawn from the respective Gaussian distributions of the planetary parameters. Next, a simulation object is created from rebound, to which all planetary parameters and the mass of the star of a certain random configuration are passed on. Then, this simulation object is examined through SPOCK for the stability probability after $10^9$ orbits of the innermost planet. The same parameters were also used to estimate the stability of the system after $2 \times 10^5$ orbits using Nbody. SPOCK determines ten features for the classification of planetary systems, based on which it estimates the stability probability. Since MEGNO is one of them, it can be directly output by SPOCK and used for our analysis. Thus, all three analysis methods use the same orbital parameters and masses.

In Figure 13, the semimajor axis of AU Mic d was then plotted in a histogram for each of these configurations. Since the same number of random configurations was generated for each parameter set, the result is a mixture distribution in which the respective underlying distributions have the same weighting. The values are then weighted with the stability probability in the histogram, resulting in the overlapping histogram for SPOCK, MEGNO, and Nbody. Each histogram thus contains 200,000 values each with and without weighting by the stability probability. Unlike SPOCK, Nbody and MEGNO do not provide continuously distributed stability probabilities. Nbody provides binary stability probabilities, weighting a stable system by 1 and an unstable system by 0. For MEGNO, however, we had to set a limit above which we classify a system as unstable for comparison with the other methods. To reduce the number of systems incorrectly classified as unstable, we use the difference of the mean, $\mu_{\rm MEGNO}$, and the standard deviation, $\sigma_{\rm MEGNO}$, of the MEGNO, which can also be output by SPOCK, for the estimation of the orbital stability. If $\mu_{\rm MEGNO} - \sigma_{\rm MEGNO} > 2.1$, the system is considered as chaotic and thus unstable and receives weight 0. On the other hand, if the value is smaller, we consider the system stable and it receives weight 1. At this point, it should be emphasized once again that a chaotic system does not necessarily have to lead to instability in the near future.

Figure 13 displays the results from these aforementioned runs. The SPOCK results appear to deviate from the MEGNO and Nbody results for the inner planet d cases, while all three results appear to be consistent for the middle planet d case. For the inner d scenario, the 5.64 days case appears to be the most preferred, although the SPOCK results peak closer to the 5.86 days case. For the middle d scenario, both the 12.6 and 12.7 days cases are clearly preferred over the 11.9 and 14.1 days cases from all three results. Comparisons between the inner d orbits and the middle d orbits should be viewed with caution because of the different simulation durations due to the different innermost orbit. MEGNO and, in particular, Nbody show hardly any visible trends. One reason for the differences between SPOCK and the other methods could be that the training sample was not matched by each parameter set. However, it is more likely that the differences are due to the different number of orbits considered.

**Table 16**
TTV Model Information Criterion for the AU Mic System

| Type | $P_d$ (days) | Relative $\chi^2_{red}$ | $\Delta \ln \mathcal{L}$ | $\Delta$BIC | $\Delta$AIC$_c$ |
|---|---|---|---|---|---|
| MCMC | 12.7 | 3.95967 | 0.00000 | 0.00000 | 0.00000 |
| | 6.47 | 3.99117 | 1.56595 | 3.13190 | 3.13190 |
| | 6.20 | 3.92884 | 1.67726 | 3.35452 | 3.35452 |
| | 5.86 | 4.08053 | 1.75398 | 3.50796 | 3.50796 |
| | 14.1 | 4.12141 | 2.37983 | 4.75966 | 4.75966 |
| | 5.39 | 4.14006 | 2.78037 | 5.56074 | 5.56074 |
| | 12.6 | 4.33368 | 5.83824 | 11.67648 | 11.67648 |
| | 11.9 | 4.44417 | 7.12662 | 14.25324 | 14.25324 |
| | 5.08 | 4.45799 | 8.78461 | 17.56922 | 17.56922 |
| | 5.64 | 4.55658 | 9.62125 | 19.24250 | 19.24250 |
| | no d (high e) | 5.66526 | 52.65304 | 78.06333 | 69.43680 |
| | no d (low e) | 64.88111 | 1192.49499 | 2357.74723 | 2349.12070 |
| Best Fit | 12.7 | 4.05575 | 0.00000 | 0.00000 | 0.00000 |
| | 5.86 | 4.08923 | 0.56826 | 1.13652 | 1.13652 |
| | 6.20 | 4.25992 | 2.95667 | 5.91334 | 5.91334 |
| | 14.1 | 4.28073 | 3.27556 | 6.55112 | 6.55112 |
| | 5.39 | 4.30368 | 3.52700 | 7.05400 | 7.05400 |
| | 6.47 | 4.30787 | 3.53291 | 7.06582 | 7.06582 |
| | 12.6 | 4.36285 | 4.37647 | 8.75294 | 8.75294 |
| | 11.9 | 4.43253 | 5.40495 | 10.80990 | 10.80990 |
| | 5.64 | 4.46849 | 5.87727 | 11.75454 | 11.75454 |
| | 5.08 | 4.47444 | 5.94329 | 11.88658 | 11.88658 |
| | no d (high e) | 5.46622 | 39.22908 | 51.21541 | 42.58888 |
| | no d (low e) | 118.95179 | 2023.71529 | 4020.18783 | 4011.56130 |

**Note.** The numbers of degrees of freedom used to calculate the relative $\chi^2_{red}$ are $N_{dof} = 14$ for a two-planet model and $N_{dof} = 21$ for a three-planet model.

**Table 17**
High-precision (TESS + Spitzer + SPIRou + CHEOPS) TTV Model Information Criterion for the AU Mic System

| Type | $P_d$ (days) | Relative $\chi^2_{red}$ | $\Delta \ln \mathcal{L}$ | $\Delta$BIC | $\Delta$AIC$_c$ |
|---|---|---|---|---|---|
| MCMC | 14.1 | 10.24154 | 0.00000 | 0.00000 | 0.00000 |
| | 12.7 | 10.88606 | 1.42079 | 2.84158 | 2.84158 |
| | 5.39 | 11.96840 | 2.76171 | 5.52342 | 5.52342 |
| | 6.20 | 12.10677 | 3.84762 | 7.69524 | 7.69524 |
| | 5.86 | 14.15778 | 6.27514 | 12.55028 | 12.55028 |
| | 12.6 | 14.71546 | 7.24787 | 14.49574 | 14.49574 |
| | 6.47 | 14.72007 | 7.58335 | 15.16670 | 15.16670 |
| | 11.9 | 16.53061 | 9.83512 | 19.67024 | 19.67024 |
| | 5.08 | 16.89976 | 11.34680 | 22.69360 | 22.69360 |
| | 5.64 | 17.35204 | 12.42087 | 24.84174 | 24.84174 |
| | No d (high e) | 13.55832 | 40.32199 | 59.33232 | 1060.64398 |
| | No d (low e) | 164.49125 | 601.87497 | 1182.43828 | 2183.74994 |
| Best Fit | 12.7 | 10.96391 | 0.00000 | 0.00000 | 0.00000 |
| | 14.1 | 11.56410 | 0.83980 | 1.67960 | 1.67960 |
| | 6.20 | 13.89642 | 4.46176 | 8.92352 | 8.92352 |
| | 5.39 | 13.94522 | 4.50562 | 9.01124 | 9.01124 |
| | 5.86 | 14.65509 | 5.64192 | 11.28384 | 11.28384 |
| | 12.6 | 14.77799 | 5.72267 | 11.44534 | 11.44534 |
| | 6.47 | 15.66435 | 7.16597 | 14.33194 | 14.33194 |
| | 11.9 | 16.41644 | 8.26575 | 16.53150 | 16.53150 |
| | 5.08 | 16.54831 | 8.46338 | 16.92676 | 16.92676 |
| | 5.64 | 16.68665 | 8.69418 | 17.38836 | 17.38836 |
| | No d (high e) | 14.39713 | 34.30994 | 47.30822 | 1048.61988 |
| | No d (low e) | 312.57388 | 1077.13307 | 2132.95448 | 3134.26614 |

**Notes.** The numbers of degrees of freedom used to calculate the relative $\chi^2_{red}$ are $N_{dof} = 14$ for a two-planet model and $N_{dof} = 18$ for a three-planet model. $N_{dof} = 18$ is used instead of 21 due to there being 21 data observations in this high-precision model comparison.

To check whether this is indeed the case, we ran 100 `Nbody` simulations over $10^7$ orbits for each of the ten parameter sets. This is still two orders of magnitude smaller than the $10^9$ orbits according to which `SPOCK` estimates the stability probability, but a smaller value was chosen because of the numerical effort. In fact, after $10^7$ orbits, the systems tended to become unstable more often. The clearest difference occurred in the 5.39 days case. While 85% of the generated configurations were still

**Table 18**
Exo-Striker-generated Best-fit and MCMC Modeling Parameters for $P_d = 12.7$ Days

| Parameter | Unit | Best Fit | | | MCMC | | |
|---|---|---|---|---|---|---|---|
| | | AU Mic b | AU Mic c | AU Mic d | AU Mic b | AU Mic c | AU Mic d |
| $K$ | m s$^{-1}$ | 1.65668 | 0.45119 | 0.30658 | $0.31290 \pm 0.26983$ | $0.18450 \pm 0.07362$ | $0.45150 \pm 0.21874$ |
| $P_{orb}$ | day | 8.46318 | 18.86027 | 12.73174 | $8.46308 \pm 0.00006$ | $18.85969 \pm 0.00008$ | $12.73596 \pm 0.00793$ |
| $e$ | ... | 0.01013 | 0.00000 | 0.00339 | $0.00577 \pm 0.00101$ | $0.00338 \pm 0.00164$ | $0.00305 \pm 0.00104$ |
| $\omega$ | deg | 89.99210 | 224.07980 | 160.53522 | $88.43038 \pm 0.05783$ | $223.28438 \pm 1.68357$ | $160.78945 \pm 2.59947$ |
| $M_0$ | deg | 0.00003 | 0.00003 | 0.00013 | $1.58566 \pm 1.46718$ | $0.51338 \pm 0.41839$ | $2.11220 \pm 1.97561$ |
| $i$ | deg | 89.57141 | 89.42889 | 89.53818 | $89.57917 \pm 0.37639$ | $89.22655 \pm 0.21654$ | $89.31812 \pm 1.15800$ |
| $\Omega$ | deg | 0.00015 | 0.00000 | 0.00000 | $0.31487 \pm 0.15366$ | $2.29724 \pm 2.17643$ | $0.39499 \pm 0.27136$ |
| $\chi^2$ | ... | 109.75800 | 3.80307 | ... | 106.33254 | 4.53826 | ... |
| $\chi^2_{red}$ | ... | 4.73171 | 28.39027 | ... | 4.61962 | 27.71770 | ... |
| $\ln \mathcal{L}$ | ... | | 215.40728 | | | 228.75014 | |
| BIC | ... | | -349.08633 | | | -375.77205 | |
| AIC$_c$ | ... | | -354.59234 | | | -381.27806 | |

**Note.** The $K$'s listed here are unconstrained, but see Section 6 for discussion regarding the planets' low $K$'s generated by Exo-Striker.

stable after $2 \times 10^5$ orbits, only 37% were stable after $10^7$ orbits. For the 6.47 days case and the 14.1 days case, the number of stable configurations fell by about 9% from 97% to 88% and from 100% to 91%, respectively. For the other cases, only minor effects or, in some cases, no effects at all were observed. However, the results are still consistent with SPOCK, since the 5.39 days case and the 6.47 days case are clearly disfavored here as well. For this reason, we assume that the SPOCK results provide a sound basis for assessing probable parameters for AU Mic d.

To make sure that the configurations' evolving instabilities over the larger timescale match the SPOCK results, we analyzed the fraction of equally classified configurations by SPOCK and Nbody. As SPOCK provides a stability probability instead of a binary stability classification, we have to set a limit above which all configurations are classified as stable in order to be able to compare the results with Nbody and MEGNO. For a first approach, we set this limit to 0.34 because Tamayo et al. (2020) used this limit to analyze the reliability of SPOCK as well. As Tamayo et al. (2021) remark that the chosen limit can influence the false-positive rate, we additionally try the limits 0.2 and 0.5 to make sure that differences in the results are not due to the selected threshold. Therefore, each configuration exceeding a stability probability of 0.34 is classified as stable, and each configuration below this limit is classified as unstable. It is important to mention that this limit is only necessary to directly compare SPOCK with Nbody and MEGNO. To weight the values in the histogram, the stability probabilities are used without a certain stability limit.

Due to the difference in the number of orbits after which the stability probability is predicted ($10^9$ for SPOCK and $2 \times 10^5$ and $10^7$ for Nbody), we cannot consider the fraction of different classified configurations as the false-positive or false-negative rate, respectively. Nevertheless, we expect that the number of equally classified configurations should increase for the $10^7$ run as the time span in which instabilities can occur grows. For most parameter sets the fraction of different classified systems is clearly below 10% for both the $2 \times 10^5$ and the $10^7$ runs. Nevertheless, the cases of 5.39 days, 6.20 days, 6.47 days, and 14.1 days are exceptions and show stronger deviating results. For 6.47 days and 14.1 days, the fraction of different classified systems decreased from 13% and 12% to 7% and 5%. For these cases, the number of considered orbits seems to be the main reason for the differences in the $2 \times 10^5$ run, and we assume that the Nbody results will approach closer to SPOCK for a longer Nbody run. However, the cases of 6.20 days and 5.39 days show a different behavior: Both parameter sets show large discrepancies for the $2 \times 10^5$ Nbody run (41% for 6.20 days and 46% for 5.39 days). Despite the decrease from 41% to 37% for the 6.20 day case, the fraction of different classified systems is still much larger than for the other parameter sets. For the 5.39 days case, the rate even increases from 46% to 53%, which corresponds to an almost random classification. To check whether the choice of the stability limit causes this effect, we compared the results again for a stability limit of 0.2 and 0.5 for SPOCK. For both limits, the fraction of differently classified configurations was about 50%. Although we cannot exclude the possibility that the parameter set develops instabilities on larger timescales, we would like to mention that both the 5.39 days case as well as the 6.20 days case belong to the sets for which the mutual inclinations do not match the SPOCK training sample. So, it is quite possible that this could be the reason for the deviations.

However, the behavior of MEGNO is particularly striking here. In the comparison with Nbody after $10^7$ orbits, the proportion of differently classified systems for the case of 5.39 days was 64%. For the 6.20 days case the proportion is about 19%. Since SPOCK uses, among other features, MEGNO to estimate the stability of planetary configurations, this could be a decisive factor for the deviations. Nevertheless, for most of the parameter sets there is a very good agreement between SPOCK and Nbody, and even for the case of 5.39 days the trend indicates a higher number of unstable systems after a high number of orbits for both methods. This suggests that the trend shown by the SPOCK histogram may well be used as an indication of the stability of the system to at least partly limit the parameter space.

### *4.7. Most Favored Configuration for AU Mic d*

Based on the calculated super-period (Section 4.1), the TTV model comparisons (Section 4.5), and the stability test (Section 4.6), the 12.7 days configuration is the most favored model and thus is presented in this section (Figures 14, 15, and 16, and Table 18), while the other TTV cases are presented in the Appendix. More discussions regarding the results can be found in Section 6.

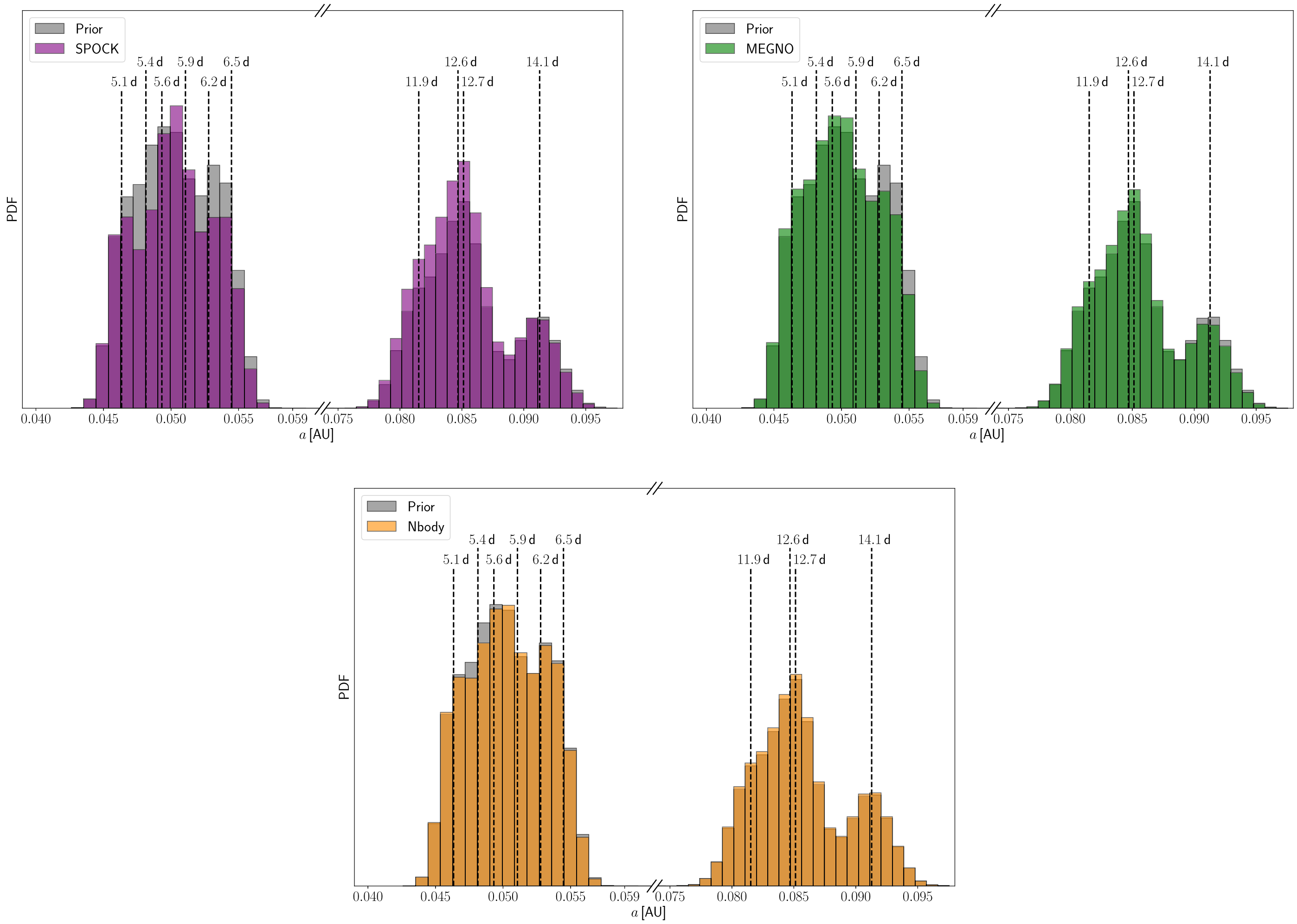


**Figure 13.** Histograms of the semimajor axis of AU Mic d with `SPOCK` (top left), `MEGNO` (top right), and `Nbody` (bottom), each marked with the corresponding orbital periods of AU Mic d. `SPOCK` and `Nbody` estimates the stability probability after $10^9$ and $2 \times 10^5$ orbits, respectively, of the innermost planet, while `MEGNO` is a fast indicator for chaotic orbits. For each parameter set, 20,000 random configurations of masses and orbital parameters were generated following the respective Gaussian distributions of planetary parameters from `Exo-Striker`; each of these random configurations was given its own stability probability by `SPOCK`, and the semimajor axis of AU Mic d is then plotted in the histogram for each of these configurations. Since the same number of random configurations was generated for each parameter set, the result is a mixture distribution in which the respective underlying distributions have the same weighting. The values were then weighted with the stability probability in the histogram, resulting in the overlapping histogram for `SPOCK`, `MEGNO`, and `Nbody`. Thus, each histogram contains 200,000 values. `Nbody` uses the same aforementioned simulation object generated by `rebound` to perform `Nbody` simulations and outputs either 0 (unstable) or 1 (stable); these outputs are then used for weighting. `Nbody` is more accurate than `SPOCK` but is much more computationally intensive over a large simulation time, so both the 200,000-orbit integrations were performed and the pretrained classifier was used. The `MEGNO` value threshold is set to 2.1, so any configurations that lead to their `MEGNO` value exceeding this threshold are considered unstable and given a weight of 0 while all other configurations that are considered stable are given a weight of 1. By weighting with the `SPOCK` or `MEGNO` outputs, the 5.64 days case appears to be favored over other inner d cases, and both 12.6 and 12.7 days appear to be preferred among the middle d cases.

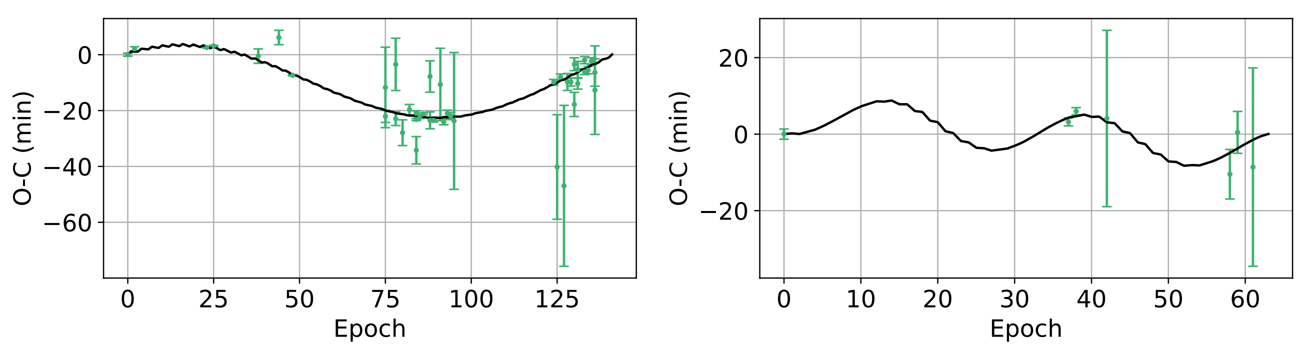


**Figure 14.** $O-C$ diagrams of AU Mic b (left) and AU Mic c (right), with comparison between TTVs (green) and `Exo-Striker`-generated MCMC models (black) for $P_{\rm d} = 12.7$ days.

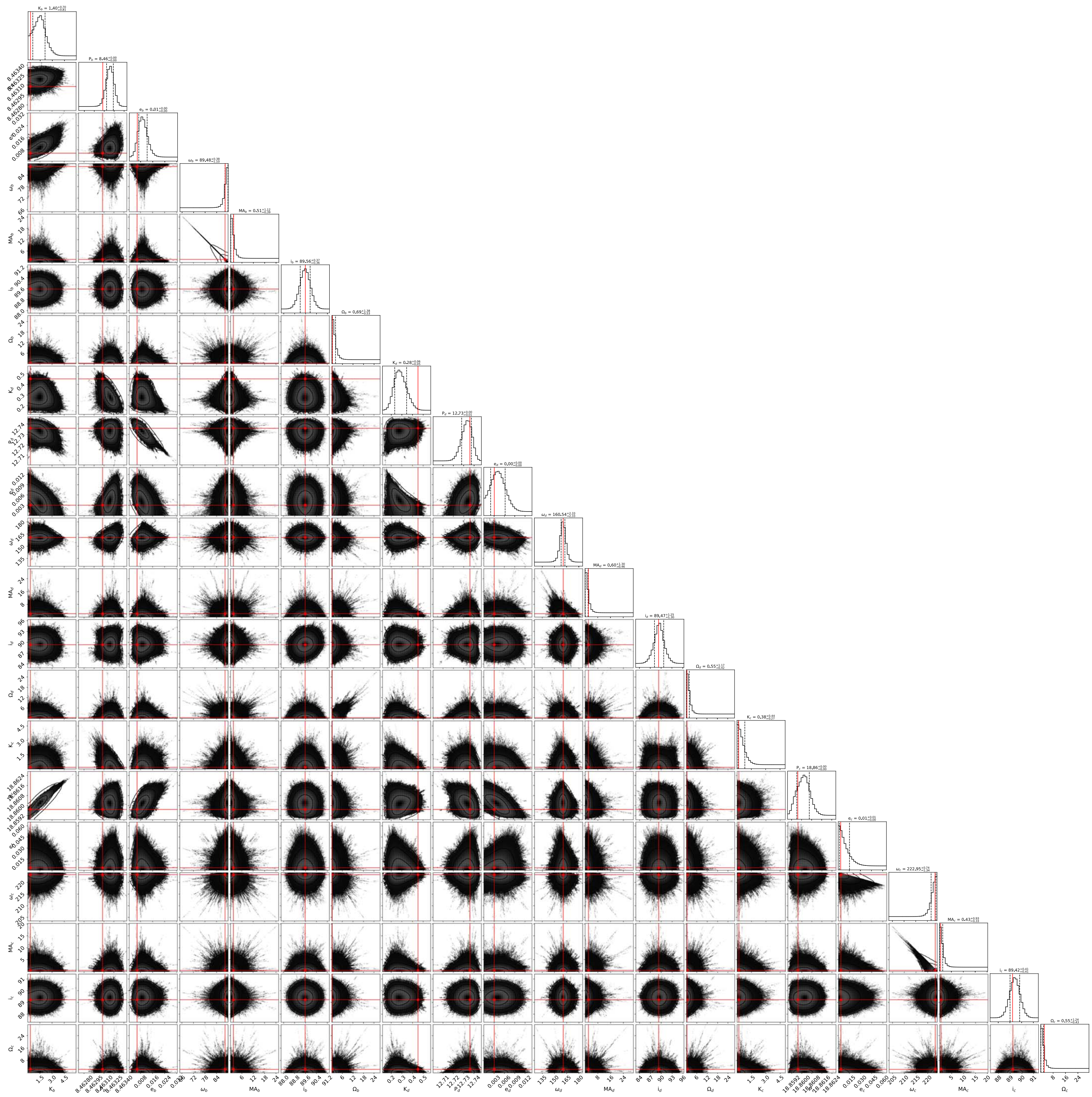

**Figure 15.** Corner plot of AU Mic b and c's orbital parameters from Exo-Striker MCMC analysis for $P_{\mathrm{d}} = 12.7$ days.

## 5. Radial Velocity Vetting of Transit Timing Variation Analysis

Cale et al. (2021) modeled the RVs of the AU Mic system and searched for additional candidate nontransiting planet signals. Their RV models indicated a candidate RV signal between the orbits of AU Mic b and c with an orbital period of 12.742 days but were ruled inconclusive.

We repeat the analysis of Cale et al. (2021) with the addition of the SERVAL-generated (Zechmeister et al. 2018) High Accuracy Radial Velocity Planet Searcher (HARPS) RVs from Zicher et al. (2022) to see if the RVs exhibit consistent behavior with the TTVs. We compute two generalized Lomb–Scargle (GLS) periodograms, one without HARPS RV data and another with HARPS data included (Figure 17). The planet d's signal was present in the periodogram without HARPS data; however, after adding HARPS data to the GLS periodogram, the signal vanishes. We also note the 16 days peak in the bottom row of the periodogram is not credible in terms of orbital dynamics stability.

We compute an $\ln \mathcal{L}$ brute-force periodogram (Figure 18) over a range of possible periods for AU Mic d. We do not see any clearly identified peaks consistent with d's periods derived from the TTVs, but there is additional power in the periodogram, particularly near 12.75 (which is the exact 2:3

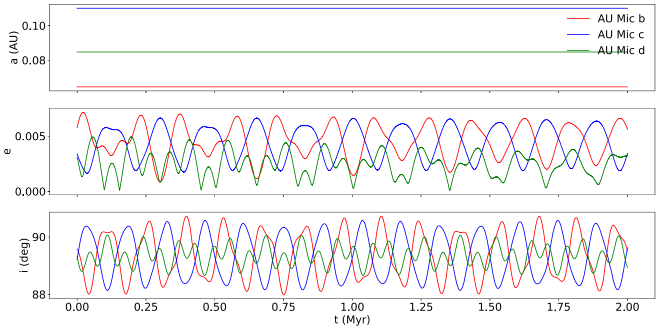


**Figure 16.** `rebound` model of the stability of the AU Mic system on a timescale of 2 Myr for $P_d = 12.7$ days.

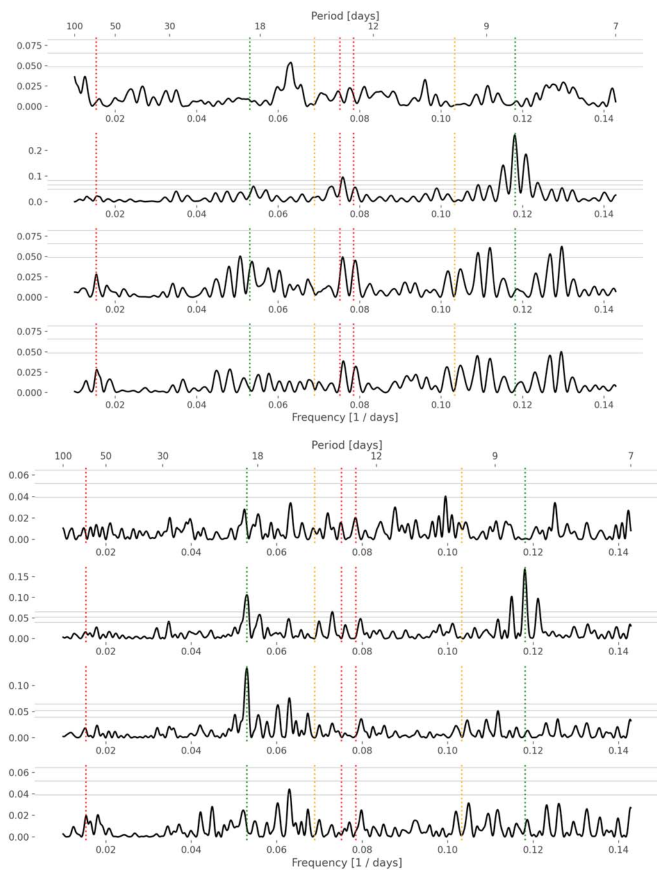


**Figure 17.** GLS periodograms of the AU Mic system. Top four panels: GLS generated without HARPS data. Bottom four panels: GLS generated with HARPS data. From top to bottom: zero-point corrected, activity corrected, planet b corrected, planet c corrected. The dotted vertical lines, from right to left, are $P_b$, $2^*P_{rot}$, $P_d = 12.74$ days, $P_d = 13.31$ days, $3^*P_{rot}$, $P_c$, $P_{candidate} = 65.22$ days. AU Mic d's signal vanishes when HARPS data are added to the GLS periodogram. Also, the 16 days peak in the bottom row of the periodogram is not credible in term of orbital dynamics stability.

orbital resonance and our TTV period) and 13.3 days, indicating our RV model is incomplete and, therefore, our RV analysis is inconclusive in confirming AU Mic d. The 22 days peak would not be dynamically stable, and there is the possibility of a 65 days planetary candidate in the RVs.

We explore the RV model comparison for ten different periods of AU Mic d (Table 19). The three-planet configuration is favored relative to the two-planet configuration for 6.20 days ($\Delta\mathrm{AIC}_c = 104.83$), 5.39 days ($\Delta\mathrm{AIC}_c = 48.64$), 5.64 days ($\Delta\mathrm{AIC}_c = 36.77$), 12.7 days ($\Delta\mathrm{AIC}_c = 23.63$), 6.47 days

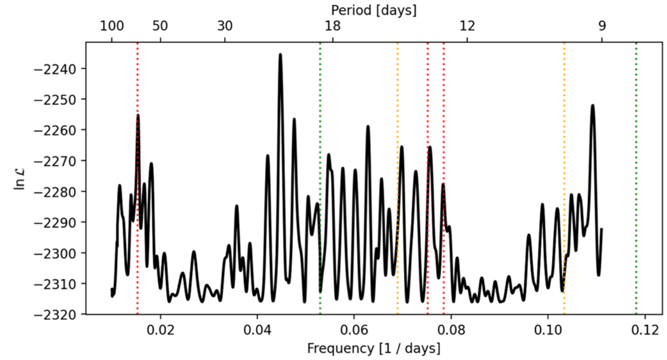


**Figure 18.** ln $\mathcal{L}$ brute-force periodogram of AU Mic's RVs, including models for both AU Mic b and c. AU Mic d's $T_C$ was allowed to vary. The dotted vertical lines, from right to left, are $P_b$, $2^*P_{rot}$, $P_d = 12.74$ days, $P_d = 13.31$ days, $3^*P_{rot}$, $P_c$, $P_{candidate} = 65.22$ days. There appears to be no obvious peaks consistent with d's periods derived from the TTVs, but there is additional power in the periodogram, particularly near 12.75 and 13.3 days. Also note that the 22 days peak would not be dynamically stable, and that there is the possibility of a 65 days planetary candidate in the RVs.

($\Delta\mathrm{AIC}_c = 19.12$), 11.9 days ($\Delta\mathrm{AIC}_c = 12.66$), and 5.08 days ($\Delta\mathrm{AIC}_c = 11.74$) cases, while the two-planet configuration is favored relative to the three-planet configuration for 12.6 days ($\Delta\mathrm{AIC}_c = 9.61$), 14.1 days ($\Delta\mathrm{AIC}_c = 46.22$), and 5.86 days ($\Delta\mathrm{AIC}_c = 69.79$) cases. Based on the log-likelihood, $\Delta$BIC, and $\Delta\mathrm{AIC}_c$, the 6.20 days is the most favored one overall and the 12.7 days is the most favored among the three-planet cases. However, the TTV analysis indicated that planet d is of very small mass compared to AU Mic b and c, so it is not surprising that the RV model struggles to detect AU Mic d with any statistical significance.

## 6. Discussion

We modeled the transits of AU Mic b and c to obtain the midpoint times, which we then use to model the TTVs of the AU Mic system. We attempted both two-planet and three-planet dynamical models and found that the three-planet model adequately describes the observed TTVs, including its super-period. Moreover, we generated TTV periodograms and found ten possible solutions for the period of the nontransiting planet AU Mic d. In the next subsections, we discuss the impact of AU Mic's stellar activity on the TTVs, the convergence of transit models, the TTV and RV model comparisons, the coplanarity of AU Mic system, the planetary resonant chains, the mass of AU Mic d, the inner d orbits versus middle d orbits, and the validation versus confirmation of AU Mic d.

### *6.1. Impact of AU Mic's Stellar Activity on Transit Timing Variations*

Wittrock et al. (2022) explored the impacts that stellar flares and spot modulations may have on the TTV profile. Given the 7:4 spin–orbital commensurability between AU Mic and planet b (Szabó et al. 2021) and the long lifetime of AU Mic's starspots, Wittrock et al. (2022) modeled the TTVs induced by AU Mic's spot crossing during AU Mic b's transit and found the effect to be relatively minimal (no more than ∼2 minutes) compared to TTVs of planet b induced by planets c and d and with no clear pattern. Martioli et al. (2020), Palle et al. (2020), Gilbert et al. (2022), Wittrock et al. (2022), and Szabó et al. (2021, 2022) modeled the stellar flares from SPIRou, ESPRESSO, TESS, Spitzer, and CHEOPS observations,

**Table 19**
RV Model Information Criterion for the AU Mic System

| $P_d$ (days) | Planets | $\chi^2_{red}$ | $\ln \mathcal{L}$ | ΔBIC | $\Delta\mathrm{AIC}_c$ |
|---|---|---|---|---|---|
| 5.08 | b, c, d | 4.00978 | −2248.46411 | 0.00000 | 0.00000 |
| | b, c | 4.10715 | −2257.68857 | 0.85803 | 11.74349 |
| | b, d | 4.16747 | −2271.93853 | 41.0852 | 44.70022 |
| | b | 4.14185 | −2280.01400 | 39.64525 | 54.18589 |
| | c, d | 4.15293 | −2283.78303 | 64.7742 | 68.38922 |
| | c | 4.24211 | −2302.43094 | 84.47913 | 99.01977 |
| | d | 4.33652 | −2320.10267 | 131.54986 | 138.79341 |
| | - | 4.27910 | −2327.09888 | 127.95138 | 146.16034 |
| 5.39 | b, c, d | 3.95174 | −2248.37326 | 0.00000 | 0.00000 |
| | b, d | 4.14993 | −2269.88140 | 37.15265 | 40.76767 |
| | b, c | 4.24239 | −2276.04763 | 37.75784 | 48.64331 |
| | c, d | 4.05626 | −2275.93760 | 49.26505 | 52.88007 |
| | c | 4.19304 | −2287.77753 | 55.35401 | 69.89465 |
| | b | 4.10217 | −2298.35680 | 76.51256 | 91.05320 |
| | d | 4.19466 | −2305.18164 | 101.88949 | 109.13304 |
| | - | 4.60850 | −2353.45811 | 180.85153 | 199.06049 |
| 5.64 | b, c, d | 3.90634 | −2223.31676 | 0.00000 | 0.00000 |
| | b, c | 3.95149 | −2245.05276 | 25.88113 | 36.76659 |
| | c, d | 3.95899 | −2248.70048 | 44.90381 | 48.51884 |
| | b, d | 3.91049 | −2252.70267 | 52.90820 | 56.52322 |
| | b | 4.18677 | −2279.81918 | 89.55033 | 104.09097 |
| | c | 4.24168 | −2292.44964 | 114.81124 | 129.35188 |
| | - | 4.24294 | −2311.41267 | 146.87368 | 165.08264 |
| | d | 4.37061 | −2332.12947 | 205.89816 | 213.14171 |
| 5.86 | b, c | 3.95261 | −2247.52212 | 0.00000 | 0.00000 |
| | b | 3.99113 | −2267.43656 | 33.96527 | 37.62044 |
| | b, c, d | 4.24926 | −2279.06355 | 80.67377 | 69.78830 |
| | b, d | 4.26988 | −2287.46508 | 91.61319 | 84.34275 |
| | c, d | 4.24476 | −2291.16124 | 99.00551 | 91.73507 |
| | d | 4.24737 | −2307.05552 | 124.93044 | 121.28852 |
| | c | 4.27718 | −2315.40526 | 129.90265 | 133.55782 |
| | - | 4.33599 | −2318.39795 | 130.02440 | 137.34790 |
| 6.20 | b, c, d | 3.76222 | −2223.32578 | 0.00000 | 0.00000 |
| | b | 4.04026 | −2266.56250 | 63.01893 | 77.55957 |
| | b, c | 4.11199 | −2279.09511 | 93.94778 | 104.83324 |
| | b, d | 4.19250 | −2280.76895 | 109.02271 | 112.63774 |
| | c | 4.18665 | −2289.96236 | 109.81864 | 124.35928 |
| | c, d | 4.20633 | −2299.23938 | 145.96358 | 149.57860 |
| | - | 4.22326 | −2311.14636 | 146.32301 | 164.53197 |
| | d | 4.41166 | −2331.23825 | 204.09768 | 211.34123 |
| 6.47 | b, d | 3.82012 | −2242.37068 | 0.00000 | 0.00000 |
| | b, c, d | 4.17966 | −2268.82978 | 58.78184 | 55.16681 |
| | b, c | 4.06131 | −2281.74255 | 67.01647 | 74.28691 |
| | b | 4.16875 | −2290.60045 | 78.86866 | 89.79428 |
| | c, d | 4.11485 | −2289.43973 | 94.13811 | 94.13811 |
| | c | 4.28375 | −2313.19199 | 124.05174 | 134.97736 |
| | - | 4.27356 | −2315.79337 | 123.39086 | 137.98480 |
| | d | 4.48229 | −2339.34545 | 188.08591 | 191.71444 |
| 11.9 | b, c, d | 4.06977 | −2256.91123 | 0.00000 | 0.00000 |
| | b | 4.08732 | −2266.27497 | -4.72704 | 9.81360 |
| | b, c | 4.13643 | −2266.59584 | 1.77833 | 12.66379 |
| | b, d | 4.11093 | −2270.03862 | 20.39115 | 24.00618 |
| | c | 4.29308 | −2306.57442 | 75.87187 | 90.41251 |
| | d | 4.31650 | −2317.55744 | 109.56516 | 116.80871 |
| | - | 4.39886 | −2321.13976 | 99.13891 | 117.34787 |
| | c, d | 4.42181 | −2342.39152 | 165.09695 | 168.71197 |
| 12.6 | b, c | 3.93956 | −2242.04753 | 0.00000 | 0.00000 |
| | b, c, d | 3.95070 | −2243.49828 | 20.49239 | 9.60693 |
| | b, d | 4.03554 | −2253.46944 | 34.57107 | 27.30063 |
| | c, d | 4.16405 | −2283.63677 | 94.90575 | 87.6353 |
| | c | 4.15953 | −2288.90894 | 87.85919 | 91.51436 |
| | b | 4.21603 | −2299.51198 | 109.06527 | 112.72045 |
| | d | 4.37735 | −2325.24047 | 172.24951 | 168.6076 |
| | - | 5.01924 | −2454.82572 | 413.82911 | 421.15261 |
| 12.7 | b, d | 3.82300 | −2230.60095 | 0.00000 | 0.00000 |
| | b, c, d | 3.93925 | −2244.69089 | 34.04350 | 30.42848 |
| | b, c | 4.03965 | −2259.85878 | 46.78839 | 54.05884 |
| | c, d | 4.06094 | −2265.50468 | 69.80745 | 69.80745 |
| | b | 4.06797 | −2276.96998 | 75.14716 | 86.07278 |
| | d | 4.15544 | −2283.89919 | 100.73284 | 104.36137 |
| | - | 4.21856 | −2316.20370 | 147.75097 | 162.34491 |
| | c | 4.32722 | −2330.15944 | 181.52608 | 192.45169 |
| 14.1 | b, d | 4.00062 | −2264.98707 | 0.00000 | 0.00000 |
| | b, c | 4.08155 | −2278.10035 | 14.49931 | 21.76975 |
| | b | 4.32125 | −2291.32638 | 35.08774 | 46.01336 |
| | c | 4.25284 | −2293.92168 | 40.27834 | 51.20395 |
| | c, d | 4.20466 | −2290.74089 | 51.50765 | 51.50765 |
| | b, c, d | 4.35643 | −2297.85791 | 71.60532 | 67.99030 |
| | d | 4.42068 | −2319.25242 | 102.66709 | 106.29561 |
| | - | 4.66740 | −2392.62944 | 231.83023 | 246.42417 |

respectively, which marginalized the effect of flares on the observed TTVs. While `AIJ` and `EXOFASTv2` are not yet capable of jointly modeling the flares during transits, the ground-based observations have relatively lower photometric precision and larger timing uncertainties, so the flares' effect on the TTVs are significantly down-weighted within the photometric precision timing uncertainties (Wittrock et al. 2022).

### *6.2. Convergence of Transit Models*

It can be challenging to get transit model convergence when using standard MCMC methods such as the `emcee` package uses (Foreman-Mackey et al. 2013), especially with a large number of model parameters. However, as mentioned in Section 3, `EXOFASTv2` is written in `IDL` and uses the differential evolution MCMC algorithm instead of the `emcee` package. As part of the convergence criteria, `EXOFASTv2` simultaneously employs two metrics, the Gelman–Rubin statistic and the number of independent draws, to help minimize the individual shortcomings of these convergence criteria (Gelman & Rubin 1992; Goodman & Weare 2010). We were able to use fairly tight priors on most of the parameters (Table 4) and had `rejectflatmodel` switched on to ease the convergence of our transit models. Numerous different walkers, while not fully independent from each other, are found to produce posteriors that are relatively consistent with one another, convincing us that the independent chains do converge. See Eastman et al. (2013) and Eastman et al. (2019) for more information on `EXOFASTv2`'s use of the MCMC algorithm and convergence criteria, and Section 3 of this paper for details on our process with `EXOFASTv2`.

### *6.3. Dynamically Settled Assumption of the AU Mic System*

In Section 4.3, we presented a high-eccentricity two-planet TTV model that does exhibit the super-period (Figure 4), making it seems a potentially good fit for a two-planet system with a stable but unlikely eccentric-aligned configuration with abnormally small masses inconsistent with the RV masses from Cale et al. (2021) and Donati et al. (2023). After having the very small masses replaced with those RV masses, the high-eccentricity two-planet model provides an example of an unstable eccentric system that does model the TTVs and does persist for 20 Myr, as seen in Figure 6, but it is clearly not dynamically settled given the apparent orbital migrations of AU Mic b and c and the extreme fluctuations in both planets' eccentricities and inclinations in the `rebound` simulations.

We must caution that `rebound` does not include tidal circularization and general relativity (GR) precession, which are relevant at these orbital periods, and highly eccentric planets do not exist in older systems. So, in theory, planet d may not exist if the system is currently dynamically unstable. However, future TTVs will clearly rule out this case, and current RVs from Cale et al. (2021) and Donati et al. (2023), while challenging to constrain the eccentricity, do not give any clear indication that this system is highly eccentric. Additionally, the secondary-eclipse model of AU Mic b by K. I. Collins et al. (2023, in preparation) rules out high eccentricity and provides a vastly different argument of periastron (∼90° as opposed to our 173° from Table 12). The dynamically unstable case does not account for the fact that the host star was larger in the recent past, so the planets would have likely collided with the star prior to the 20 Myr mark at these high eccentricities. Thus, we likely can rule out this scenario, but more work is needed on dynamical simulations that include GR precession, tidal circularization, and any disk drag from the past for this star.

### 6.4. Overall Model Comparisons of the AU Mic System

In Section 4.4, we modeled our TTVs and then generated the TTV log-likelihood periodograms to explore a set of planet d's orbital periods that would be in agreement with the observed TTVs of the AU Mic system; it was through the periodograms that we obtained ten possible orbital periods and orbital configurations for AU Mic d. Given that the high-eccentricity two-planet configuration is ruled out for reasons provided in the previous section (Section 6.3), that the low-eccentricity two-planet configuration has both b and c being misaligned despite their well-known transiting status (Plavchan et al. 2020; Martioli et al. 2021; Gilbert et al. 2022; Wittrock et al. 2022), and that both two-planet models are statistically ruled out at high confidence (Tables 16 and 17), this validates AU Mic d, and AU Mic d must possess one of these ten orbital periods and orbital configurations. Based on our TTV model comparison (Tables 16 and 17), our calculated super-period (Figure 3 and Table 9), our RV analysis, and our stability tests (Figure 13), the 12.7 days configuration is the most favored period for AU Mic d.

In the meanwhile, the 5.64 days case is favored by the RVs and the dynamical stability tests but is strongly disfavored by the TTVs. The 5.39, 6.20, and 6.47 days cases are favored by the TTVs and RVs but are disfavored by the stability tests. The 5.08 and 11.9 days cases are favored by the RVs but are disfavored by the TTVs and stability tests. The 12.6 days case is favored by the stability tests but is disfavored by the TTVs and RVs. Lastly, the 5.86 and 14.1 days cases are favored by the TTV but are disfavored by the RVs and stability tests.

Thus, while we do not statistically rule out the other nine potential periods for AU Mic d, they are all statistically disfavored to varying degrees for one reason or another. Since we do not statistically rule out these other potential orbital periods for AU Mic d, we do not consider AU Mic d to be confirmed, only statistically validated. Further, in addition to AU Mic d at its likely orbital period of 12.7 days, it is entirely plausible there could be an additional fourth planet at 5.39, 6.20, or 6.47 days interior to AU Mic b, which is favored by the TTVs and RVs and is disfavored by the dynamical stability tests. Our existing data are unable to explore this latter possibility.

### 6.5. Coplanarity of the AU Mic System

One curious feature among the `Exo-Striker` MCMC models is the inclination of AU Mic d for these ten candidate periods of AU Mic d. AU Mic d is nearly coplanar for the 5.64, 12.6, and 12.7 days cases, with $i_d = 90.08° \pm 4.99°$, $89.63° \pm 1.71°$, and $89.32° \pm 1.16°$, respectively, but the 5.64 days case is strongly disfavored by the TTVs and the 12.6 days case is disfavored by both the TTVs and RVs. For the 6.47 days case, AU Mic d is slightly misaligned at $i_d = 93.57° \pm 3.26°$ but is strongly disfavored from the dynamical stability tests. The remaining candidate periods required considerable misalignment with $i_d = 76.88° \pm 3.05°$, $57.19° \pm 1.83°$, $99.59° \pm 6.78°$, $107.16° \pm 14.19°$, $81.89° \pm 0.64°$, and $74.27° \pm 0.40°$ for the 5.08, 5.39, 5.86, 6.20, 11.9, and 14.1 cases, respectively.

We do not know if the planet formation process could produce such a highly misaligned planet in this young system, especially for the cases between the two coplanar, transiting planets, but we can invoke Occam's razor, which argues that the simplest configurations are the 5.64, 12.6, and 12.74 days cases since these configuration have AU Mic d being coplanar with the system. As discussed in Picogna & Marzari (2014), misalignments are considered to be a particular signature of a past flyby, with a maximum tilting value of 9°, while multiple flybys can lead to higher misalignments. However, after reconstructing the flybys of debris disks using the Gaia Early Data Release 3 data, Bertini et al. (2023) found that AU Mic did not experience any flyby in the last 5 Myr, so any misalignment induced by a recent close flyby appears unlikely. It is also important to point out that if a flyby had occurred, we would expect to see both AU Mic b and c become highly misaligned along with AU Mic d. Moreover, most of the Kepler compact multiplanet systems are well-aligned with a scatter of $\pm 3°$ (Lissauer et al. 2011; Fang & Margot 2012; Fabrycky et al. 2014). These are yet further reasons why we favor the 12.74 days period for the validated AU Mic d, but additional TTV observations will be needed to confirm that this is the case.

### 6.6. Near-resonant Chains of the AU Mic System

Since AU Mic b exhibits such strong TTVs, one consequence of all ten candidate periods for AU Mic d is that they all place the AU Mic system near a resonant chain of varying order. For the inner d scenario, the near resonances between d and b are 3:5 for 5.08 days, 5:8 for 5.39 days, 2:3 for 5.64 days, 5:7 for 5.86 days, 3:4 for 6.20 days, and 7:9 for 6.47 days. The near-orbital resonance between planets b and c for all inner d cases is 4:9, so the overall near-resonant chains are 12:20:45 for 5.08 days, 5:8:18 for 5.39 days, 8:12:27 for 5.64 days, 20:28:63 for 5.86 days, 3:4:9 for 6.20 days, and 28:36:81 for 6.47 days. For the 11.9 days case, the near resonances between b and d and between d and c are 5:7 and 5:8, or near a 25:35:56 chain overall. Both the 12.6 days and 12.7 days cases have both pairs near a 2:3 chain, or near a 4:6:9 chain overall. The 14.1 days case pairs are near 3:5 and 3:4 chains, or near a 9:15:20 chain overall. These near-MMR chains are the reason why our

**Table 20**
Masses, Radii, and Time of Conjunctions of AU Mic d

| $P_{\rm d}$ (days) | $M_{\rm d}$ ($M_\oplus$) | $M_{\rm d}$ ($M_J$) | $R_{\rm d}$ ($R_\oplus$) | $R_{\rm d}$ ($R_J$) | $T_{C,{\rm d}}$ (BJD) |
|---|---|---|---|---|---|
| 5.08 | 0.737 ± 0.083 | 0.00232 ± 0.00026 | 0.926 ± 0.029 | 0.0826 ± 0.0002 | 2458330.88624 ± 0.16079 |
| 5.39 | 0.667 ± 0.042 | 0.00210 ± 0.00013 | 0.900 ± 0.016 | 0.0803 ± 0.0001 | 2458330.79993 ± 0.29196 |
| 5.64 | 0.469 ± 0.045 | 0.00148 ± 0.00014 | 0.816 ± 0.022 | 0.0728 ± 0.0001 | 2458331.07793 ± 0.30077 |
| 5.86 | 1.049 ± 0.239 | 0.00330 ± 0.00075 | 1.021 ± 0.065 | 0.0911 ± 0.0005 | 2458331.46003 ± 0.28115 |
| 6.20 | 0.904 ± 0.482 | 0.00284 ± 0.00152 | 0.980 ± 0.146 | 0.0874 ± 0.0011 | 2458331.66688 ± 1.08314 |
| 6.47 | 0.510 ± 0.112 | 0.00161 ± 0.00035 | 0.836 ± 0.051 | 0.0745 ± 0.0003 | 2458331.03312 ± 0.33184 |
| 11.9 | 0.392 ± 0.079 | 0.00123 ± 0.00025 | 0.776 ± 0.044 | 0.0693 ± 0.0003 | 2458339.91558 ± 0.08663 |
| 12.6 | 0.522 ± 0.147 | 0.00164 ± 0.00046 | 0.841 ± 0.066 | 0.0750 ± 0.0004 | 2458339.99167 ± 0.18465 |
| 12.7 | 1.053 ± 0.511 | 0.00331 ± 0.00161 | 1.023 ± 0.139 | 0.0912 ± 0.0011 | 2458340.55781 ± 0.11641 |
| 14.1 | 0.628 ± 0.092 | 0.00198 ± 0.00029 | 0.885 ± 0.036 | 0.0790 ± 0.0003 | 2458341.05771 ± 0.20391 |

**Notes.** The masses were calculated using the parameters from `Exo-Striker` MCMC models. AU Mic d is not known to transit, so its measured radius and density are unknown. However, we use the Chen–Kipping mass–radius relation (Chen & Kipping 2017) to estimate the radii of AU Mic d.

TTV periodograms (Figures 10 and 12) yielded ten possible solutions, each with relatively high log-likelihood.

Suggestively, as per the Occam's razor argument, the near 4:6:9 resonant chain (or near 3:2 pairings between d and b and between c and d) is the simplest one, given that our TTV and RV models, dynamical stability tests, and the calculated TTV super-period favor the 12.7 days case (the 12.6 days case also shares this near-MMR chain but is not as favored). The 3:2 resonance is the most common among the resonant chains; the 4:3, 5:3, 7:5, and 8:5 resonances are not as common, respectively, but are not unprecedented; and the 9:4 and 9:7 resonances do not appear to be very common (Fabrycky et al. 2014). Thus, the distribution of near-MMR chains among the known exoplanets gives stronger credence to the potential near 3:2 resonant chain pairs of the AU Mic system. Regardless of which of the ten candidates periods for AU Mic d is correct, with the 12.7 days case being most favored, all place the AU Mic system near a resonant chain, with the 12.7 days case being the simplest commensurability chain configuration. The presence of near-MMRs in such a young system poses significant constraints for the formation model and evolution of planetary systems. The similarly young V1298 Tau system is also near a similar resonant chain configuration, suggesting this may be a common characteristic of the formation of compact multiplanet systems (David et al. 2019a, 2019b; Tejada Arevalo et al. 2022). This implies that the planetary systems can develop resonant chains very early on, particularly in compact systems, which in turn would quickly establish the stability of the dynamical systems.

### 6.7. Characterizing AU Mic d

We calculate the mass of AU Mic d (Table 20) using the parameters generated from `Exo-Striker` MCMC models and Equation (3) (Cumming et al. 1999):

$$K = \left(\frac{2\pi G}{P_{\rm orb}}\right)^{1/3} \frac{M_p \sin i}{(M_* + M_p)^{2/3}} \frac{1}{\sqrt{1 - e^2}}. \tag{3}$$

Since AU Mic d is not known or observed to transit, its radius, and therefore its density, is unknown.

The mass of AU Mic b is poorly constrained from the TTVs due to the limited amount of transit data from AU Mic c and that AU Mic d is not known to be transiting, so we do not derive a TTV mass constraint for AU Mic b. AU Mic c is better constrained given the wealth of transit data from AU Mic b, but since there is no transit data from AU Mic d, we are unable to meaningfully constrain the mass of AU Mic c either. However, the mass of AU Mic d is the most constrained of the three planets due to the availability of transit data from both planets b and c. The most favored model ($P_{\rm d} = 12.7$ days) has the mass $M_{\rm d} = 1.053 \pm 0.511\ M_\oplus$, which makes AU Mic d Earth-like in mass. The 5.86 and 6.20 days cases also have AU Mic d's mass being Earth-like but smaller, while the rest of the cases have AU Mic d being of even smaller mass but still not as small as that of Mars; for comparison, the mass of Mars is $M_{\rm Mars} = 0.107\ M_\oplus$.

These relatively small masses for AU Mic d partially explain the challenges RVs face in characterizing such a planet and the divergent results between TTVs and RVs in which periods for AU Mic d were favored. Additionally, given that the host star AU Mic is highly active, it is incredibly challenging to validate AU Mic d with RVs with current-generation RV measurements and techniques for modeling and mitigating stellar activity. However, given that our RV models indicated the presence of a potential additional planet beyond AU Mic c, it will still be worthwhile to continue to intensely monitor the AU Mic system with RVs.

Given that the 12.7 days case is the most plausible one based on the super-period (Section 4.1), the stability tests (Section 4.6), overall model comparisons (Section 6.4), and the Occam's razor arguments from Sections 6.5 and 6.6, AU Mic d is most likely to have a roughly Earth-like mass. If confirmed, this would be the first known Earth-mass planet orbiting a young star. If it does transit, it will provide a crucial and valuable opportunity in probing its atmosphere and understanding the evolution of terrestrial planets' atmosphere.

We use the Chen–Kipping mass–radius relation (Chen & Kipping 2017) to estimate the radius of AU Mic d (Table 20). For $P_{\rm d} = 12.7$ days, AU Mic d has a radius $1.023 \pm 0.139\ R_\oplus$, making its size very Earth-like. The 5.86 and 6.20 days cases still have AU Mic d being Earth-like in size, while the remaining cases have it being smaller, with the smallest size being $0.776 \pm 0.044\ R_\oplus$ from the 11.9 days case (for comparison, Mars' radius is $R_{\rm Mars} = 0.532\ R_\oplus$).

We obtain $T_{C,{\rm d}} = 2458340.55781 \pm 0.11641$ BJD for $P_{\rm d} = 12.7$ days (Table 20). Assuming AU Mic d is coplanar with the other planets, we predict the time of transits for AU Mic d and map them onto the raw TESS photometry of AU Mic (Figures 19 and A14).

Any potential transit signatures of AU Mic d are not readily apparent by eye in the TESS photometry. Based on the model of AU Mic c's depth uncertainty from Gilbert et al. (2022), we

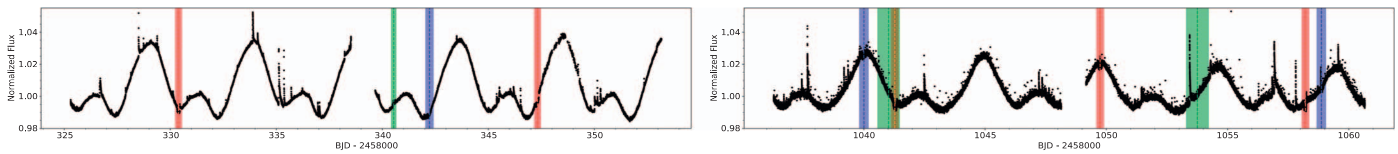


**Figure 19.** Raw TESS photometry of AU Mic overlaid with observed transits of AU Mic b (red) and c (blue) and range of predicted transit midpoint times for AU Mic d (green). This case is for $P_{\rm d} = 12.7$ days. Left panel is from Cycle 1, and right panel is from Cycle 3. Owing to AU Mic d's estimated 160 ppm depth and AU Mic's intense stellar activity, the potential transit signatures from AU Mic d are not readily apparent by eye, nor detectable at high statistical significance in the TESS light curve given the stellar activity and photon noise.

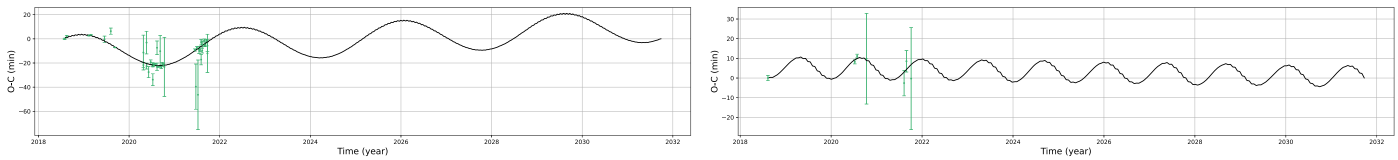


**Figure 20.** `Exo-Striker`-generated TTV models of AU Mic b (left) and c (right) projected over 10 yr since last observed transit of the AU Mic system for $P_{\rm d} = 12.7$ days. The observed TTVs (green) are included with the model (black).

place a 3$\sigma$ upper limit on AU Mic d's transit of 460 ppm. With the estimated radius $R_{\rm d} = 1.023 \pm 0.139\ R_\oplus$ for AU Mic d (Table 20), its transit depth would be ∼160 ppm. AU Mic d's small radius and very shallow transit depth could explain its lack of transit detection, especially in the presence of AU Mic's intense stellar activity. Future multiwavelength, high-precision, space-based photometry could potentially confirm whether or not AU Mic d transits.

We next estimate whether or not a transit of AU Mic d could be recovered with any statistical significance. The point-to-point white-noise scatter in the AU Mic TESS light-curves model from Gilbert et al. (2022) is 550 ppm for the 20 s cadence data and 370 ppm for the 2 minutes cadence data. There is also the variability in the Gaussian process (GP) component of their model, which has an amplitude of ∼3000 ppm and is periodic over ∼0.6 days; this periodic noise is, in principle, removable with the GP process, so the white noise is the remaining limiting factor. As an example, let us consider the 2 minutes cadence data with the 370 ppm scatter. In 1 hr, that noise averages down to ∼70 ppm. Therefore, to obtain an signal-to-noise ratio (S/N) = 7 for a 160 ppm transit, we would need approximately 10 hr of transit data. The 20 s cadence data with the 550 ppm scatter is less noisy per unit time; the reason for this is partially unknown, but is believed to be not significantly caused by the cosmic-ray correction (Huber et al. 2022). In that case, the noise averages down to ∼40 ppm in 1 hr; this would require approximately 4 hr of transit data to achieve a S/N = 7 for a 160 ppm transit. Therefore, accounting for the photon noise alone, given the transit duration of AU Mic d would be less than 4 hr if it transited, there is marginal photon noise to recover a statistically significant detection off AU Mic d in the TESS light curves, but this statistical significance would be degraded even further after accounting for the additional uncertainty introduced from the stellar activity. This is best evidenced by the recovered depth uncertainty for AU Mic c of $1.15 \pm 0.22$ ppt.

Future work is needed to involve a thorough search of all existing space-based light curves of the AU Mic system for any statistically significant 160 ppm signal to confirm AU Mic d's transiting nature and to tighten the predicted timing of its transits. This will also require additional transit observations of AU Mic to minimize the photon shot noise such that AU Mic d's transits can potentially be detected. To further constrain this system, and confirm and distinguish the 12.7 days period for AU Mid d relative to the other nine candidate periods, additional precise space-based transit timing observations of AU Mic b and especially AU Mic c are needed. For this purpose, we modeled the projected TTVs of AU Mic b and c over the course of 10 yr since the last observed transit in the AU Mic system (Figures 20 and A15).

### 6.8. Inner d Orbits versus Middle d Orbits

Is AU Mic d interior or exterior to AU Mic b? The TTV analysis (Tables 16 and 17) favors AU Mic d to be between AU Mic b and c, and this is additionally supported by the Occam's razor arguments covered in Sections 6.5 and 6.6, whereas the `SPOCK`, `MEGNO`, and `Nbody` stability analyses (Figure 13) and the RV analysis (Table 19) appear to favor AU Mic d lying interior to AU Mic b. However, this kind of comparison can only be done to a limited extent because the time periods after which the stability is estimated vary. For instance, `SPOCK` can only predict the stability probability after $10^9$ orbits of the innermost planet. If AU Mic d is interior to b, this corresponds to about 14 Myr, but if AU Mic d is between b and d, this corresponds to about 23 Myr. Therefore, the results for the two ranges are not directly comparable, since the longer timescale could naturally make more systems unstable, sorting out more configurations, and making the AU Mic d between b and c case seem less likely than it is. Additionally, the current RV models, including those from Cale et al. (2021) and Zicher et al. (2022), struggle in detecting low-mass planets with $K_{\rm d} < 1$ m s$^{-1}$ like AU Mic d and most especially in the presence of heightened stellar activity such as that of AU Mic.

The determination of these cases is further complicated by the fact that AU Mic d's transiting nature is unknown. If AU Mic d does not appear to transit, it can mean that either the planet is misaligned or is so small such that its transit signature is masked by the instrumental and photon noise and/or host star's activity. Notably, almost all of the TTV orbital configurations that were explored in this paper require d to be misaligned with the other two planets, with the exception of the 5.64, 12.6, and 12.7 days cases. Additionally, AU Mic d in the inner d cases would have a higher probability of transiting AU Mic than in the middle d cases (Table 21). We also found AU Mic d to be relatively small (∼1.02 $R_\oplus$ assuming d is Earth-like in density), so its transit signature would be very

**Table 21**
Probabilities of AU Mic d Transiting Based on Its Corresponding Distances from the Host Star Using the Simplest Estimate $P_{tr} = R_{\star}/a_d$ (Borucki & Summers 1984; Sackett 1999)

| $P_d$ (days) | $a_d$ (au) | $P_{tr}$ |
|---|---|---|
| 5.08 | 0.0462 ± 0.0008 | 0.0749 ± 0.0027 |
| 5.39 | 0.0481 ± 0.0009 | 0.0720 ± 0.0026 |
| 5.64 | 0.0495 ± 0.0009 | 0.0698 ± 0.0025 |
| 5.86 | 0.0508 ± 0.0009 | 0.0681 ± 0.0024 |
| 6.20 | 0.0528 ± 0.0010 | 0.0655 ± 0.0024 |
| 6.47 | 0.0543 ± 0.0010 | 0.0637 ± 0.0023 |
| 11.9 | 0.0813 ± 0.0015 | 0.0425 ± 0.0015 |
| 12.6 | 0.0849 ± 0.0016 | 0.0408 ± 0.0015 |
| 12.7 | 0.0853 ± 0.0016 | 0.0406 ± 0.0015 |
| 14.1 | 0.0912 ± 0.0017 | 0.0380 ± 0.0014 |

shallow (∼160 ppm, which is below the 460 ppm limit for resolving transits in the AU Mic TESS light curves).

Given the complexity of the resonance orders of the different candidate periods, Occam's razor suggests that the 12.7 days period (and thus the middle d case) is the most likely scenario, given that this configuration has the simplest near-MMR chains and with planet d being coplanar with the system (as discussed in Sections 6.6 and 6.5, respectively). However, we do not rule out the possibility of an interior planet to AU Mic b and the near-2:3 resonance.

With the small mass $M_d = 1.053 \pm 0.511\ M_{\oplus}$ of AU Mic d (based on 12.7 days being the most plausible case), this would make d the first Earth-mass planet orbiting a known young star. Thus, d will serve as a very valuable target for a test case study involving the evolution of terrestrial planets and their atmosphere, provided that AU Mid d does transit. Kane et al. (2022) determined that AU Mic d presently does not lie within the habitable zone (HZ). While it is true that AU Mic is still in its pre-main sequence phase and that the HZ regions are predicted to migrate relatively quickly toward the host star until AU Mic becomes a main sequence star (Kane et al. 2022), AU Mic d will still be well interior to the innermost boundary of the HZ. This implies that AU Mic d may become more like Venus instead of Earth. Additionally, the compact near-MMR orbits mentioned in Section 6.6 could lead to significant tidal heating of AU Mic planets' interior, particularly that of AU Mic d (e.g., Bolmont et al. 2013; Van Laerhoven et al. 2014; Luger et al. 2017), but this effect is not further explored herein.

### *6.9. Is AU Mic d a Candidate, Validated, or Confirmed Planet?*

Throughout this work, we have characterized AU Mic d as a "validated" planet and not as a "confirmed" or "candidate" planet. We consider the threshold for "confirmed" planet to be that it is detected through a second technique that unequivocally rules out false-positive scenarios (even if its orbital period is not well-known), for "validated" planet to be that the planet is statistically verified (even if its orbital period is ambiguous), and for "candidate planet" to be that there is a signal which may be due to a planet but is not statistically verified. Thus, by our definition, "validated" is more conservative than "confirmed." The main point of "validation" is that we have statistically proven AU Mic d must exist (TTV model comparisons from Tables 16 and 17 and most of RV model comparisons from Table 19 consistently ruled out the two-planet configurations), even if there is some ambiguity in its orbital period, and Wittrock et al. (2022) ruled out TTVs driven by stellar flares and spot modulations. Moreover, we have come across several published examples where the planets that are "confirmed" via the TTV detection technique apparently may have several possible orbital periods or do not need their orbital period to be well-defined or even known; such examples include Kepler-19 c (Ballard et al. 2011), Kepler-82 f (Freudenthal et al. 2019), Kepler-160 d (Heller et al. 2020), Kepler-448 c (Masuda 2017), Kepler-539 c (Mancini et al. 2016), and KOI-984 c (Sun et al. 2022). We should also point out that many direct-imaging planets are considered confirmed without precise knowledge of their orbital period.

Based on the sensitivity of RVs from Cale et al. (2021) and Zicher et al. (2022), and since $K_d < 1$ m s$^{-1}$, further characterization of AU Mic d is out of reach of the current RV sensitivity, especially in the presence of substantial stellar activity. Furthermore, this planet is too close to the host star for direct imaging at ∼0.1 au, which is a ∼0.01″ maximum angular separation from the host star at 9.7 pc. Thus, TTVs and transits (if AU Mic d does transit) are the only near-term methods to further characterize this system and confirm planet d. Additional TTVs of AU Mic b and, in particular, AU Mic c are critical for the coming decade with space-based photometry and in further distinguishing the inner d and middle d scenarios. Follow-up with current and future space-based transit observing missions such as the Hubble Space Telescope, CHEOPS, PLAnetary Transits and Oscillation of stars (PLATO), and Pandora would be greatly beneficial in searching for and/or ruling out any transit signatures for AU Mic d. To this end, both AU Mic b's and c's predicted transit midpoint times in Barycentric Julian Date (BJD), after accounting for the TTVs, over the next three years for each three-planet configuration are listed in Tables A10 through A13.

## 7. Conclusion

AU Mic is a young, nearby system hosting a dusty disk and two transiting planets. It is known to be very active, which made RV and TTV observations of the AU Mic system quite challenging. However, Wittrock et al. (2022) determined that the impact of spot modulation on observed TTVs are minimal with respect to the observed TTV variability, and the effect of stellar flares had been mitigated in SPIRou (Martioli et al. 2020), ESPRESSO (Palle et al. 2020), TESS (Gilbert et al. 2022), Spitzer (Wittrock et al. 2022), and CHEOPS (Szabó et al. 2021, 2022) data and masked in the ground data due to larger transit timing uncertainties.

We presented the validation of the new planet, AU Mic d, likely orbiting between planets b and c. We collected 50 data sets from 4 yr of observations on the AU Mic system, including 18 new observations presented herein. We modeled the photometric transits with `EXOFASTv2` and the TTVs with `Exo-Striker`. We determined the super-period of AU Mic b's TTVs, which we then used to estimate the orbital period of AU Mic d. We modeled the high-eccentricity and low-eccentricity two-planet configurations. The high-eccentricity configurations' high eccentricities ($e > 0.2$) and very small inferred masses ($K < 0.07$ m s$^{-1}$) are in strong disagreement with those from RV models (Cale et al. 2021; Donati et al. 2023) and a secondary-eclipse search (Kevin et al. 2023, in preparation). While this configuration does model a TTV super-period, it is clearly not dynamically settled given the apparent orbital migrations of AU Mic b and c and the extreme fluctuations in both planets' eccentricities and inclinations in the rebound simulations. Unlike the high-eccentricity configuration, the low-eccentricity two-planet counterpart does not exhibit the super-period in AU Mic b's TTVs; this configuration also has both b and c being misaligned, which contradicts with transit models and observations (Plavchan et al. 2020; Martioli et al. 2021; Gilbert et al. 2022; Wittrock et al. 2022). Lastly, the TTV model comparisons statistically ruled out both two-planet models. We then developed the TTV log-likelihood periodograms to explore a range of possible orbital periods for AU Mic d; through this technique, we obtained ten possible solutions, which we then follow up with `Exo-Striker`'s Bayesian analysis, stability test packages, including `rebound` and `SPOCK`, and RV modeling.

After performing the TTV and RV model comparisons, the stability tests, and the calculation of the super-period of AU Mic b's TTVs, and taking into consideration the Occam's razor arguments regarding the near-MMR chains and coplanarity of the AU Mic system, we determined that the most favored orbital period for AU Mic d is $P_{\rm d} = 12.73596 \pm 0.00793$ days. The nine other possible periods for AU Mic d are statistically and dynamically disfavored, but not ruled out. The favored solution for AU Mic d places the three planets near the 2:3 orbital resonance pairs, or near 4:6:9 orbital resonance overall. The near-3:2 resonant chain is the most common pairing among the known exoplanets (Fabrycky et al. 2014). Moreover, this particular configuration is statistically the most stable one. The presence of resonant chains among the planets in a very young yet stable system is significant, as it indicates that a compact system can quickly establish resonant chains very early on and which can become dynamically stable within a few hundred short orbital periods. The other disfavored candidate periods for AU Mic d that we modeled would also establish the AU Mic system of three planets in a near-MMR chain, but in higher-order and less commonly occurring resonances. Either way, the scenario with no AU Mic d is statistically ruled out through the TTV and RV model comparisons, and the system must be in a near-resonant chain.

For the period of 12.7 days, our modeling determined the mass $M_{\rm d} = 1.053 \pm 0.511$ $M_\oplus$ and the time of conjunction $T_{C,{\rm d}} = 2458340.55781 \pm 0.11641$ BJD for AU Mic d. This will make AU Mic d the first known Earth-mass planet to orbit a young star and which will serve as a fundamental target for young terrestrial planets' atmospheric characterization and evolution, provided that it does transit. If one assumes AU Mic d is transiting and its density is Earth-like, then its transit depth would be $\sim$160 ppm. This very shallow depth in face of AU Mic's heightened stellar activity may explain the apparent lack of transit signals from AU Mic d in the TESS light curves. Future work could involve thoroughly searching all existing space-based light curves of the AU Mic system for any statistically significant 160 ppm signals. The calculated time of conjunction provided in this paper will simplify the search as it provides a constraint on the timing of the expected transits of AU Mic d.

Our RV analysis implies that there may be additional planets beyond AU Mic c, including the 65 days candidate signature from our $\ln \mathcal{L}$ brute-force periodogram. We recommend additional ground- and space-based TTV observations to further characterize AU Mic d and confirm its orbital period, and to search for additional planets beyond AU Mic c. Given the youthfulness of the AU Mic system and the numerous exciting discoveries emerging from it, AU Mic will serve as an excellent target for HST, CHEOPS, PLATO, Pandora, and future space-based transit observing missions.

## Acknowledgments

P.P.P. acknowledges support from NASA (Exoplanet Research Program Award No. 80NSSC20K0251, TESS Cycle 3 Guest Investigator Program Award No. 80NSSC21K0349, JPL Research and Technology Development, and Keck Observatory Data Analysis) and the NSF (Astronomy and Astrophysics grants Nos. 1716202 and 2006517), and the Mt Cuba Astronomical Foundation.

E.G. acknowledges support from the NASA Exoplanets Research Program Award No. 80NSSC20K0251. The material is based upon work supported by NASA under award No. 80GSFC21M0002.

L.D.V. acknowledges funding support from the Heising-Simons Astrophysics Postdoctoral Launch Program, through a grant to Vanderbilt University.

V.R. acknowledges the support of the Italian National Institute of Astrophysics (INAF) through the INAF GTO Grant "ERIS and SHARK GTO data exploitation."

This paper includes data collected by the TESS mission, which are publicly available from the Mikulski Archive for Space Telescopes (MAST). Funding for the TESS mission is provided by NASA's Science Mission directorate. Resources supporting this work were provided by the NASA High-End Computing (HEC) Program through the NASA Advanced Supercomputing (NAS) Division at Ames Research Center for the production of the SPOC data products.

This work is based (in part) on observations made with the Spitzer Space Telescope, which was operated by the Jet Propulsion Laboratory, California Institute of Technology under a contract with NASA. Support for this work was provided by NASA through an award issued by JPL/Caltech. This research has made use of the NASA/IPAC Infrared Science Archive, which is funded by the National Aeronautics and Space Administration and operated by the California Institute of Technology.

This work makes use of observations from the Las Cumbres Observatory global telescope network. Part of the LCOGT telescope time was granted by NOIRLab through the Mid-Scale Innovations Program (MSIP). MSIP is funded by NSF.

This research made use of the PEST photometry pipeline[39] by Thiam-Guan Tan.

This work makes use of observations from the ASTEP telescope. ASTEP benefited from the support of the French and Italian polar agencies IPEV and PNRA in the framework of the Concordia station program, from OCA, INSU, and Idex UCAJEDI (ANR- 15-IDEX-01).

This research received funding from the European Research Council (ERC) under the European Union's Horizon 2020 research and innovation program (grant agreement No. 803193/BEBOP), and from the Science and Technology Facilities Council (STFC; grant No. ST/S00193X/1).

This research has made use of the NASA Exoplanet Archive, which is operated by the California Institute of Technology, under contract with the National Aeronautics and Space Administration under the Exoplanet Exploration Program.

This research has made use of the Exoplanet Follow-up Observation Program (ExoFOP; DOI: 10.26134/ExoFOP5) website, which is operated by the California Institute of

[39] http://pestobservatory.com

Technology, under contract with the National Aeronautics and Space Administration under the Exoplanet Exploration Program.

This research has made use of the SIMBAD database, operated at CDS, Strasbourg, France.

This research has made use of NASA's Astrophysics Data System Bibliographic Services.

This research has made use of an online calculator that converts a list of Barycentric Julian Dates in Barycentric Dynamical Time (BJD_TDB) to JD in UT (Eastman et al. 2010)[40].

We also give thanks to Trifon Trifonov for his assistance in the use of the `Exo-Striker` package and analysis of the AU Mic system.

*Facilities*: ASTEP 400:0.4m (FLI Proline 16800E), Brierfield:0.36m (Moravian G4-16000 KAF-16803), CFHT (SPIRou), CHEOPS, ExoFOP, Exoplanet Archive, IRSA, IRTF (iSHELL), LCOGT (CTIO:1m, SAAO:1m, SSO:1m, and TO:1 m; Sinistro), MAST, MKO CDK700:0.7m (U16), PEST:0.30m (SBIG ST-8XME), Spitzer (IRAC), TESS, VLT:Antu (ESPRESSO)

*Software*: `AstroImageJ` (Collins et al. 2017), `astropy` (Astropy Collaboration et al. 2013, 2018), `batman` (Kreidberg 2015), `celerite` (Foreman-Mackey et al. 2017), `celerite2` (Foreman-Mackey et al. 2017; Foreman-Mackey 2018), `emcee` (Foreman-Mackey et al. 2013), `EXOFAST` (Eastman et al. 2013), `EXOFASTv2` (Eastman et al. 2019), `exoplanet` (Foreman-Mackey et al. 2021), `Exo-Striker` (Trifonov 2019), `ipython` (Perez & Granger 2007), `lightkurve` (Lightkurve Collaboration et al.), `matplotlib` (Hunter 2007), `MEGNO` (Cincotta & Simó 2000; Cincotta et al. 2003), `numpy` (Harris et al. 2020), `rebound` (Rein & Liu 2012; Rein & Spiegel 2015), `scipy` (Virtanen et al. 2020), `SPOCK` (Tamayo et al. 2020), `TAPIR` (Jensen 2013)

## Appendix
## Outputs from Alternative Cases

This appendix lists the $O-C$ diagrams (Figures A1–A3), MCMC posteriors (Tables A1–A9), corner plots (Figures A4–A12), rebound plots (Figure A13), predicted transit times (Figure A14 and Tables A10–A13), and future (10 yrs) TTV models (Figure A15) for $P_{\mathrm{d}} = (5.08,\ 5.39,\ 5.64,\ 5.86,\ 6.20,\ 6.47,\ 11.9,\ 12.6,\ \text{and}\ 14.1)$ days. The 12.7 days case is statistically most favored and is presented in the main text (Sections 4 and 6).

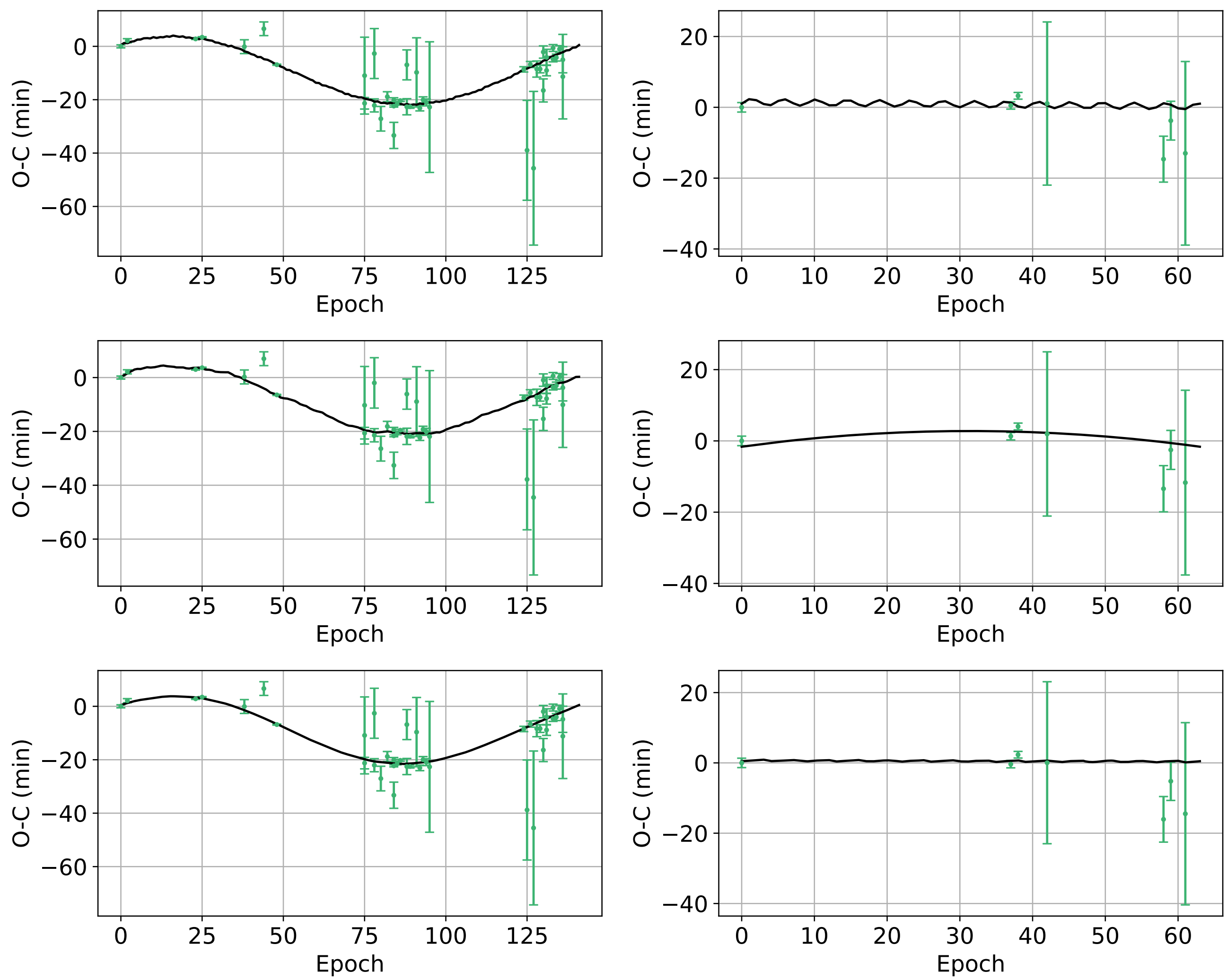


**Figure A1.** $O-C$ diagrams of AU Mic b (left) and AU Mic c (right), with comparison between TTVs (green) and `Exo-Striker`-generated MCMC models (black) for $P_{\mathrm{d}} = 5.08$ days (top row), 5.39 days (middle row), and 5.64 days (bottom row).

[40] https://astroutils.astronomy.osu.edu/time/bjd2utc.html

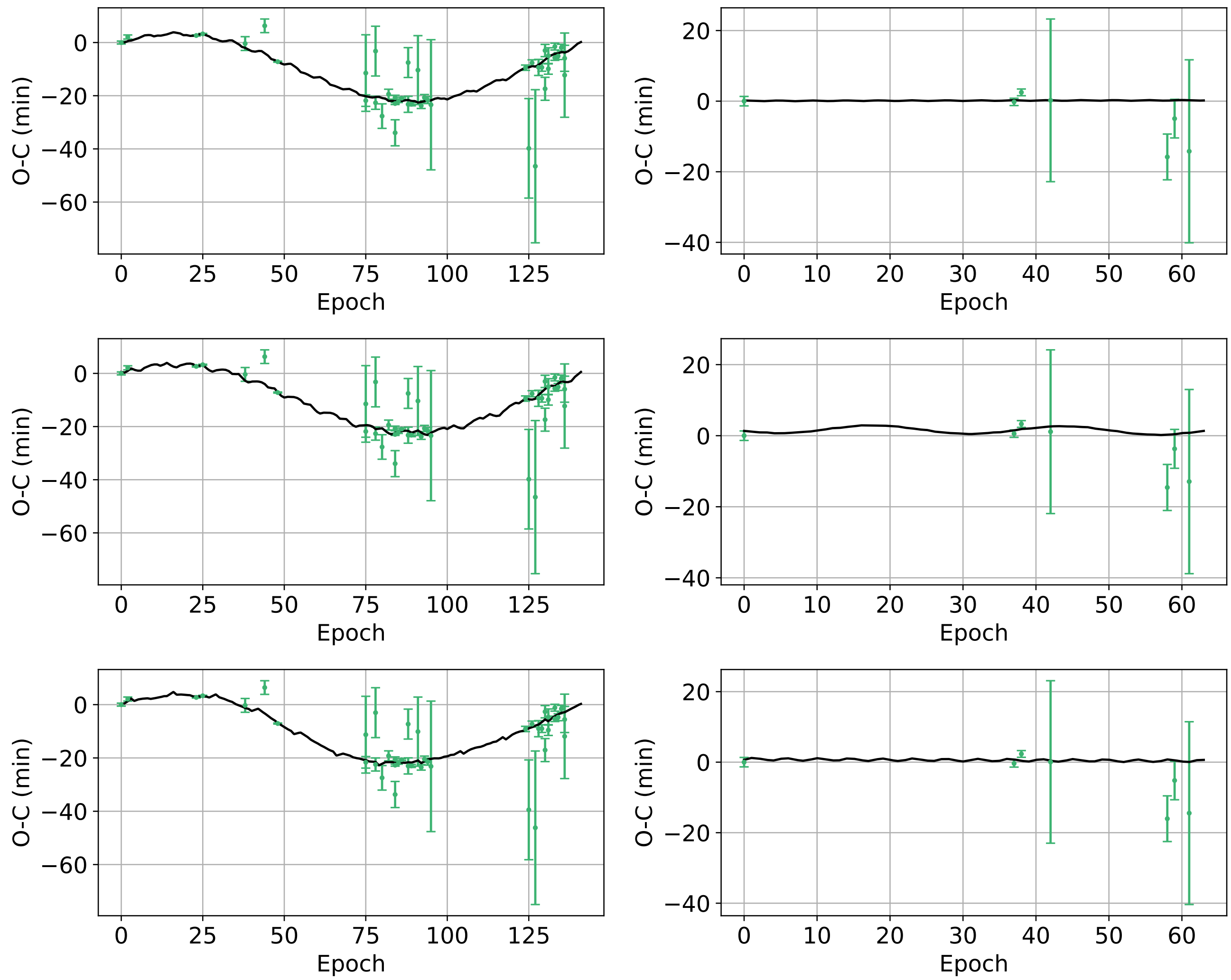


**Figure A2.** $O-C$ diagrams of AU Mic b (left) and AU Mic c (right), with comparison between TTVs (green) and `Exo-Striker`-generated MCMC models (black) for $P_{\mathrm{d}} = 5.86$ days (top row), 6.20 days (middle row), and 6.47 days (bottom row).

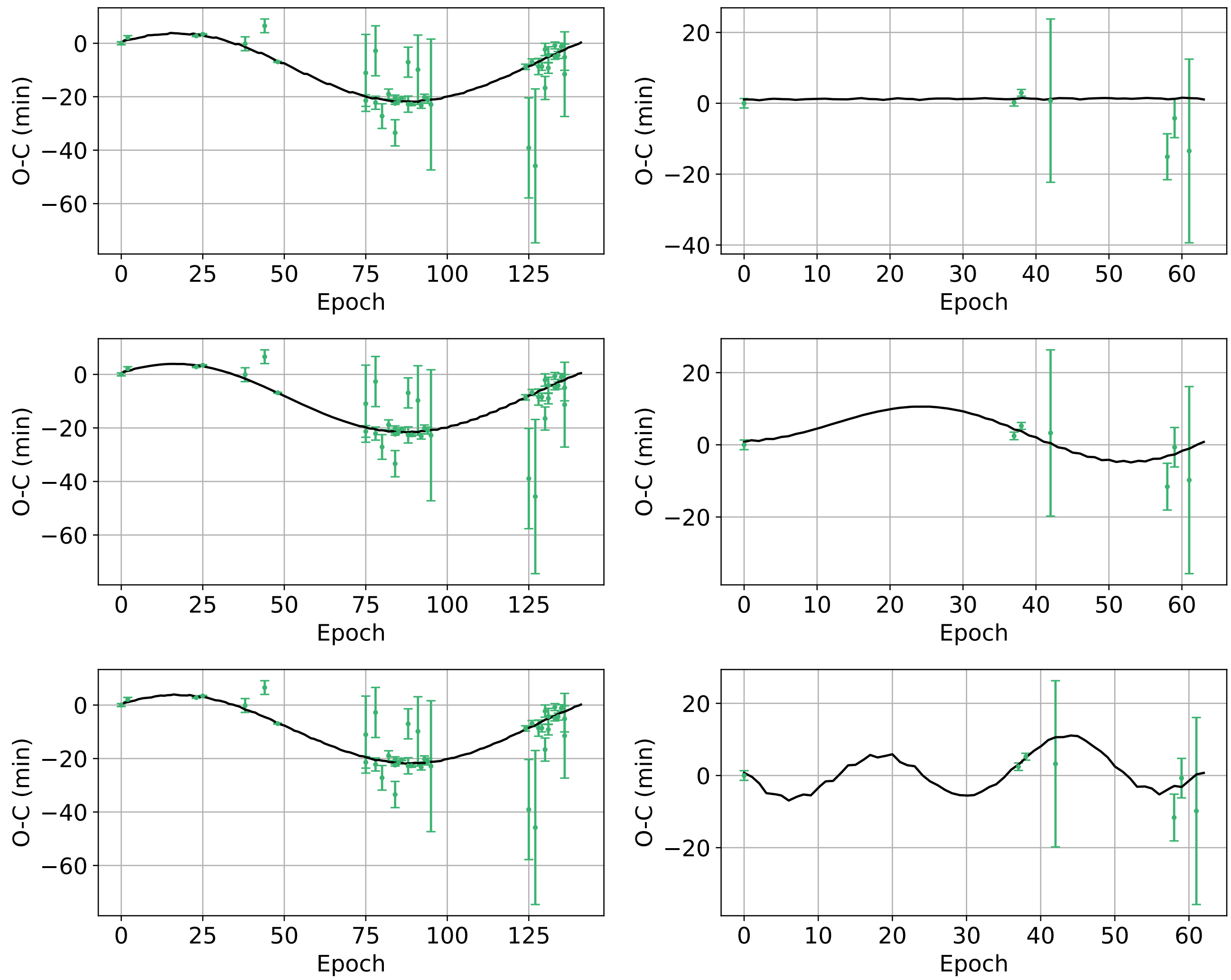


**Figure A3.** $O-C$ diagrams of AU Mic b (left) and AU Mic c (right), with comparison between TTVs (green) and `Exo-Striker`-generated MCMC models (black) for 11.9 days (top row), 12.6 days (*middle row*), and 14.1 days (bottom row).

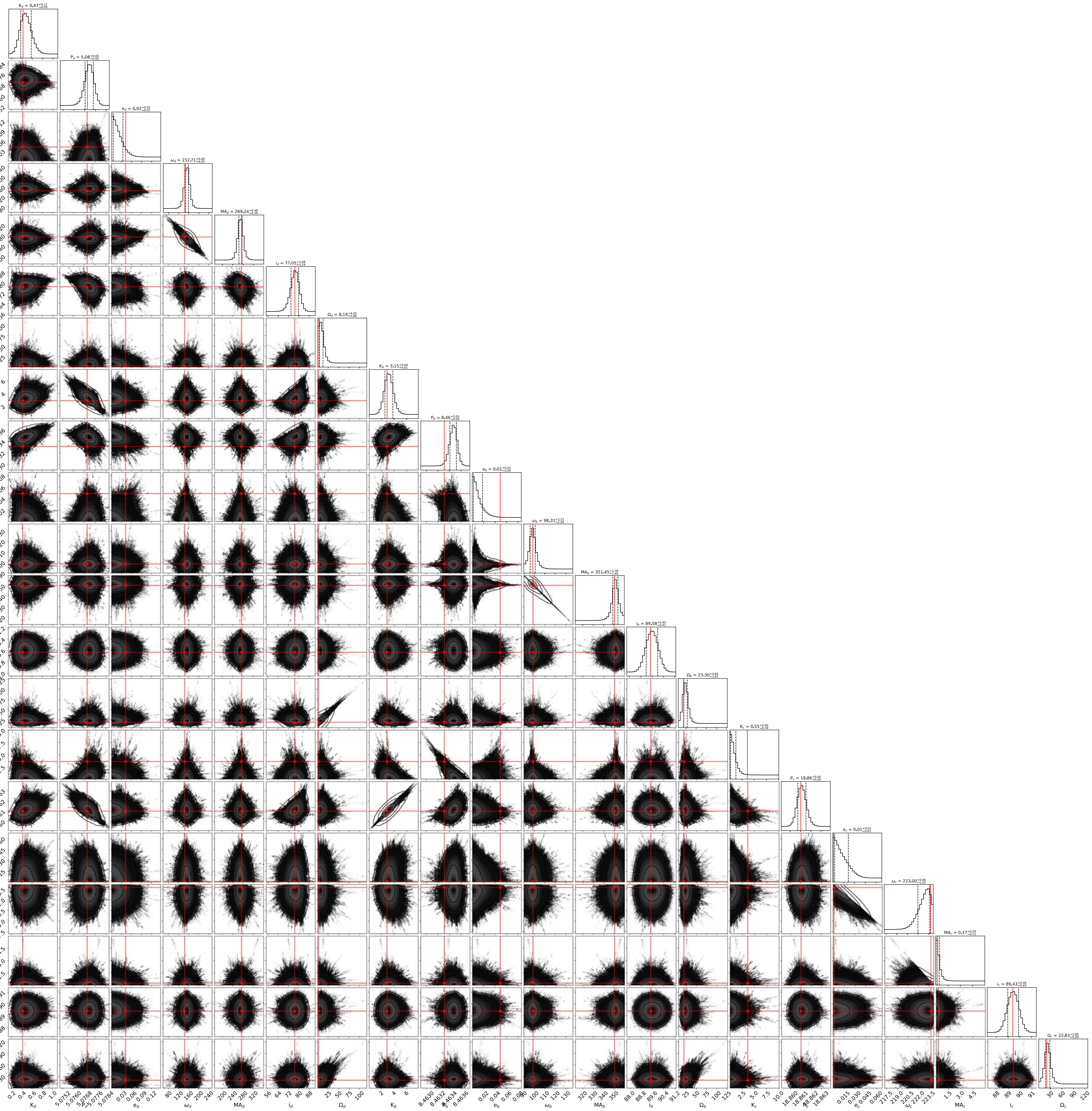

**Figure A4.** Corner plot of AU Mic b and c's orbital parameters from Exo-Striker MCMC analysis for $P_{\rm d} = 5.08$ days.

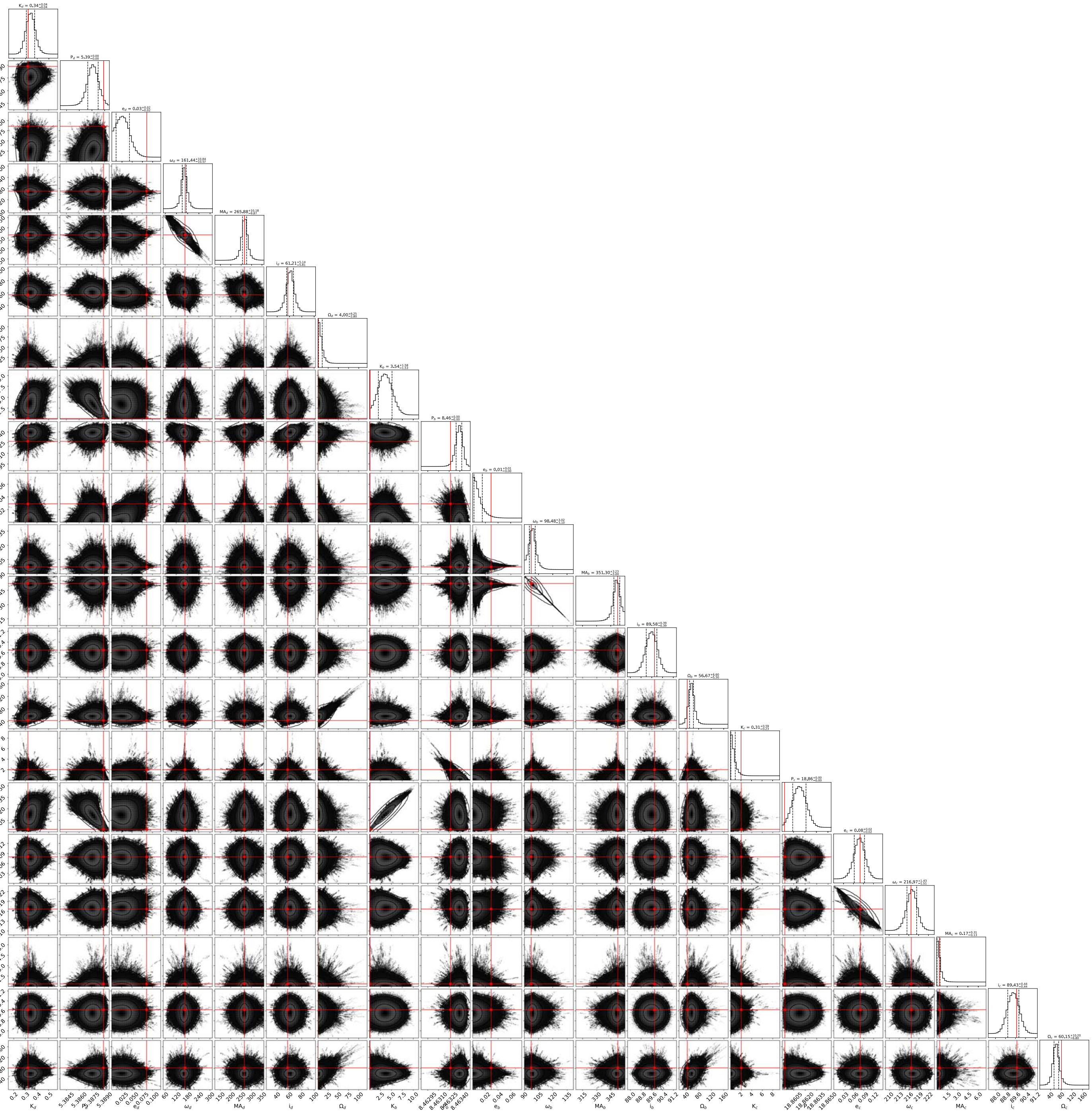

**Figure A5.** Corner plot of AU Mic b and c's orbital parameters from `Exo-Striker` MCMC analysis for $P_{\rm d} = 5.39$ days.

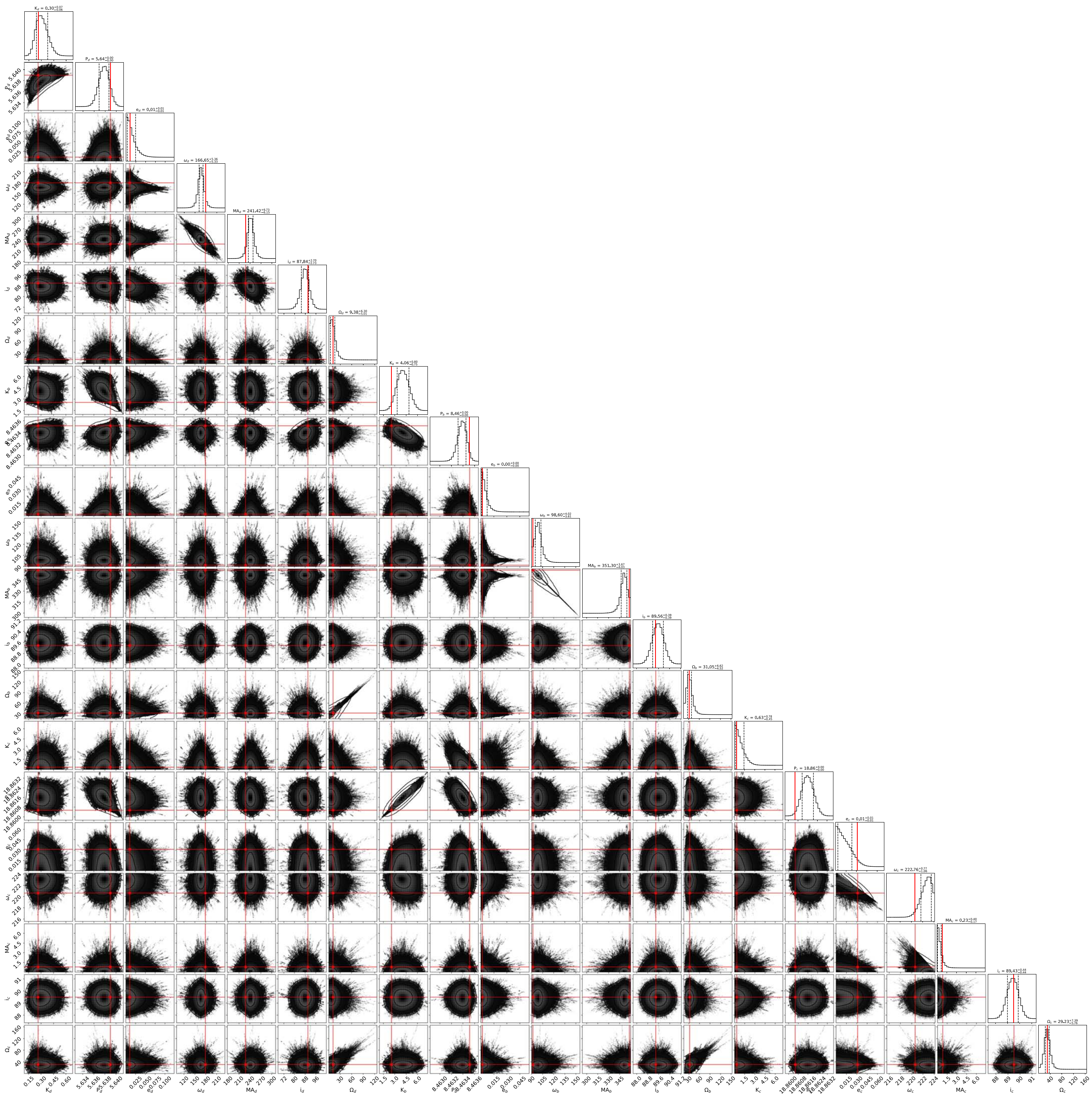

**Figure A6.** Corner plot of AU Mic b and c's orbital parameters from `Exo-Striker` MCMC analysis for $P_{\rm d} = 5.64$ days.

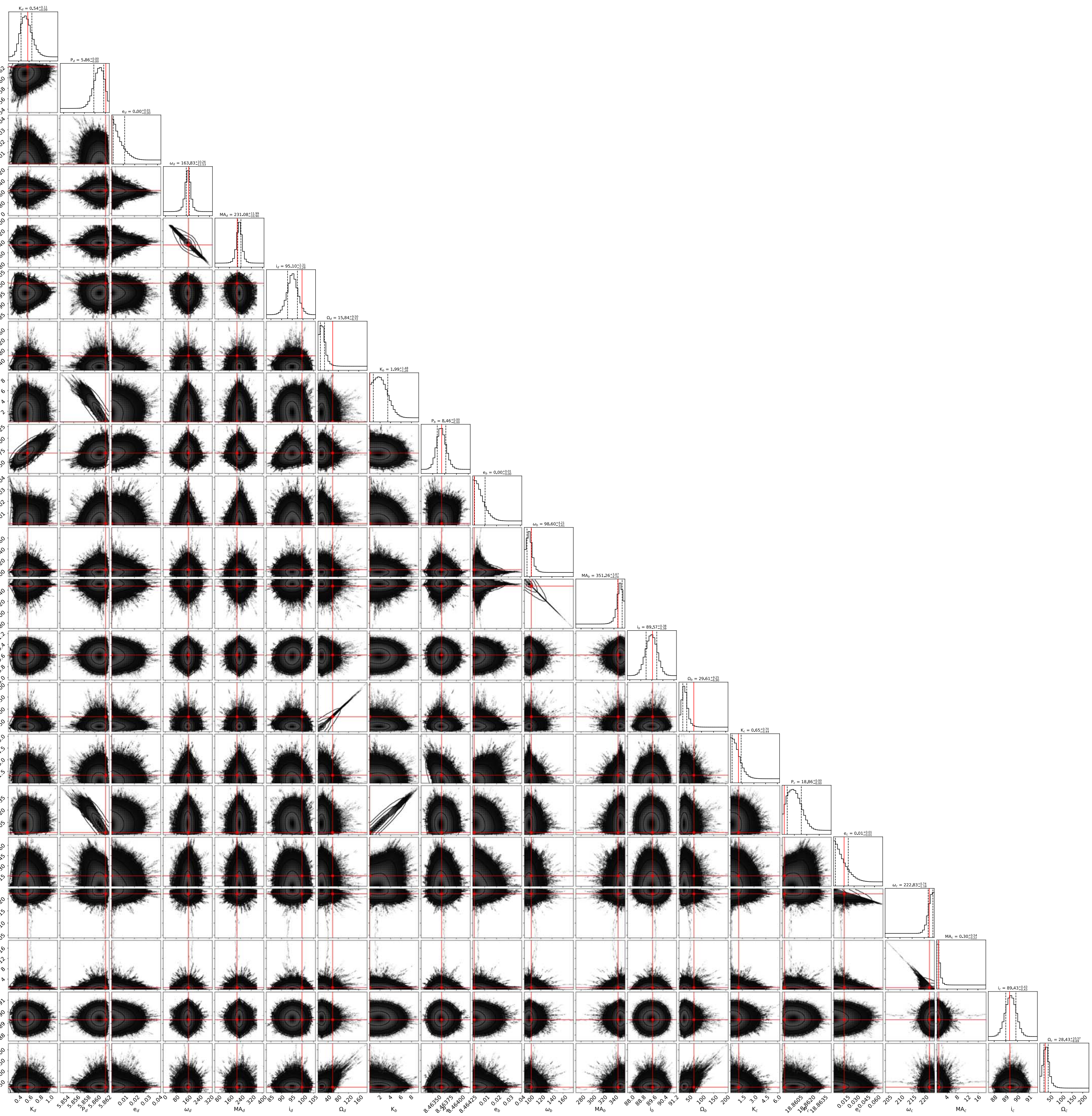

**Figure A7.** Corner plot of AU Mic b and c's orbital parameters from `Exo-Striker` MCMC analysis for $P_{\rm d} = 5.86$ days.

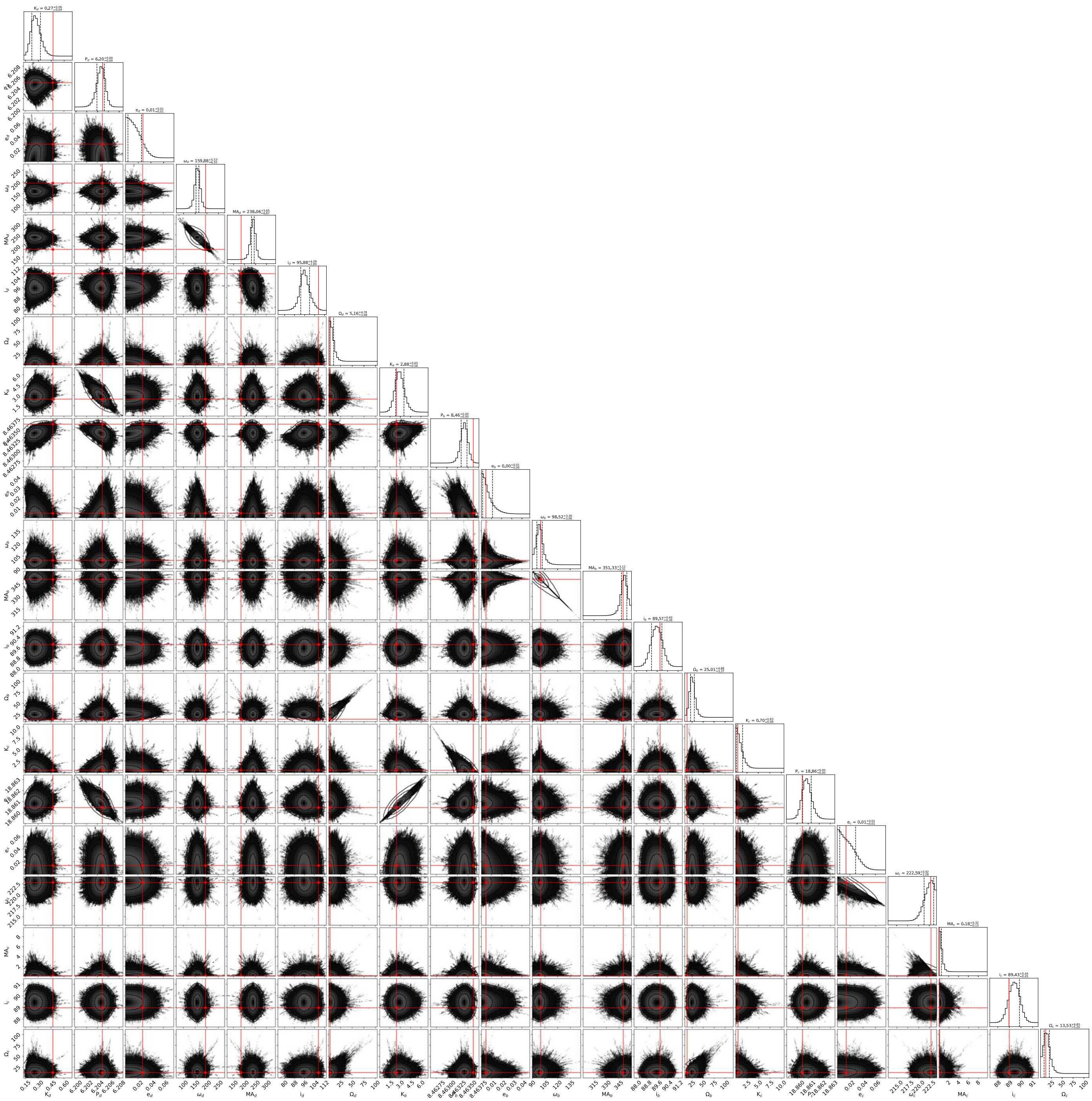

**Figure A8.** Corner plot of AU Mic b and c's orbital parameters from `Exo-Striker` MCMC analysis for $P_{\rm d} = 6.20$ days.

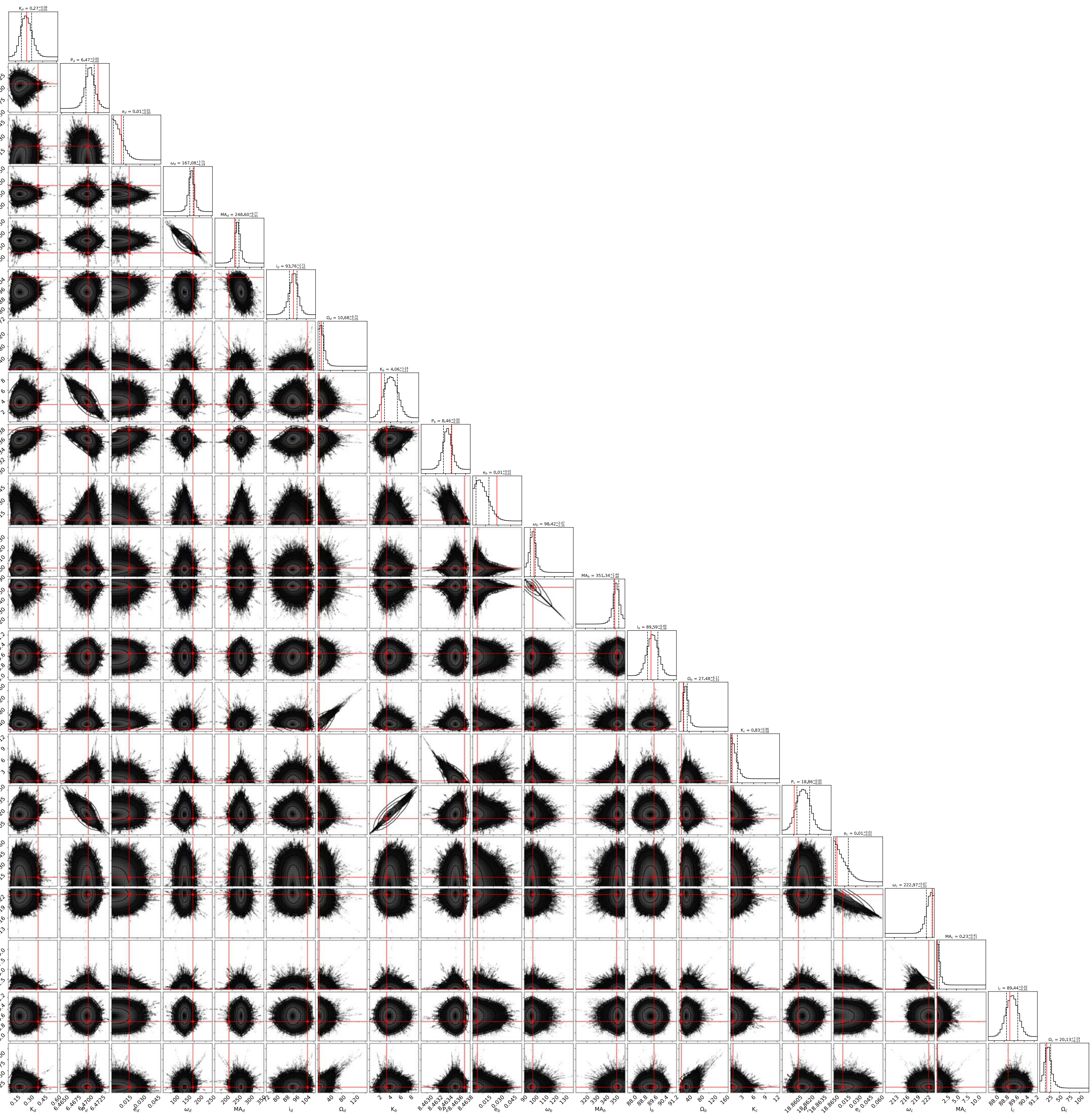

**Figure A9.** Corner plot of AU Mic b and c's orbital parameters from `Exo-Striker` MCMC analysis for $P_{\rm d} = 6.47$ days.

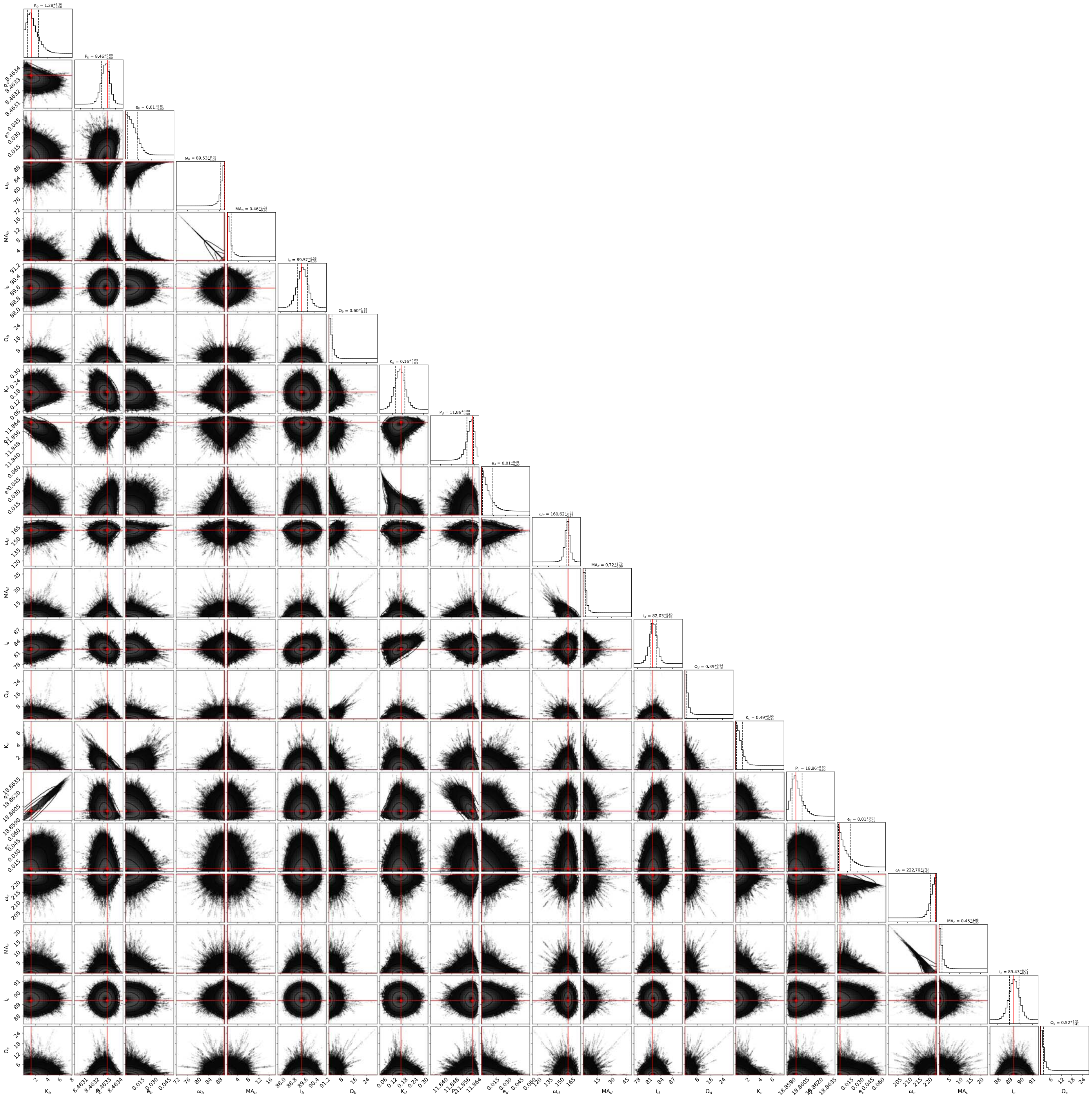

**Figure A10.** Corner plot of AU Mic b and c's orbital parameters from Exo-Striker MCMC analysis for $P_{\rm d} = 11.9$ days.

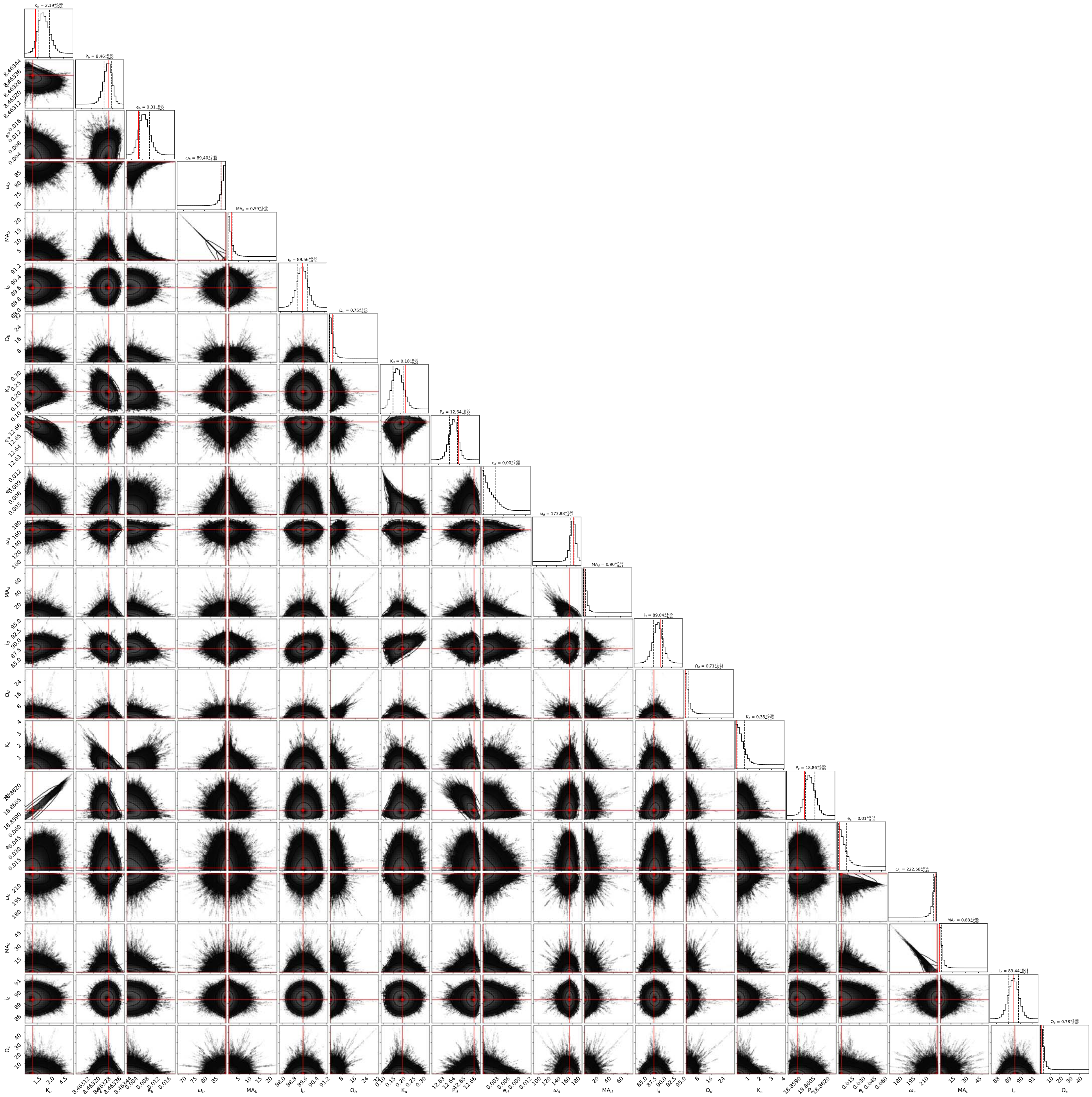

**Figure A11.** Corner plot of AU Mic b and c's orbital parameters from Exo-Striker MCMC analysis for $P_{\rm d} = 12.6$ days.

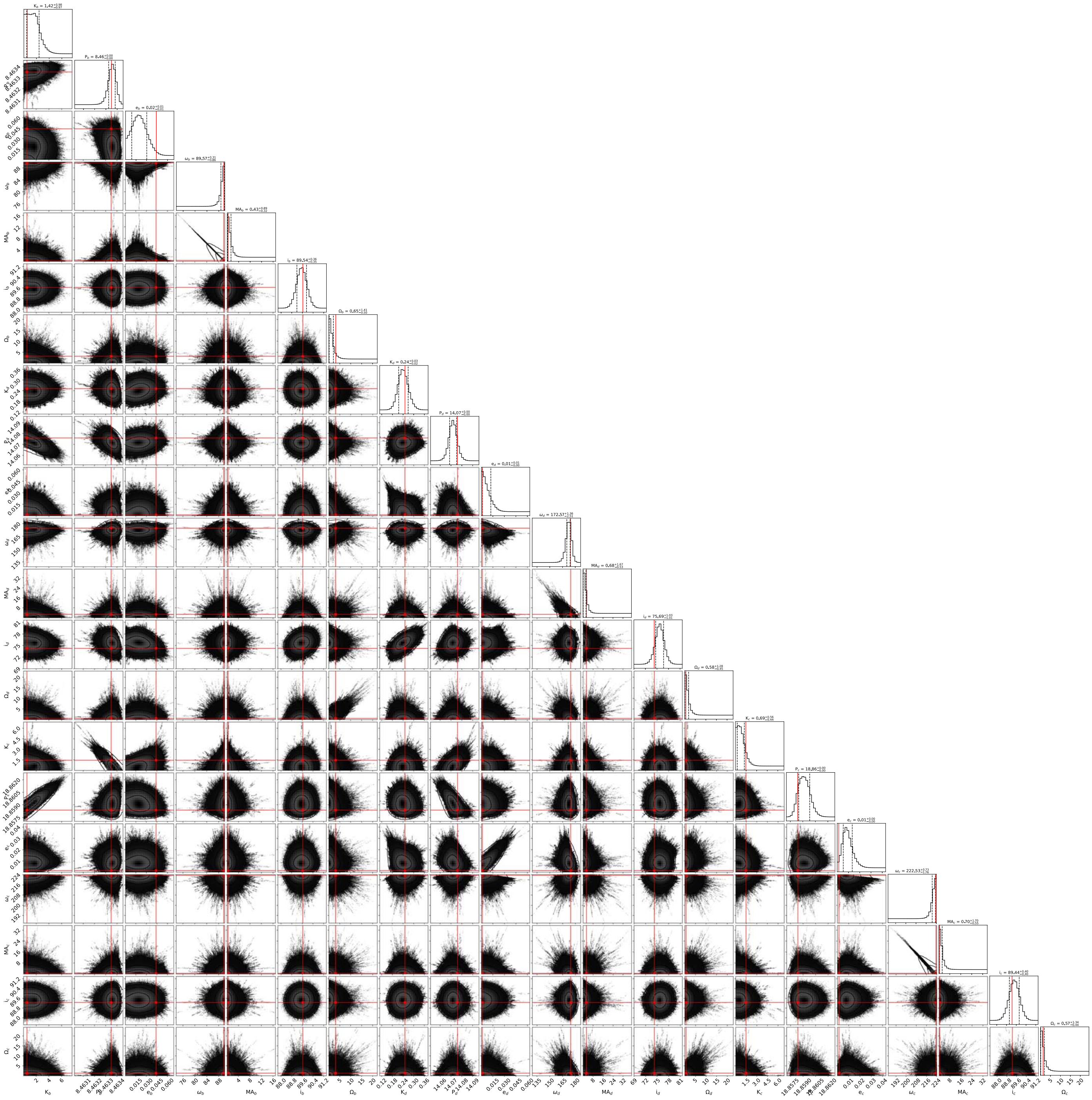

**Figure A12.** Corner plot of AU Mic b and c's orbital parameters from `Exo-Striker` MCMC analysis for $P_{\rm d} = 14.1$ days.

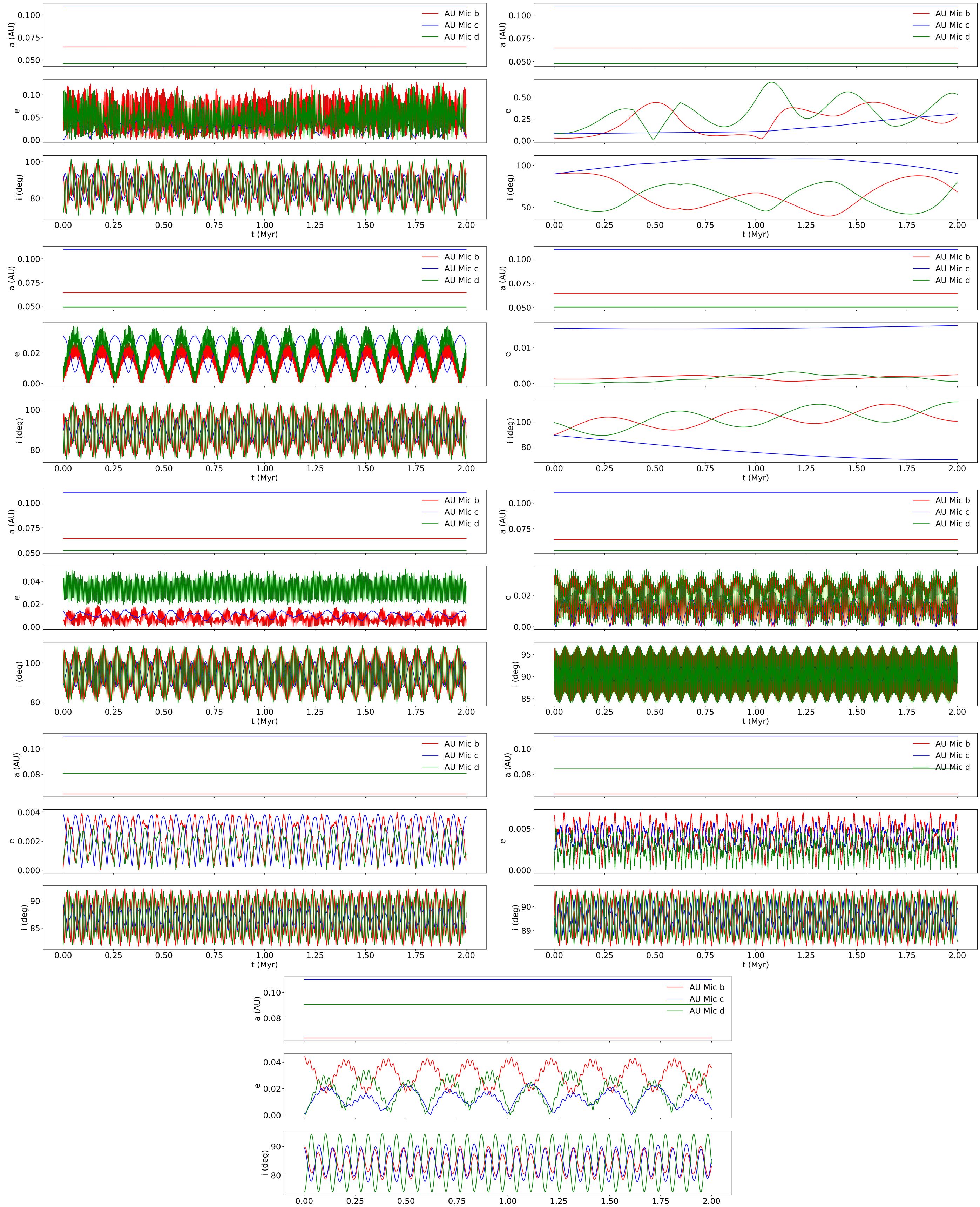


**Figure A13.** `rebound` models of the stability of the AU Mic system on a timescale of 2 Myr for $P_d = 5.08$ days (first row left), 5.39 days (first row right), 5.64 days (second row left), 5.86 days (second row right), 6.20 days (third row left), 6.47 days (third row right), 11.9 days (fourth row left), 12.6 days (fourth row right), and 14.1 days (fifth row).

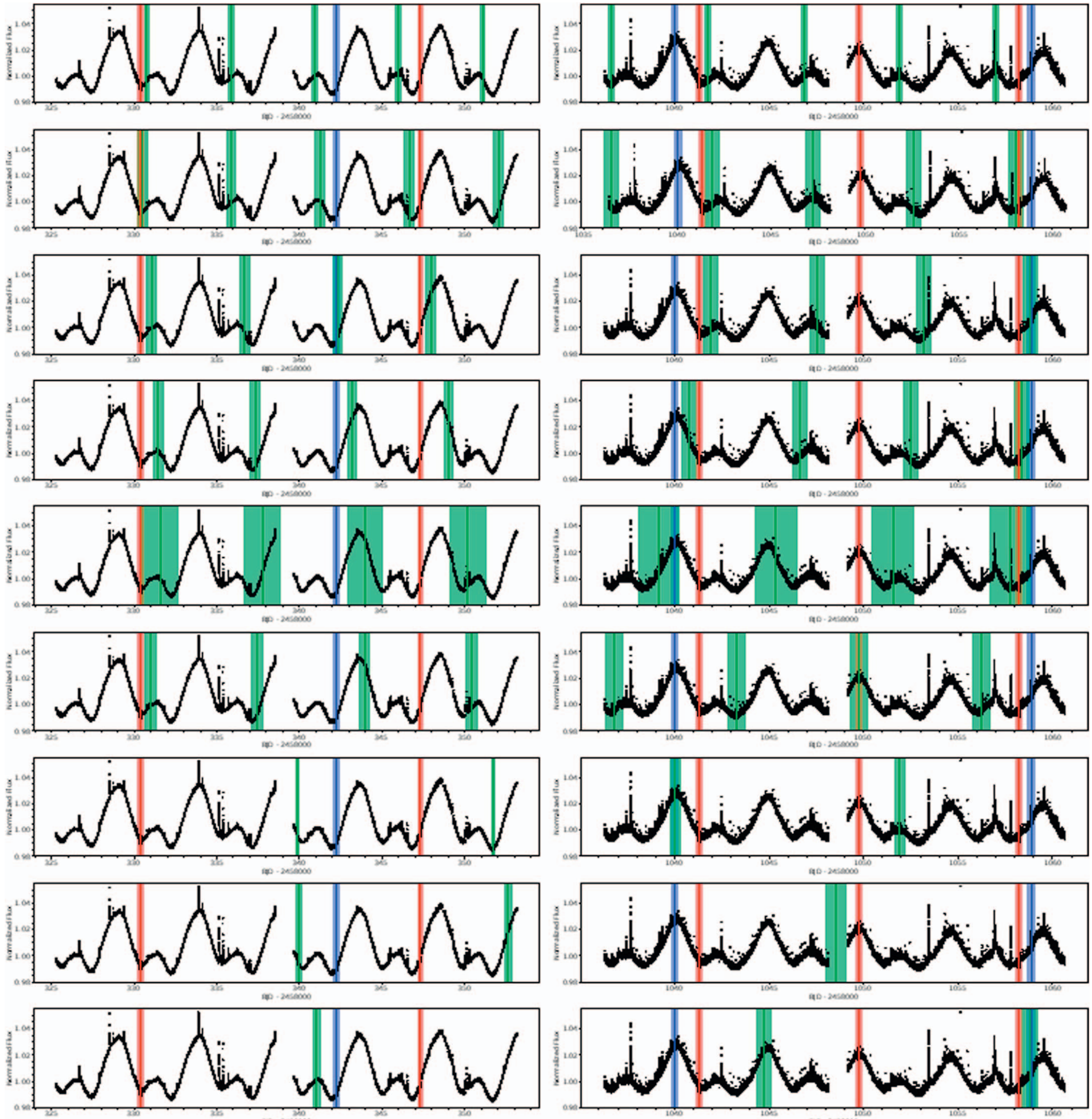

**Figure A14.** Raw TESS photometry of AU Mic overlaid with observed transits of AU Mic b (red) and c (blue) and a range of predicted transit midpoint times for AU Mic d (green), with $P_d = 5.07$ days (first row), 5.39 days (second row), 5.64 days (third row), 5.86 days (fourth row), 6.20 days (fifth row), 6.47 days (sixth row), 11.9 days (seventh row), 12.6 days (eighth row), and 14.1 days (ninth row). Left column is from Cycle 1, and right column is from Cycle 3. Owing to AU Mic d's estimated 160 ppm depth and AU Mic's intense stellar activity, the potential transit signatures from AU Mic d are not obvious in these plots.

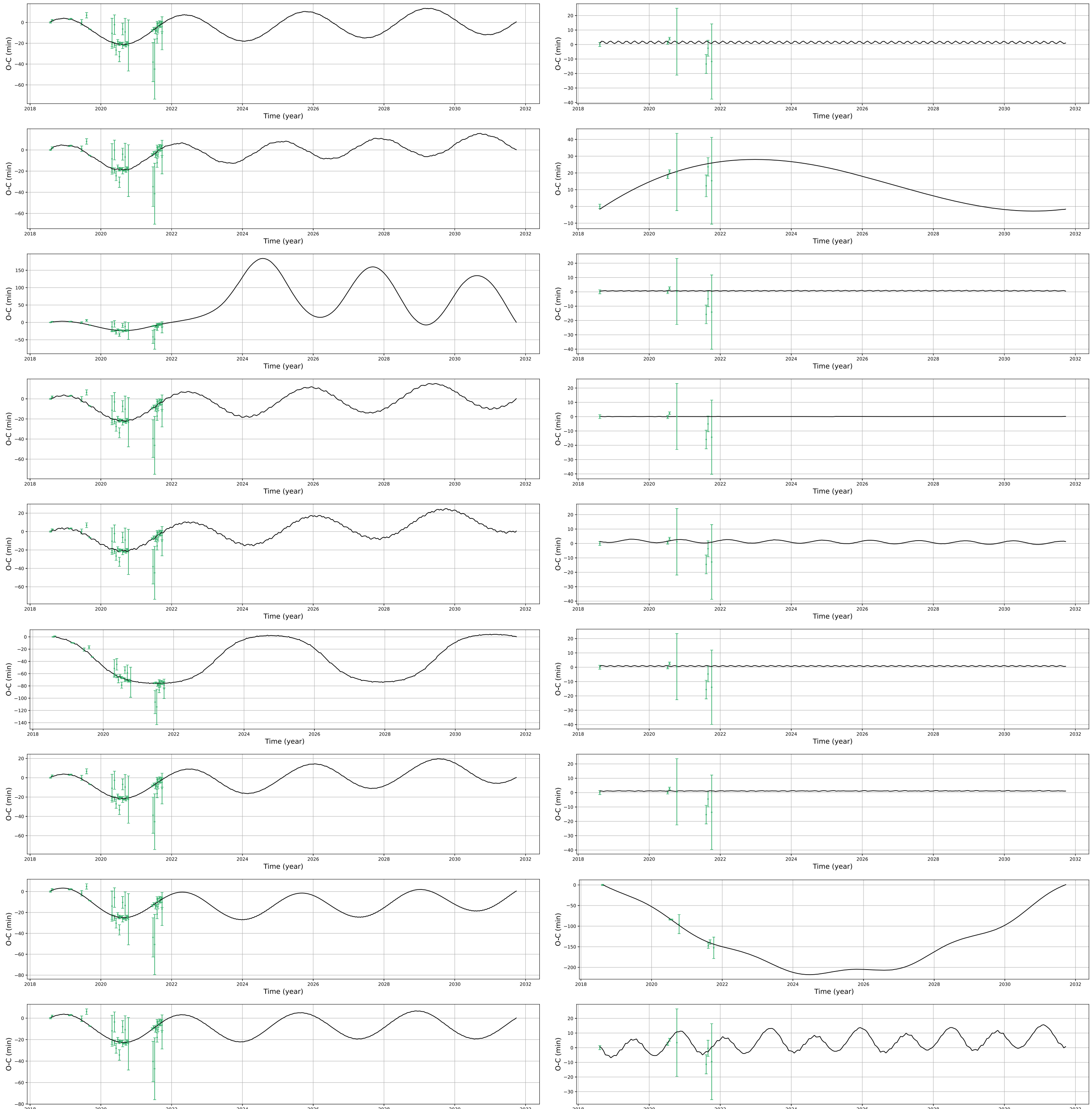


**Figure A15.** `Exo-Striker`-generated TTV models of AU Mic b (left) and c (right) projected over 10 yr since last observed transit of the AU Mic system. The observed TTVs (green) are included with the model (black), with $P_{\mathrm{d}} = 5.07$ days (first row), 5.39 days (second row), 5.64 days (third row), 5.86 days (fourth row), 6.20 days (fifth row), 6.47 days (sixth row), 11.9 days (seventh row), 12.6 days (eighth row), and 14.1 days (ninth row).

**Table A1**
Exo-Striker-Generated Best-fit and MCMC Modeling Parameters for $P_d = 5.08$ Days

| Parameter | Unit | Best Fit | | | MCMC | | |
|---|---|---|---|---|---|---|---|
| | | AU Mic b | AU Mic c | AU Mic d | AU Mic b | AU Mic c | AU Mic d |
| $K$ | m s$^{-1}$ | 3.35536 | 0.22986 | 0.50720 | 2.87947 ± 0.34321 | 3.60029 ± 3.44133 | 0.41877 ± 0.04442 |
| $P_{orb}$ | day | 8.46351 | 18.86127 | 5.07706 | 8.46331 ± 0.00010 | 18.86102 ± 0.00029 | 5.07701 ± 0.00017 |
| $e$ | ... | 0.00000 | 0.00592 | 0.00016 | 0.04872 ± 0.04662 | 0.00103 ± 0.00159 | 0.04209 ± 0.03778 |
| $\omega$ | deg | 98.37057 | 223.59289 | 152.78962 | 98.57816 ± 2.54783 | 223.75374 ± 1.77297 | 144.16841 ± 2.43169 |
| $M_0$ | deg | 351.61077 | 0.00025 | 268.90220 | 350.54357 ± 1.58108 | 0.24484 ± 0.20155 | 274.43129 ± 10.64027 |
| $i$ | deg | 89.57924 | 89.43188 | 77.33666 | 89.48110 ± 0.31229 | 89.39871 ± 0.42666 | 76.88456 ± 3.04551 |
| $\Omega$ | deg | 23.10249 | 22.62173 | 8.17561 | 19.11756 ± 0.53911 | 20.71402 ± 3.01682 | 2.55408 ± 1.56684 |
| $\chi^2$ | ... | 114.02094 | 11.26343 | ... | 106.79515 | 18.02865 | ... |
| $\chi^2_{red}$ | ... | 5.22018 | 31.32109 | ... | 5.20099 | 31.20595 | ... |
| $\ln \mathcal{L}$ | ... | | 209.46399 | | | 219.96553 | |
| BIC | ... | | -337.19975 | | | -358.20283 | |
| AIC$_c$ | ... | | -342.70576 | | | -363.70884 | |

**Note.** The $K$'s listed here are unconstrained, but see Section 6 for discussion regarding the planets' low $K$'s generated by Exo-Striker.

**Table A2**
Exo-Striker-generated Best-fit and MCMC Modeling Parameters for $P_d = 5.39$ Days

| Parameter | Unit | Best Fit | | | MCMC | | |
|---|---|---|---|---|---|---|---|
| | | AU Mic b | AU Mic c | AU Mic d | AU Mic b | AU Mic c | AU Mic d |
| $K$ | m s$^{-1}$ | 5.16537 | 0.50637 | 0.34978 | 0.10817 ± 1.90115 | 2.00680 ± 1.92941 | 0.32173 ± 0.01505 |
| $P_{orb}$ | day | 8.46341 | 18.86196 | 5.38693 | 8.46327 ± 0.00008 | 18.85933 ± 0.00107 | 5.38888 ± 0.00188 |
| $e$ | ... | 0.00001 | 0.07780 | 0.00299 | 0.02897 ± 0.02697 | 0.07978 ± 0.01753 | 0.08579 ± 0.07529 |
| $\omega$ | deg | 98.55512 | 217.22994 | 161.43928 | 97.22742 ± 1.87410 | 216.68146 ± 1.23336 | 166.41581 ± 15.66255 |
| $M_0$ | deg | 351.43634 | 0.00001 | 265.97175 | 352.33787 ± 4.06365 | 0.36773 ± 0.32286 | 265.55255 ± 9.64814 |
| $i$ | deg | 89.57209 | 89.42620 | 61.86109 | 89.79654 ± 0.61080 | 89.68914 ± 0.70596 | 57.18937 ± 1.827605 |
| $\Omega$ | deg | 55.99639 | 58.92122 | 2.10453 | 43.45119 ± 7.68065 | 81.23160 ± 27.93638 | 6.51204 ± 6.20803 |
| $\chi^2$ | ... | 115.39770 | 5.10544 | ... | 105.90689 | 10.01490 | ... |
| $\chi^2_{red}$ | ... | 5.02096 | 30.12578 | ... | 4.83007 | 28.98045 | ... |
| $\ln \mathcal{L}$ | ... | | 211.88028 | | | 225.96977 | |
| BIC | ... | | -342.03233 | | | -370.21131 | |
| AIC$_c$ | ... | | -347.53834 | | | -375.71732 | |

**Note.** The $K$'s listed here are unconstrained, but see Section 6 for discussion regarding the planets' low $K$'s generated by Exo-Striker.

**Table A3**
Exo-Striker-generated Best-fit and MCMC Modeling Parameters for $P_d = 5.64$ Days

| Parameter | Unit | Best Fit | | | MCMC | | |
|---|---|---|---|---|---|---|---|
| | | AU Mic b | AU Mic c | AU Mic d | AU Mic b | AU Mic c | AU Mic d |
| $K$ | m s$^{-1}$ | 4.40058 | 0.46675 | 0.33788 | 2.56609 ± 0.74131 | 0.32794 ± 0.14726 | 0.26404 ± 0.02325 |
| $P_{orb}$ | day | 8.46339 | 18.86185 | 5.63768 | 8.46351 ± 0.00020 | 18.86055 ± 0.00059 | 5.63897 ± 0.00207 |
| $e$ | ... | 0.00000 | 0.00677 | 0.00029 | 0.00179 ± 0.00085 | 0.03117 ± 0.02806 | 0.00997 ± 0.00676 |
| $\omega$ | deg | 98.50502 | 223.51766 | 166.51374 | 91.68412 ± 3.26572 | 220.60684 ± 1.08879 | 179.09135 ± 17.81811 |
| $M_0$ | deg | 351.47597 | 0.00094 | 241.03825 | 358.29595 ± 11.06134 | 0.80625 ± 0.74415 | 228.08583 ± 7.13443 |
| $i$ | deg | 89.52517 | 89.43744 | 87.60186 | 89.38133 ± 0.21181 | 89.48992 ± 0.50234 | 90.07831 ± 4.98962 |
| $\Omega$ | deg | 30.10388 | 28.65682 | 9.84080 | 31.92354 ± 5.43454 | 30.65984 ± 7.23061 | 11.45968 ± 7.13193 |
| $\chi^2$ | ... | 113.88847 | 11.22925 | ... | 115.86957 | 11.71456 | ... |
| $\chi^2_{red}$ | ... | 5.21324 | 31.27943 | ... | 5.31601 | 31.89603 | ... |
| $\ln \mathcal{L}$ | ... | | 209.53001 | | | 219.12889 | |
| BIC | ... | | -337.33179 | | | -356.52955 | |
| AIC$_c$ | ... | | -342.83780 | | | -362.03556 | |

**Note.** The $K$'s listed here are unconstrained, but see Section 6 for discussion regarding the planets' low $K$'s generated by Exo-Striker.

**Table A4**
Exo-Striker-generated Best-fit and MCMC Modeling Parameters for $P_{\rm d} = 5.86$ Days

| Parameter | Unit | Best Fit | | | MCMC | | |
|---|---|---|---|---|---|---|---|
| | | AU Mic b | AU Mic c | AU Mic d | AU Mic b | AU Mic c | AU Mic d |
| $K$ | m s$^{-1}$ | 2.16456 | 0.23630 | 0.53136 | $0.03744 \pm 0.66777$ | $1.01987 \pm 0.81217$ | $0.57447 \pm 0.12867$ |
| $P_{\rm orb}$ | day | 8.46367 | 18.86055 | 5.86086 | $8.46369 \pm 0.00009$ | $18.85928 \pm 0.00036$ | $5.86210 \pm 0.00231$ |
| $e$ | ... | 0.00000 | 0.00311 | 0.00003 | $0.00129 \pm 0.00025$ | $0.01538 \pm 0.01280$ | $0.00011 \pm 0.00110$ |
| $\omega$ | deg | 98.48083 | 223.82709 | 164.24881 | $102.58694 \pm 7.62158$ | $222.06323 \pm 0.41503$ | $168.01295 \pm 16.83654$ |
| $M_0$ | deg | 351.49999 | 0.00131 | 231.06872 | $347.37523 \pm 0.39120$ | $0.73499 \pm 0.65918$ | $216.24219 \pm 3.82607$ |
| $i$ | deg | 89.55965 | 89.42747 | 95.02796 | $89.64773 \pm 0.46690$ | $89.32042 \pm 0.32416$ | $99.58862 \pm 6.78176$ |
| $\Omega$ | deg | 29.19644 | 28.21852 | 15.22950 | $68.15507 \pm 45.50567$ | $25.26173 \pm 5.59688$ | $57.61649 \pm 48.55583$ |
| $\chi^2$ | ... | 102.74262 | 11.75572 | ... | 100.82281 | 13.43211 | ... |
| $\chi^2_{\rm red}$ | ... | 4.77076 | 28.62458 | ... | 4.76062 | 28.56373 | ... |
| $\ln \mathcal{L}$ | ... | | 214.83902 | | | 226.99616 | |
| BIC | ... | | -347.94981 | | | -372.26409 | |
| AIC$_c$ | ... | | -353.45582 | | | -377.77010 | |

**Note.** The $K$'s listed here are unconstrained, but see Section 6 for discussion regarding the planets' low $K$'s generated by Exo-Striker.

**Table A5**
Exo-Striker-generated Best-fit and MCMC Modeling Parameters for $P_{\rm d} = 6.20$ Days

| Parameter | Unit | Best Fit | | | MCMC | | |
|---|---|---|---|---|---|---|---|
| | | AU Mic b | AU Mic c | AU Mic d | AU Mic b | AU Mic c | AU Mic d |
| $K$ | m s$^{-1}$ | 2.90791 | 0.46992 | 0.26161 | $2.45919 \pm 0.14618$ | $0.49589 \pm 0.28947$ | $0.47104 \pm 0.24820$ |
| $P_{\rm orb}$ | day | 8.46343 | 18.86090 | 6.20441 | $8.46362 \pm 0.00029$ | $18.86047 \pm 0.00004$ | $6.20494 \pm 0.00105$ |
| $e$ | ... | 0.00000 | 0.01115 | 0.00018 | $0.00452 \pm 0.00323$ | $0.01386 \pm 0.00986$ | $0.02737 \pm 0.02352$ |
| $\omega$ | deg | 98.48979 | 223.15789 | 160.36483 | $99.85587 \pm 4.41672$ | $222.82523 \pm 1.52204$ | $194.59296 \pm 41.32711$ |
| $M_0$ | deg | 351.49117 | 0.00036 | 238.43986 | $350.03934 \pm 2.04421$ | $0.09010 \pm 0.04308$ | $184.33273 \pm 46.79969$ |
| $i$ | deg | 89.55720 | 89.42914 | 94.74564 | $89.82232 \pm 0.65141$ | $88.96846 \pm 0.01337$ | $107.15764 \pm 14.18751$ |
| $\Omega$ | deg | 24.51329 | 12.84297 | 4.91602 | $13.49562 \pm 8.12320$ | $12.11611 \pm 3.83135$ | $2.67773 \pm 0.61209$ |
| $\chi^2$ | ... | 107.43664 | 11.84116 | ... | 99.94369 | 10.06389 | ... |
| $\chi^2_{\rm red}$ | ... | 4.96991 | 29.81945 | ... | 4.58365 | 27.50189 | ... |
| $\ln \mathcal{L}$ | ... | | 212.45061 | | | 227.07288 | |
| BIC | ... | | -343.17299 | | | -372.41753 | |
| AIC$_c$ | ... | | -348.67900 | | | -377.92354 | |

**Note.** The $K$'s listed here are unconstrained, but see Section 6 for discussion regarding the planets' low $K$'s generated by Exo-Striker.

**Table A6**
Exo-Striker-generated Best-fit and MCMC Modeling Parameters for $P_{\rm d} = 6.47$ Days

| Parameter | Unit | Best Fit | | | MCMC | | |
|---|---|---|---|---|---|---|---|
| | | AU Mic b | AU Mic c | AU Mic d | AU Mic b | AU Mic c | AU Mic d |
| $K$ | m s$^{-1}$ | 5.22397 | 0.51394 | 0.30268 | $2.24280 \pm 0.60448$ | $0.44272 \pm 0.19449$ | $0.27380 \pm 0.05928$ |
| $P_{\rm orb}$ | day | 8.46343 | 18.86244 | 6.47074 | $8.46352 \pm 0.00016$ | $18.86056 \pm 0.00033$ | $6.47251 \pm 0.00249$ |
| $e$ | ... | 0.00000 | 0.00442 | 0.00023 | $0.02862 \pm 0.02473$ | $0.00453 \pm 0.00215$ | $0.01002 \pm 0.00819$ |
| $\omega$ | deg | 98.49871 | 223.71495 | 166.62198 | $99.63829 \pm 3.59581$ | $223.56221 \pm 1.61921$ | $178.62168 \pm 17.77984$ |
| $M_0$ | deg | 351.48520 | 0.00062 | 248.45972 | $349.79295 \pm 0.95313$ | $0.15047 \pm 0.08931$ | $236.71532 \pm 4.90333$ |
| $i$ | deg | 89.57471 | 89.46389 | 94.91569 | $89.45294 \pm 0.26172$ | $89.25326 \pm 0.26737$ | $93.57266 \pm 3.26340$ |
| $\Omega$ | deg | 27.67490 | 19.55833 | 10.23918 | $20.65656 \pm 1.45446$ | $17.43367 \pm 3.48630$ | $11.01673 \pm 5.42317$ |
| $\chi^2$ | ... | 109.38331 | 11.23694 | ... | 97.94533 | 13.80731 | ... |
| $\chi^2_{\rm red}$ | ... | 5.02584 | 30.15506 | ... | 4.65636 | 27.93816 | ... |
| $\ln \mathcal{L}$ | ... | | 211.87437 | | | 227.18419 | |
| BIC | ... | | -342.02051 | | | -372.64015 | |
| AIC$_c$ | ... | | -347.52652 | | | -378.14616 | |

**Note.** The $K$'s listed here are unconstrained, but see Section 6 for discussion regarding the planets' low $K$'s generated by Exo-Striker.

**Table A7**
Exo-Striker-generated Best-fit and MCMC Modeling Parameters for $P_d = 11.9$ Days

| Parameter | Unit | Best Fit | | | MCMC | | |
|---|---|---|---|---|---|---|---|
| | | AU Mic b | AU Mic c | AU Mic d | AU Mic b | AU Mic c | AU Mic d |
| $K$ | m s$^{-1}$ | 0.97504 | 0.38690 | 0.17182 | $1.24696 \pm 0.65028$ | $0.02093 \pm 0.13709$ | $0.17048 \pm 0.03388$ |
| $P_{\rm orb}$ | day | 8.46331 | 18.85981 | 11.86306 | $8.46333 \pm 0.00005$ | $18.85996 \pm 0.00043$ | $11.86292 \pm 0.00406$ |
| $e$ | ... | 0.00000 | 0.00109 | 0.00000 | $0.00018 \pm 0.00189$ | $0.00385 \pm 0.00196$ | $0.00051 \pm 0.00087$ |
| $\omega$ | deg | 89.99086 | 223.99440 | 160.83877 | $89.81844 \pm 1.31482$ | $223.69121 \pm 2.55320$ | $160.94662 \pm 2.61504$ |
| $M_0$ | deg | 0.00005 | 0.00014 | 0.00032 | $0.17304 \pm 0.06999$ | $0.06776 \pm 0.02942$ | $0.01696 \pm 0.13710$ |
| $i$ | deg | 89.58985 | 89.43145 | 82.02998 | $89.50347 \pm 0.29017$ | $89.33758 \pm 0.31993$ | $81.88651 \pm 0.63757$ |
| $\Omega$ | deg | 0.00012 | 0.00000 | 0.00000 | $0.00494 \pm 0.12589$ | $0.01833 \pm 0.09216$ | $0.11655 \pm 0.03333$ |
| $\chi^2$ | ... | 112.83347 | 11.27744 | ... | 113.01980 | 11.41707 | ... |
| $\chi^2_{\rm red}$ | ... | 5.17129 | 31.02773 | ... | 5.18487 | 31.10922 | ... |
| $\ln \mathcal{L}$ | ... | | 210.00233 | | | 221.62352 | |
| BIC | ... | | -338.27643 | | | -361.51881 | |
| AIC$_c$ | ... | | -343.78244 | | | -367.02482 | |

**Note.** The $K$'s listed here are unconstrained, but see Section 6 for discussion regarding the planets' low $K$'s generated by Exo-Striker.

**Table A8**
Exo-Striker-generated Best-fit and MCMC Modeling Parameters for $P_d = 12.6$ Days

| Parameter | Unit | Best Fit | | | MCMC | | |
|---|---|---|---|---|---|---|---|
| | | AU Mic b | AU Mic c | AU Mic d | AU Mic b | AU Mic c | AU Mic d |
| $K$ | m s$^{-1}$ | 2.90332 | 0.48084 | 0.18469 | $1.25408 \pm 0.39741$ | $0.03573 \pm 0.07120$ | $0.22424 \pm 0.06278$ |
| $P_{\rm orb}$ | day | 8.46334 | 18.86145 | 12.64081 | $8.46333 \pm 0.00004$ | $18.86027 \pm 0.00009$ | $12.64921 \pm 0.00874$ |
| $e$ | ... | 0.00849 | 0.00278 | 0.00341 | $0.00646 \pm 0.00045$ | $0.00257 \pm 0.00086$ | $0.00000 \pm 0.00039$ |
| $\omega$ | deg | 89.99407 | 223.85721 | 174.65177 | $88.35089 \pm 0.42306$ | $223.25926 \pm 2.84483$ | $174.35726 \pm 4.76760$ |
| $M_0$ | deg | 0.00002 | 0.00048 | 0.00012 | $1.65671 \pm 1.52820$ | $0.60281 \pm 0.41896$ | $2.35570 \pm 2.16294$ |
| $i$ | deg | 89.57125 | 89.43113 | 89.06083 | $89.58284 \pm 0.38234$ | $89.45028 \pm 0.41961$ | $89.63258 \pm 1.70943$ |
| $\Omega$ | deg | 0.00001 | 0.00000 | 0.00000 | $2.17332 \pm 2.01326$ | $0.78666 \pm 0.62801$ | $0.15814 \pm 0.01661$ |
| $\chi^2$ | ... | 114.85574 | 7.30405 | ... | 113.68872 | 7.65425 | ... |
| $\chi^2_{\rm red}$ | ... | 5.08999 | 30.53995 | ... | 5.05596 | 30.33574 | ... |
| $\ln \mathcal{L}$ | ... | | 211.03081 | | | 222.91190 | |
| BIC | ... | | -340.33339 | | | -364.09557 | |
| AIC$_c$ | ... | | -345.83940 | | | -369.60158 | |

**Note.** The $K$'s listed here are unconstrained, but see Section 6 for discussion regarding the planets' low $K$'s generated by Exo-Striker.

**Table A9**
Exo-Striker-generated Best-fit and MCMC Modeling Parameters for $P_d = 14.1$ Days

| Parameter | Unit | Best Fit | | | MCMC | | |
|---|---|---|---|---|---|---|---|
| | | AU Mic b | AU Mic c | AU Mic d | AU Mic b | AU Mic c | AU Mic d |
| $K$ | m s$^{-1}$ | 1.94679 | 0.79913 | 0.23459 | $0.53676 \pm 0.09009$ | $1.45679 \pm 1.21270$ | $0.25084 \pm 0.03547$ |
| $P_{\rm orb}$ | day | 8.46336 | 18.85942 | 14.07157 | $8.46335 \pm 0.00002$ | $18.85837 \pm 0.00013$ | $14.07595 \pm 0.00724$ |
| $e$ | ... | 0.01119 | 0.00631 | 0.00109 | $0.04387 \pm 0.03502$ | $0.00142 \pm 0.00394$ | $0.00120 \pm 0.00028$ |
| $\omega$ | deg | 89.99234 | 223.54696 | 173.15636 | $89.68870 \pm 0.98273$ | $223.47563 \pm 2.72212$ | $174.56600 \pm 4.52321$ |
| $M_0$ | deg | 0.00001 | 0.00034 | 0.00010 | $0.33416 \pm 0.23087$ | $0.46562 \pm 0.31050$ | $2.71969 \pm 2.57135$ |
| $i$ | deg | 89.47507 | 89.44010 | 75.59741 | $89.63164 \pm 0.44523$ | $89.25623 \pm 0.21991$ | $74.27032 \pm 0.40173$ |
| $\Omega$ | deg | 0.00000 | 0.00000 | 0.00000 | $3.15613 \pm 3.01037$ | $1.28301 \pm 1.15840$ | $0.55842 \pm 0.42973$ |
| $\chi^2$ | ... | 116.76747 | 3.09309 | ... | 112.45805 | 2.94137 | ... |
| $\chi^2_{\rm red}$ | ... | 4.99419 | 29.96514 | ... | 4.80831 | 28.84985 | ... |
| $\ln \mathcal{L}$ | ... | | 212.13172 | | | 226.37031 | |
| BIC | ... | | -342.53521 | | | -371.01239 | |
| AIC$_c$ | ... | | -348.04122 | | | -376.51840 | |

**Note.** The $K$'s listed here are unconstrained, but see Section 6 for discussion regarding the planets' low $K$'s generated by Exo-Striker.

**Table A10**
List of Predicted Midpoint Times in BJD for AU Mic b (After Accounting for TTVs) Over the Next Three Years (Part I)

| $P_d = 5.08$ days | $P_d = 5.39$ days | $P_d = 5.64$ days | $P_d = 5.86$ days | $P_d = 6.20$ days |
|---|---|---|---|---|
| 2460310.79154 ± 0.02340 | 2460310.78763 ± 0.01872 | 2460310.93889 ± 0.04680 | 2460310.88002 ± 0.02106 | 2460310.86700 ± 0.06786 |
| 2460319.25458 ± 0.02350 | 2460319.25095 ± 0.01880 | 2460319.40485 ± 0.04700 | 2460319.34368 ± 0.02115 | 2460319.33064 ± 0.06815 |
| 2460327.71804 ± 0.02360 | 2460327.71452 ± 0.01888 | 2460327.87082 ± 0.04720 | 2460327.80741 ± 0.02124 | 2460327.79364 ± 0.06844 |
| 2460336.18110 ± 0.02370 | 2460336.17825 ± 0.01896 | 2460336.33675 ± 0.04740 | 2460336.27118 ± 0.02133 | 2460336.25668 ± 0.06873 |
| 2460344.64459 ± 0.02380 | 2460344.64199 ± 0.01904 | 2460344.80265 ± 0.04760 | 2460344.73512 ± 0.02142 | 2460344.72013 ± 0.06902 |
| 2460353.10786 ± 0.02390 | 2460353.10580 ± 0.01912 | 2460353.26849 ± 0.04780 | 2460353.19922 ± 0.02151 | 2460353.18421 ± 0.06931 |
| 2460361.57145 ± 0.02400 | 2460361.56936 ± 0.01920 | 2460361.73427 ± 0.04800 | 2460361.66304 ± 0.02160 | 2460361.64811 ± 0.06960 |
| 2460370.03469 ± 0.02410 | 2460370.03278 ± 0.01928 | 2460370.19998 ± 0.04820 | 2460370.12646 ± 0.02169 | 2460370.11201 ± 0.06989 |
| 2460378.49828 ± 0.02420 | 2460378.49640 ± 0.01936 | 2460378.66560 ± 0.04840 | 2460378.59002 ± 0.02178 | 2460378.57573 ± 0.07018 |
| 2460386.96159 ± 0.02430 | 2460386.95994 ± 0.01944 | 2460387.13115 ± 0.04860 | 2460387.05323 ± 0.02187 | 2460387.03920 ± 0.07047 |
| 2460395.42481 ± 0.02440 | 2460395.42333 ± 0.01952 | 2460395.59662 ± 0.04880 | 2460395.51698 ± 0.02196 | 2460395.50235 ± 0.07076 |
| 2460403.88841 ± 0.02450 | 2460403.88681 ± 0.01960 | 2460404.06208 ± 0.04900 | 2460403.98082 ± 0.02205 | 2460403.96615 ± 0.07105 |
| 2460412.35159 ± 0.02460 | 2460412.35041 ± 0.01968 | 2460412.52738 ± 0.04920 | 2460412.44467 ± 0.02214 | 2460412.43004 ± 0.07134 |
| 2460420.81518 ± 0.02470 | 2460420.81415 ± 0.01976 | 2460420.99267 ± 0.04940 | 2460420.90872 ± 0.02223 | 2460420.89319 ± 0.07163 |
| 2460429.27859 ± 0.02480 | 2460429.27787 ± 0.01984 | 2460429.45779 ± 0.04960 | 2460429.37297 ± 0.02232 | 2460429.35645 ± 0.07192 |
| 2460437.74230 ± 0.02490 | 2460437.74135 ± 0.01992 | 2460437.92285 ± 0.04980 | 2460437.83701 ± 0.02241 | 2460437.82002 ± 0.07221 |
| 2460446.20564 ± 0.02500 | 2460446.20485 ± 0.02000 | 2460446.38774 ± 0.05000 | 2460446.30059 ± 0.02250 | 2460446.28426 ± 0.07250 |
| 2460454.66949 ± 0.02510 | 2460454.66833 ± 0.02008 | 2460454.85251 ± 0.05020 | 2460454.76424 ± 0.02259 | 2460454.74828 ± 0.07279 |
| 2460463.13292 ± 0.02520 | 2460463.13172 ± 0.02016 | 2460463.31713 ± 0.05040 | 2460463.22757 ± 0.02268 | 2460463.21231 ± 0.07308 |
| 2460471.59633 ± 0.02530 | 2460471.59544 ± 0.02024 | 2460471.78164 ± 0.05060 | 2460471.69149 ± 0.02277 | 2460471.67619 ± 0.07337 |
| 2460480.06005 ± 0.02540 | 2460480.05920 ± 0.02032 | 2460480.24605 ± 0.05080 | 2460480.15552 ± 0.02286 | 2460480.13991 ± 0.07366 |
| 2460488.52335 ± 0.02550 | 2460488.52269 ± 0.02040 | 2460488.71030 ± 0.05100 | 2460488.61950 ± 0.02295 | 2460488.60321 ± 0.07395 |
| 2460496.98704 ± 0.02560 | 2460496.98634 ± 0.02048 | 2460497.17447 ± 0.05120 | 2460497.08361 ± 0.02304 | 2460497.06726 ± 0.07424 |
| 2460505.45054 ± 0.02570 | 2460505.45012 ± 0.02056 | 2460505.63849 ± 0.05140 | 2460505.54795 ± 0.02313 | 2460505.53132 ± 0.07453 |
| 2460513.91434 ± 0.02580 | 2460513.91388 ± 0.02064 | 2460514.10239 ± 0.05160 | 2460514.01220 ± 0.02322 | 2460513.99467 ± 0.07482 |
| 2460522.37779 ± 0.02590 | 2460522.37766 ± 0.02072 | 2460522.56610 ± 0.05180 | 2460522.47594 ± 0.02331 | 2460522.45808 ± 0.07511 |
| 2460530.84178 ± 0.02600 | 2460530.84125 ± 0.02080 | 2460531.02967 ± 0.05200 | 2460530.93972 ± 0.02340 | 2460530.92182 ± 0.07540 |
| 2460539.30532 ± 0.02610 | 2460539.30476 ± 0.02088 | 2460539.49307 ± 0.05220 | 2460539.40317 ± 0.02349 | 2460539.38615 ± 0.07569 |
| 2460547.76895 ± 0.02620 | 2460547.76855 ± 0.02096 | 2460547.95635 ± 0.05240 | 2460547.86722 ± 0.02358 | 2460547.85031 ± 0.07598 |
| 2460556.23269 ± 0.02630 | 2460556.23214 ± 0.02104 | 2460556.41945 ± 0.05260 | 2460556.33140 ± 0.02367 | 2460556.31450 ± 0.07627 |
| 2460564.69612 ± 0.02640 | 2460564.69540 ± 0.02112 | 2460564.88244 ± 0.05280 | 2460564.79548 ± 0.02376 | 2460564.77852 ± 0.07656 |
| 2460573.15988 ± 0.02650 | 2460573.15890 ± 0.02120 | 2460573.34534 ± 0.05300 | 2460573.25962 ± 0.02385 | 2460573.24241 ± 0.07685 |
| 2460581.62343 ± 0.02660 | 2460581.62253 ± 0.02128 | 2460581.80808 ± 0.05320 | 2460581.72393 ± 0.02394 | 2460581.70586 ± 0.07714 |
| 2460590.08726 ± 0.02670 | 2460590.08624 ± 0.02136 | 2460590.27072 ± 0.05340 | 2460590.18822 ± 0.02403 | 2460590.17012 ± 0.07743 |
| 2460598.55080 ± 0.02680 | 2460598.54997 ± 0.02144 | 2460598.73317 ± 0.05360 | 2460598.65214 ± 0.02412 | 2460598.63431 ± 0.07772 |
| 2460607.01483 ± 0.02690 | 2460607.01342 ± 0.02152 | 2460607.19552 ± 0.05380 | 2460607.11609 ± 0.02421 | 2460607.09781 ± 0.07801 |
| 2460615.47840 ± 0.02700 | 2460615.47669 ± 0.02160 | 2460615.65771 ± 0.05400 | 2460615.57963 ± 0.02430 | 2460615.56131 ± 0.07830 |
| 2460623.94226 ± 0.02710 | 2460623.94002 ± 0.02168 | 2460624.11977 ± 0.05420 | 2460624.04371 ± 0.02439 | 2460624.02512 ± 0.07859 |
| 2460632.40598 ± 0.02720 | 2460632.40333 ± 0.02176 | 2460632.58167 ± 0.05440 | 2460632.50792 ± 0.02448 | 2460632.48959 ± 0.07888 |
| 2460640.86950 ± 0.02730 | 2460640.86665 ± 0.02184 | 2460641.04349 ± 0.05460 | 2460640.97210 ± 0.02457 | 2460640.95386 ± 0.07917 |
| 2460649.33327 ± 0.02740 | 2460649.33003 ± 0.02192 | 2460649.50523 ± 0.05480 | 2460649.43629 ± 0.02466 | 2460649.41819 ± 0.07946 |
| 2460657.79684 ± 0.02750 | 2460657.79339 ± 0.02200 | 2460657.96686 ± 0.05500 | 2460657.90053 ± 0.02475 | 2460657.88231 ± 0.07975 |
| 2460666.26065 ± 0.02760 | 2460666.25692 ± 0.02208 | 2460666.42842 ± 0.05520 | 2460666.36474 ± 0.02484 | 2460666.34630 ± 0.08004 |
| 2460674.72419 ± 0.02770 | 2460674.72036 ± 0.02216 | 2460674.88986 ± 0.05540 | 2460674.82873 ± 0.02493 | 2460674.80991 ± 0.08033 |
| 2460683.18821 ± 0.02780 | 2460683.18361 ± 0.02224 | 2460683.35122 ± 0.05560 | 2460683.29284 ± 0.02502 | 2460683.27418 ± 0.08062 |
| 2460691.65174 ± 0.02790 | 2460691.64697 ± 0.02232 | 2460691.81248 ± 0.05580 | 2460691.75647 ± 0.02511 | 2460691.73852 ± 0.08091 |
| 2460700.11571 ± 0.02800 | 2460700.11020 ± 0.02240 | 2460700.27363 ± 0.05600 | 2460700.22052 ± 0.02520 | 2460700.20200 ± 0.08120 |
| 2460708.57941 ± 0.02810 | 2460708.57332 ± 0.02248 | 2460708.73470 ± 0.05620 | 2460708.68470 ± 0.02529 | 2460708.66557 ± 0.08149 |
| 2460717.04299 ± 0.02820 | 2460717.03680 ± 0.02256 | 2460717.19570 ± 0.05640 | 2460717.14898 ± 0.02538 | 2460717.12943 ± 0.08178 |
| 2460725.50671 ± 0.02830 | 2460725.50029 ± 0.02264 | 2460725.65668 ± 0.05660 | 2460725.61326 ± 0.02547 | 2460725.59397 ± 0.08207 |
| 2460733.97025 ± 0.02840 | 2460733.96330 ± 0.02272 | 2460734.11758 ± 0.05680 | 2460734.07740 ± 0.02556 | 2460734.05828 ± 0.08236 |
| 2460742.43400 ± 0.02850 | 2460742.42651 ± 0.02280 | 2460742.57852 ± 0.05700 | 2460742.54148 ± 0.02565 | 2460742.52266 ± 0.08265 |
| 2460750.89748 ± 0.02860 | 2460750.88996 ± 0.02288 | 2460751.03936 ± 0.05720 | 2460751.00541 ± 0.02574 | 2460750.98679 ± 0.08294 |
| 2460759.36144 ± 0.02870 | 2460759.35342 ± 0.02296 | 2460759.50024 ± 0.05740 | 2460759.46964 ± 0.02583 | 2460759.45084 ± 0.08323 |
| 2460767.82489 ± 0.02880 | 2460767.81683 ± 0.02304 | 2460767.96102 ± 0.05760 | 2460767.93336 ± 0.02592 | 2460767.91438 ± 0.08352 |
| 2460776.28881 ± 0.02890 | 2460776.28002 ± 0.02312 | 2460776.42181 ± 0.05780 | 2460776.39737 ± 0.02601 | 2460776.37865 ± 0.08381 |
| 2460784.75245 ± 0.02900 | 2460784.74313 ± 0.02320 | 2460784.88254 ± 0.05800 | 2460784.86151 ± 0.02610 | 2460784.84292 ± 0.08410 |
| 2460793.21611 ± 0.02910 | 2460793.20634 ± 0.02328 | 2460793.34328 ± 0.05820 | 2460793.32578 ± 0.02619 | 2460793.30642 ± 0.08439 |
| 2460801.67968 ± 0.02920 | 2460801.66937 ± 0.02336 | 2460801.80400 ± 0.05840 | 2460801.79003 ± 0.02628 | 2460801.76998 ± 0.08468 |
| 2460810.14318 ± 0.02930 | 2460810.13226 ± 0.02344 | 2460810.26476 ± 0.05860 | 2460810.25404 ± 0.02637 | 2460810.23389 ± 0.08497 |
| 2460818.60682 ± 0.02940 | 2460818.59531 ± 0.02352 | 2460818.72558 ± 0.05880 | 2460818.71797 ± 0.02646 | 2460818.69842 ± 0.08526 |
| 2460827.07017 ± 0.02950 | 2460827.05838 ± 0.02360 | 2460827.18640 ± 0.05900 | 2460827.18170 ± 0.02655 | 2460827.16273 ± 0.08555 |
| 2460835.53400 ± 0.02960 | 2460835.52160 ± 0.02368 | 2460835.64730 ± 0.05920 | 2460835.64585 ± 0.02664 | 2460835.62707 ± 0.08584 |
| 2460843.99736 ± 0.02970 | 2460843.98483 ± 0.02376 | 2460844.10818 ± 0.05940 | 2460844.10963 ± 0.02673 | 2460844.09111 ± 0.08613 |

**Table A10**
(Continued)

| $P_d = 5.08$ days | $P_d = 5.39$ days | $P_d = 5.64$ days | $P_d = 5.86$ days | $P_d = 6.20$ days |
|---|---|---|---|---|
| 2460852.46114 ± 0.02980 | 2460852.44773 ± 0.02384 | 2460852.56913 ± 0.05960 | 2460852.57361 ± 0.02682 | 2460852.55501 ± 0.08642 |
| 2460860.92465 ± 0.02990 | 2460860.91051 ± 0.02392 | 2460861.03006 ± 0.05980 | 2460861.03768 ± 0.02691 | 2460861.01849 ± 0.08671 |
| 2460869.38834 ± 0.03000 | 2460869.37345 ± 0.02400 | 2460869.49108 ± 0.06000 | 2460869.50184 ± 0.02700 | 2460869.48264 ± 0.08700 |
| 2460877.85175 ± 0.03010 | 2460877.83630 ± 0.02408 | 2460877.95210 ± 0.06020 | 2460877.96596 ± 0.02709 | 2460877.94681 ± 0.08729 |
| 2460886.31518 ± 0.03020 | 2460886.29928 ± 0.02416 | 2460886.41321 ± 0.06040 | 2460886.42987 ± 0.02718 | 2460886.41026 ± 0.08758 |
| 2460894.77867 ± 0.03030 | 2460894.76232 ± 0.02424 | 2460894.87439 ± 0.06060 | 2460894.89369 ± 0.02727 | 2460894.87378 ± 0.08787 |
| 2460903.24188 ± 0.03040 | 2460903.22526 ± 0.02432 | 2460903.33566 ± 0.06080 | 2460903.35724 ± 0.02736 | 2460903.33759 ± 0.08816 |
| 2460911.70554 ± 0.03050 | 2460911.68830 ± 0.02440 | 2460911.79703 ± 0.06100 | 2460911.82122 ± 0.02745 | 2460911.80212 ± 0.08845 |
| 2460920.16876 ± 0.03060 | 2460920.15136 ± 0.02448 | 2460920.25847 ± 0.06120 | 2460920.28496 ± 0.02754 | 2460920.26633 ± 0.08874 |
| 2460928.63236 ± 0.03070 | 2460928.61446 ± 0.02456 | 2460928.71997 ± 0.06140 | 2460928.74890 ± 0.02763 | 2460928.73053 ± 0.08903 |
| 2460937.09570 ± 0.03080 | 2460937.07762 ± 0.02464 | 2460937.18155 ± 0.06160 | 2460937.21290 ± 0.02772 | 2460937.19443 ± 0.08932 |
| 2460945.55932 ± 0.03090 | 2460945.54050 ± 0.02472 | 2460945.64317 ± 0.06180 | 2460945.67694 ± 0.02781 | 2460945.65814 ± 0.08961 |
| 2460954.02259 ± 0.03100 | 2460954.00333 ± 0.02480 | 2460954.10489 ± 0.06200 | 2460954.14093 ± 0.02790 | 2460954.12149 ± 0.08990 |
| 2460962.48599 ± 0.03110 | 2460962.46653 ± 0.02488 | 2460962.56664 ± 0.06220 | 2460962.60472 ± 0.02799 | 2460962.58542 ± 0.09019 |
| 2460970.94928 ± 0.03120 | 2460970.92961 ± 0.02496 | 2460971.02854 ± 0.06240 | 2460971.06843 ± 0.02808 | 2460971.04954 ± 0.09048 |
| 2460979.41236 ± 0.03130 | 2460979.39222 ± 0.02504 | 2460979.49049 ± 0.06260 | 2460979.53180 ± 0.02817 | 2460979.51282 ± 0.09077 |
| 2460987.87583 ± 0.03140 | 2460987.85523 ± 0.02512 | 2460987.95263 ± 0.06280 | 2460987.99555 ± 0.02826 | 2460987.97629 ± 0.09106 |
| 2460996.33887 ± 0.03150 | 2460996.31841 ± 0.02520 | 2460996.41476 ± 0.06300 | 2460996.45914 ± 0.02835 | 2460996.44001 ± 0.09135 |
| 2461004.80231 ± 0.03160 | 2461004.78156 ± 0.02528 | 2461004.87708 ± 0.06320 | 2461004.92297 ± 0.02844 | 2461004.90439 ± 0.09164 |
| 2461013.26548 ± 0.03170 | 2461013.24474 ± 0.02536 | 2461013.33939 ± 0.06340 | 2461013.38690 ± 0.02853 | 2461013.36842 ± 0.09193 |
| 2461021.72894 ± 0.03180 | 2461021.70771 ± 0.02544 | 2461021.80186 ± 0.06360 | 2461021.85087 ± 0.02862 | 2461021.83240 ± 0.09222 |
| 2461030.19206 ± 0.03190 | 2461030.17054 ± 0.02552 | 2461030.26431 ± 0.06380 | 2461030.31475 ± 0.02871 | 2461030.29610 ± 0.09251 |
| 2461038.65547 ± 0.03200 | 2461038.63342 ± 0.02560 | 2461038.72692 ± 0.06400 | 2461038.77832 ± 0.02880 | 2461038.75964 ± 0.09280 |
| 2461047.11853 ± 0.03210 | 2461047.09637 ± 0.02568 | 2461047.18953 ± 0.06420 | 2461047.24181 ± 0.02889 | 2461047.22275 ± 0.09309 |
| 2461055.58151 ± 0.03220 | 2461055.55922 ± 0.02576 | 2461055.65232 ± 0.06440 | 2461055.70502 ± 0.02898 | 2461055.68655 ± 0.09338 |
| 2461064.04481 ± 0.03230 | 2461064.02212 ± 0.02584 | 2461064.11518 ± 0.06460 | 2461064.16859 ± 0.02907 | 2461064.15048 ± 0.09367 |
| 2461072.50768 ± 0.03240 | 2461072.48504 ± 0.02592 | 2461072.57815 ± 0.06480 | 2461072.63200 ± 0.02916 | 2461072.61368 ± 0.09396 |
| 2461080.97095 ± 0.03250 | 2461080.94821 ± 0.02600 | 2461081.04121 ± 0.06500 | 2461081.09561 ± 0.02925 | 2461081.07701 ± 0.09425 |
| 2461089.43397 ± 0.03260 | 2461089.41134 ± 0.02608 | 2461089.50438 ± 0.06520 | 2461089.55943 ± 0.02934 | 2461089.54061 ± 0.09454 |
| 2461097.89726 ± 0.03270 | 2461097.87420 ± 0.02616 | 2461097.96760 ± 0.06540 | 2461098.02335 ± 0.02943 | 2461098.00475 ± 0.09483 |
| 2461106.36021 ± 0.03280 | 2461106.33721 ± 0.02624 | 2461106.43092 ± 0.06560 | 2461106.48715 ± 0.02952 | 2461106.46863 ± 0.09512 |
| 2461114.82363 ± 0.03290 | 2461114.80020 ± 0.02632 | 2461114.89427 ± 0.06580 | 2461114.95046 ± 0.02961 | 2461114.93241 ± 0.09541 |
| 2461123.28654 ± 0.03300 | 2461123.26304 ± 0.02640 | 2461123.35775 ± 0.06600 | 2461123.41373 ± 0.02970 | 2461123.39588 ± 0.09570 |
| 2461131.74947 ± 0.03310 | 2461131.72622 ± 0.02648 | 2461131.82127 ± 0.06620 | 2461131.87685 ± 0.02979 | 2461131.85921 ± 0.09599 |
| 2461140.21262 ± 0.03320 | 2461140.18948 ± 0.02656 | 2461140.28495 ± 0.06640 | 2461140.34037 ± 0.02988 | 2461140.32220 ± 0.09628 |
| 2461148.67535 ± 0.03330 | 2461148.65246 ± 0.02664 | 2461148.74866 ± 0.06660 | 2461148.80366 ± 0.02997 | 2461148.78585 ± 0.09657 |
| 2461157.13848 ± 0.03340 | 2461157.11560 ± 0.02672 | 2461157.21260 ± 0.06680 | 2461157.26706 ± 0.03006 | 2461157.24968 ± 0.09686 |
| 2461165.60138 ± 0.03350 | 2461165.57900 ± 0.02680 | 2461165.67653 ± 0.06700 | 2461165.73073 ± 0.03015 | 2461165.71273 ± 0.09715 |
| 2461174.06453 ± 0.03360 | 2461174.04240 ± 0.02688 | 2461174.14063 ± 0.06720 | 2461174.19464 ± 0.03024 | 2461174.17589 ± 0.09744 |
| 2461182.52733 ± 0.03370 | 2461182.50579 ± 0.02696 | 2461182.60471 ± 0.06740 | 2461182.65840 ± 0.03033 | 2461182.63925 ± 0.09773 |
| 2461190.99071 ± 0.03380 | 2461190.96895 ± 0.02704 | 2461191.06898 ± 0.06760 | 2461191.12155 ± 0.03042 | 2461191.10326 ± 0.09802 |
| 2461199.45355 ± 0.03390 | 2461199.43211 ± 0.02712 | 2461199.53324 ± 0.06780 | 2461199.58469 ± 0.03051 | 2461199.56693 ± 0.09831 |
| 2461207.91651 ± 0.03400 | 2461207.89552 ± 0.02720 | 2461207.99766 ± 0.06800 | 2461208.04767 ± 0.03060 | 2461208.03053 ± 0.09860 |
| 2461216.37955 ± 0.03410 | 2461216.35878 ± 0.02728 | 2461216.46209 ± 0.06820 | 2461216.51115 ± 0.03069 | 2461216.49390 ± 0.09889 |
| 2461224.84222 ± 0.03420 | 2461224.82180 ± 0.02736 | 2461224.92673 ± 0.06840 | 2461224.97436 ± 0.03078 | 2461224.95709 ± 0.09918 |
| 2461233.30525 ± 0.03430 | 2461233.28507 ± 0.02744 | 2461233.39144 ± 0.06860 | 2461233.43759 ± 0.03087 | 2461233.42002 ± 0.09947 |
| 2461241.76807 ± 0.03440 | 2461241.74844 ± 0.02752 | 2461241.85627 ± 0.06880 | 2461241.90106 ± 0.03096 | 2461241.88353 ± 0.09976 |
| 2461250.23114 ± 0.03450 | 2461250.21189 ± 0.02760 | 2461250.32117 ± 0.06900 | 2461250.36491 ± 0.03105 | 2461250.34730 ± 0.10005 |
| 2461258.69388 ± 0.03460 | 2461258.67546 ± 0.02768 | 2461258.78620 ± 0.06920 | 2461258.82862 ± 0.03114 | 2461258.81013 ± 0.10034 |
| 2461267.15716 ± 0.03470 | 2461267.13873 ± 0.02776 | 2461267.25128 ± 0.06940 | 2461267.29175 ± 0.03123 | 2461267.27313 ± 0.10063 |
| 2461275.61998 ± 0.03480 | 2461275.60190 ± 0.02784 | 2461275.71645 ± 0.06960 | 2461275.75484 ± 0.03132 | 2461275.73636 ± 0.10092 |
| 2461284.08306 ± 0.03490 | 2461284.06520 ± 0.02792 | 2461284.18165 ± 0.06980 | 2461284.21766 ± 0.03141 | 2461284.20017 ± 0.10121 |
| 2461292.54600 ± 0.03500 | 2461292.52846 ± 0.02800 | 2461292.64698 ± 0.07000 | 2461292.68107 ± 0.03150 | 2461292.66371 ± 0.10150 |
| 2461301.00873 ± 0.03510 | 2461300.99178 ± 0.02808 | 2461301.11237 ± 0.07020 | 2461301.14431 ± 0.03159 | 2461301.12721 ± 0.10179 |
| 2461309.47170 ± 0.03520 | 2461309.45517 ± 0.02816 | 2461309.57791 ± 0.07040 | 2461309.60750 ± 0.03168 | 2461309.59054 ± 0.10208 |
| 2461317.93449 ± 0.03530 | 2461317.91857 ± 0.02824 | 2461318.04346 ± 0.07060 | 2461318.07084 ± 0.03177 | 2461318.05369 ± 0.10237 |
| 2461326.39753 ± 0.03540 | 2461326.38216 ± 0.02832 | 2461326.50919 ± 0.07080 | 2461326.53460 ± 0.03186 | 2461326.51652 ± 0.10266 |
| 2461334.86029 ± 0.03550 | 2461334.84575 ± 0.02840 | 2461334.97491 ± 0.07100 | 2461334.99829 ± 0.03195 | 2461334.98001 ± 0.10295 |
| 2461343.32352 ± 0.03560 | 2461343.30924 ± 0.02848 | 2461343.44073 ± 0.07120 | 2461343.46150 ± 0.03204 | 2461343.44360 ± 0.10324 |
| 2461351.78632 ± 0.03570 | 2461351.77279 ± 0.02856 | 2461351.90655 ± 0.07140 | 2461351.92463 ± 0.03213 | 2461351.90640 ± 0.10353 |
| 2461360.24955 ± 0.03580 | 2461360.23620 ± 0.02864 | 2461360.37245 ± 0.07160 | 2461360.38737 ± 0.03222 | 2461360.36925 ± 0.10382 |
| 2461368.71249 ± 0.03590 | 2461368.69954 ± 0.02872 | 2461368.83834 ± 0.07180 | 2461368.85075 ± 0.03231 | 2461368.83239 ± 0.10411 |
| 2461377.17536 ± 0.03600 | 2461377.16330 ± 0.02880 | 2461377.30429 ± 0.07200 | 2461377.31410 ± 0.03240 | 2461377.29611 ± 0.10440 |
| 2461385.63833 ± 0.03610 | 2461385.62704 ± 0.02888 | 2461385.77028 ± 0.07220 | 2461385.77738 ± 0.03249 | 2461385.75965 ± 0.10469 |

**Table A10**
(Continued)

| $P_d = 5.08$ days | $P_d = 5.39$ days | $P_d = 5.64$ days | $P_d = 5.86$ days | $P_d = 6.20$ days |
|---|---|---|---|---|
| 2461394.10116 ± 0.03620 | 2461394.09039 ± 0.02896 | 2461394.23630 ± 0.07240 | 2461394.24072 ± 0.03258 | 2461394.22317 ± 0.10498 |
| 2461402.56424 ± 0.03630 | 2461402.55399 ± 0.02904 | 2461402.70241 ± 0.07260 | 2461402.70443 ± 0.03267 | 2461402.68653 ± 0.10527 |

**Note.** The columns are for each three-planet configuration.

**Table A11**
List of Predicted Midpoint Times in BJD for AU Mic b (After Accounting for TTVs) Over the Next Three Years (Part II)

| $P_d = 6.47$ days | $P_d = 11.9$ days | $P_d = 12.6$ days | $P_d = 12.7$ days | $P_d = 14.1$ days |
|---|---|---|---|---|
| 2460310.84935 ± 0.03744 | 2460310.79751 ± 0.01171 | 2460310.78970 ± 0.00937 | 2460310.73989 ± 0.01405 | 2460310.79791 ± 0.00470 |
| 2460319.31324 ± 0.03760 | 2460319.26066 ± 0.01176 | 2460319.25322 ± 0.00941 | 2460319.20283 ± 0.01411 | 2460319.26120 ± 0.00472 |
| 2460327.77704 ± 0.03776 | 2460327.72416 ± 0.01181 | 2460327.71651 ± 0.00945 | 2460327.66589 ± 0.01417 | 2460327.72462 ± 0.00474 |
| 2460336.24126 ± 0.03792 | 2460336.18739 ± 0.01186 | 2460336.17972 ± 0.00949 | 2460336.12873 ± 0.01423 | 2460336.18794 ± 0.00476 |
| 2460344.70557 ± 0.03808 | 2460344.65064 ± 0.01191 | 2460344.64333 ± 0.00953 | 2460344.59174 ± 0.01429 | 2460344.65158 ± 0.00478 |
| 2460353.16872 ± 0.03824 | 2460353.11392 ± 0.01196 | 2460353.10664 ± 0.00957 | 2460353.05484 ± 0.01435 | 2460353.11501 ± 0.00480 |
| 2460361.63262 ± 0.03840 | 2460361.57714 ± 0.01201 | 2460361.56992 ± 0.00961 | 2460361.51776 ± 0.01441 | 2460361.57852 ± 0.00482 |
| 2460370.09642 ± 0.03856 | 2460370.04046 ± 0.01206 | 2460370.03356 ± 0.00965 | 2460369.98073 ± 0.01447 | 2460370.04188 ± 0.00484 |
| 2460378.56013 ± 0.03872 | 2460378.50369 ± 0.01211 | 2460378.49690 ± 0.00969 | 2460378.44389 ± 0.01453 | 2460378.50539 ± 0.00486 |
| 2460387.02382 ± 0.03888 | 2460386.96730 ± 0.01216 | 2460386.96022 ± 0.00973 | 2460386.90681 ± 0.01459 | 2460386.96899 ± 0.00488 |
| 2460395.48733 ± 0.03904 | 2460395.43065 ± 0.01221 | 2460395.42389 ± 0.00977 | 2460395.36982 ± 0.01465 | 2460395.43250 ± 0.00490 |
| 2460403.95106 ± 0.03920 | 2460403.89401 ± 0.01226 | 2460403.88729 ± 0.00981 | 2460403.83303 ± 0.01471 | 2460403.89609 ± 0.00492 |
| 2460412.41477 ± 0.03936 | 2460412.35744 ± 0.01231 | 2460412.35063 ± 0.00985 | 2460412.29602 ± 0.01477 | 2460412.35952 ± 0.00494 |
| 2460420.87841 ± 0.03952 | 2460420.82077 ± 0.01236 | 2460420.81439 ± 0.00989 | 2460420.75912 ± 0.01483 | 2460420.82320 ± 0.00496 |
| 2460429.34214 ± 0.03968 | 2460429.28420 ± 0.01241 | 2460429.27781 ± 0.00993 | 2460429.22237 ± 0.01489 | 2460429.28685 ± 0.00498 |
| 2460437.80578 ± 0.03984 | 2460437.74755 ± 0.01246 | 2460437.74121 ± 0.00997 | 2460437.68546 ± 0.01495 | 2460437.75058 ± 0.00500 |
| 2460446.26979 ± 0.04000 | 2460446.21127 ± 0.01251 | 2460446.20502 ± 0.01001 | 2460446.14854 ± 0.01501 | 2460446.21409 ± 0.00502 |
| 2460454.73380 ± 0.04016 | 2460454.67471 ± 0.01256 | 2460454.66846 ± 0.01005 | 2460454.61185 ± 0.01507 | 2460454.67774 ± 0.00504 |
| 2460463.19677 ± 0.04032 | 2460463.13818 ± 0.01261 | 2460463.13191 ± 0.01009 | 2460463.07496 ± 0.01513 | 2460463.14134 ± 0.00506 |
| 2460471.66050 ± 0.04048 | 2460471.60173 ± 0.01266 | 2460471.59572 ± 0.01013 | 2460471.53807 ± 0.01519 | 2460471.60507 ± 0.00508 |
| 2460480.12424 ± 0.04064 | 2460480.06515 ± 0.01271 | 2460480.05920 ± 0.01017 | 2460480.00142 ± 0.01524 | 2460480.06882 ± 0.00509 |
| 2460488.58781 ± 0.04080 | 2460488.52869 ± 0.01276 | 2460488.52268 ± 0.01021 | 2460488.46458 ± 0.01530 | 2460488.53238 ± 0.00511 |
| 2460497.05144 ± 0.04096 | 2460496.99216 ± 0.01281 | 2460496.98653 ± 0.01025 | 2460496.92778 ± 0.01536 | 2460496.99611 ± 0.00513 |
| 2460505.51486 ± 0.04112 | 2460505.45592 ± 0.01286 | 2460505.45005 ± 0.01029 | 2460505.39118 ± 0.01542 | 2460505.45977 ± 0.00515 |
| 2460513.97852 ± 0.04128 | 2460513.91947 ± 0.01291 | 2460513.91355 ± 0.01033 | 2460513.85445 ± 0.01548 | 2460513.92369 ± 0.00517 |
| 2460522.44213 ± 0.04144 | 2460522.38303 ± 0.01296 | 2460522.37746 ± 0.01037 | 2460522.31766 ± 0.01554 | 2460522.38736 ± 0.00519 |
| 2460530.90564 ± 0.04160 | 2460530.84670 ± 0.01301 | 2460530.84100 ± 0.01041 | 2460530.78110 ± 0.01560 | 2460530.85110 ± 0.00521 |
| 2460539.36925 ± 0.04176 | 2460539.31022 ± 0.01306 | 2460539.30455 ± 0.01045 | 2460539.24439 ± 0.01566 | 2460539.31473 ± 0.00523 |
| 2460547.83269 ± 0.04192 | 2460547.77383 ± 0.01311 | 2460547.76846 ± 0.01049 | 2460547.70760 ± 0.01572 | 2460547.77847 ± 0.00525 |
| 2460556.29656 ± 0.04208 | 2460556.23735 ± 0.01316 | 2460556.23199 ± 0.01053 | 2460556.17106 ± 0.01578 | 2460556.24231 ± 0.00527 |
| 2460564.76038 ± 0.04224 | 2460564.70117 ± 0.01321 | 2460564.69558 ± 0.01057 | 2460564.63441 ± 0.01584 | 2460564.70601 ± 0.00529 |
| 2460573.22328 ± 0.04240 | 2460573.16480 ± 0.01326 | 2460573.15948 ± 0.01061 | 2460573.09770 ± 0.01590 | 2460573.16978 ± 0.00531 |
| 2460581.68696 ± 0.04256 | 2460581.62842 ± 0.01331 | 2460581.62306 ± 0.01065 | 2460581.56119 ± 0.01596 | 2460581.63341 ± 0.00533 |
| 2460590.15066 ± 0.04272 | 2460590.09221 ± 0.01336 | 2460590.08666 ± 0.01069 | 2460590.02465 ± 0.01602 | 2460590.09729 ± 0.00535 |
| 2460598.61418 ± 0.04288 | 2460598.55578 ± 0.01341 | 2460598.55057 ± 0.01073 | 2460598.48796 ± 0.01608 | 2460598.56108 ± 0.00537 |
| 2460607.07774 ± 0.04304 | 2460607.01945 ± 0.01346 | 2460607.01417 ± 0.01077 | 2460606.95148 ± 0.01614 | 2460607.02492 ± 0.00539 |
| 2460615.54107 ± 0.04320 | 2460615.48303 ± 0.01351 | 2460615.47778 ± 0.01081 | 2460615.41496 ± 0.01620 | 2460615.48855 ± 0.00541 |
| 2460624.00461 ± 0.04336 | 2460623.94690 ± 0.01356 | 2460623.94171 ± 0.01085 | 2460623.87825 ± 0.01626 | 2460623.95228 ± 0.00543 |
| 2460632.46811 ± 0.04352 | 2460632.41056 ± 0.01361 | 2460632.40529 ± 0.01089 | 2460632.34177 ± 0.01632 | 2460632.41601 ± 0.00545 |
| 2460640.93147 ± 0.04368 | 2460640.87424 ± 0.01366 | 2460640.86892 ± 0.01093 | 2460640.80527 ± 0.01638 | 2460640.87979 ± 0.00547 |
| 2460649.39501 ± 0.04384 | 2460649.33808 ± 0.01371 | 2460649.33282 ± 0.01097 | 2460649.26860 ± 0.01644 | 2460649.34360 ± 0.00549 |
| 2460657.85836 ± 0.04400 | 2460657.80168 ± 0.01376 | 2460657.79640 ± 0.01101 | 2460657.73213 ± 0.01650 | 2460657.80720 ± 0.00551 |
| 2460666.32220 ± 0.04416 | 2460666.26539 ± 0.01381 | 2460666.26006 ± 0.01105 | 2460666.19574 ± 0.01656 | 2460666.27097 ± 0.00553 |
| 2460674.78595 ± 0.04432 | 2460674.72902 ± 0.01386 | 2460674.72393 ± 0.01109 | 2460674.65909 ± 0.01662 | 2460674.73467 ± 0.00555 |
| 2460683.24876 ± 0.04448 | 2460683.19288 ± 0.01391 | 2460683.18753 ± 0.01113 | 2460683.12264 ± 0.01668 | 2460683.19857 ± 0.00557 |
| 2460691.71237 ± 0.04464 | 2460691.65657 ± 0.01396 | 2460691.65116 ± 0.01117 | 2460691.58628 ± 0.01674 | 2460691.66221 ± 0.00559 |
| 2460700.17595 ± 0.04480 | 2460700.12027 ± 0.01401 | 2460700.11502 ± 0.01121 | 2460700.04960 ± 0.01680 | 2460700.12591 ± 0.00561 |
| 2460708.63936 ± 0.04496 | 2460708.58414 ± 0.01406 | 2460708.57860 ± 0.01125 | 2460708.51311 ± 0.01686 | 2460708.58950 ± 0.00563 |
| 2460717.10277 ± 0.04512 | 2460717.04777 ± 0.01411 | 2460717.04223 ± 0.01129 | 2460716.97674 ± 0.01692 | 2460717.05318 ± 0.00565 |
| 2460725.56600 ± 0.04528 | 2460725.51149 ± 0.01416 | 2460725.50607 ± 0.01133 | 2460725.44004 ± 0.01698 | 2460725.51699 ± 0.00567 |
| 2460734.02943 ± 0.04544 | 2460733.97511 ± 0.01421 | 2460733.96961 ± 0.01137 | 2460733.90355 ± 0.01704 | 2460733.98056 ± 0.00569 |

**Table A11**
(Continued)

| $P_d = 6.47$ days | $P_d = 11.9$ days | $P_d = 12.6$ days | $P_d = 12.7$ days | $P_d = 14.1$ days |
|---|---|---|---|---|
| 2460742.49287 ± 0.04560 | 2460742.43894 ± 0.01426 | 2460742.43324 ± 0.01141 | 2460742.36724 ± 0.01710 | 2460742.44424 ± 0.00571 |
| 2460750.95615 ± 0.04576 | 2460750.90264 ± 0.01431 | 2460750.89702 ± 0.01145 | 2460750.83058 ± 0.01716 | 2460750.90779 ± 0.00573 |
| 2460759.41965 ± 0.04592 | 2460759.36633 ± 0.01436 | 2460759.36056 ± 0.01149 | 2460759.29408 ± 0.01722 | 2460759.37155 ± 0.00575 |
| 2460767.88292 ± 0.04608 | 2460767.83024 ± 0.01441 | 2460767.82417 ± 0.01153 | 2460767.75781 ± 0.01728 | 2460767.83520 ± 0.00577 |
| 2460776.34666 ± 0.04624 | 2460776.29385 ± 0.01446 | 2460776.28790 ± 0.01157 | 2460776.22112 ± 0.01734 | 2460776.29886 ± 0.00579 |
| 2460784.81033 ± 0.04640 | 2460784.75755 ± 0.01451 | 2460784.75142 ± 0.01161 | 2460784.68457 ± 0.01740 | 2460784.76233 ± 0.00581 |
| 2460793.27293 ± 0.04656 | 2460793.22114 ± 0.01456 | 2460793.21500 ± 0.01165 | 2460793.14831 ± 0.01746 | 2460793.22589 ± 0.00583 |
| 2460801.73641 ± 0.04672 | 2460801.68494 ± 0.01461 | 2460801.67868 ± 0.01169 | 2460801.61153 ± 0.01752 | 2460801.68947 ± 0.00585 |
| 2460810.19978 ± 0.04688 | 2460810.14860 ± 0.01466 | 2460810.14215 ± 0.01173 | 2460810.07496 ± 0.01758 | 2460810.15305 ± 0.00587 |
| 2460818.66308 ± 0.04704 | 2460818.61227 ± 0.01471 | 2460818.60571 ± 0.01177 | 2460818.53869 ± 0.01764 | 2460818.61663 ± 0.00589 |
| 2460827.12638 ± 0.04720 | 2460827.07617 ± 0.01476 | 2460827.06935 ± 0.01181 | 2460827.00194 ± 0.01770 | 2460827.08002 ± 0.00591 |
| 2460835.58954 ± 0.04736 | 2460835.53973 ± 0.01481 | 2460835.53278 ± 0.01185 | 2460835.46535 ± 0.01776 | 2460835.54362 ± 0.00593 |
| 2460844.05285 ± 0.04752 | 2460844.00339 ± 0.01486 | 2460843.99631 ± 0.01189 | 2460843.92911 ± 0.01782 | 2460844.00710 ± 0.00595 |
| 2460852.51616 ± 0.04768 | 2460852.46696 ± 0.01491 | 2460852.45988 ± 0.01193 | 2460852.39237 ± 0.01788 | 2460852.47074 ± 0.00597 |
| 2460860.97929 ± 0.04784 | 2460860.93068 ± 0.01496 | 2460860.92327 ± 0.01197 | 2460860.85569 ± 0.01794 | 2460860.93411 ± 0.00599 |
| 2460869.44260 ± 0.04800 | 2460869.39429 ± 0.01501 | 2460869.38677 ± 0.01201 | 2460869.31948 ± 0.01800 | 2460869.39753 ± 0.00601 |
| 2460877.90573 ± 0.04816 | 2460877.85790 ± 0.01506 | 2460877.85026 ± 0.01205 | 2460877.78262 ± 0.01806 | 2460877.86090 ± 0.00603 |
| 2460886.36929 ± 0.04832 | 2460886.32173 ± 0.01511 | 2460886.31362 ± 0.01209 | 2460886.24591 ± 0.01812 | 2460886.32432 ± 0.00605 |
| 2460894.83290 ± 0.04848 | 2460894.78525 ± 0.01516 | 2460894.77706 ± 0.01213 | 2460894.70966 ± 0.01818 | 2460894.78785 ± 0.00607 |
| 2460903.29534 ± 0.04864 | 2460903.24885 ± 0.01521 | 2460903.24051 ± 0.01217 | 2460903.17278 ± 0.01824 | 2460903.25111 ± 0.00609 |
| 2460911.75861 ± 0.04880 | 2460911.71234 ± 0.01525 | 2460911.70381 ± 0.01221 | 2460911.63606 ± 0.01830 | 2460911.71449 ± 0.00611 |
| 2460920.22174 ± 0.04896 | 2460920.17596 ± 0.01530 | 2460920.16722 ± 0.01225 | 2460920.09978 ± 0.01836 | 2460920.17780 ± 0.00613 |
| 2460928.68486 ± 0.04912 | 2460928.63951 ± 0.01535 | 2460928.63060 ± 0.01229 | 2460928.56294 ± 0.01842 | 2460928.64127 ± 0.00615 |
| 2460937.14796 ± 0.04928 | 2460937.10302 ± 0.01540 | 2460937.09386 ± 0.01233 | 2460937.02610 ± 0.01848 | 2460937.10462 ± 0.00617 |
| 2460945.61089 ± 0.04944 | 2460945.56682 ± 0.01545 | 2460945.55723 ± 0.01237 | 2460945.48986 ± 0.01854 | 2460945.56792 ± 0.00619 |
| 2460954.07397 ± 0.04960 | 2460954.03026 ± 0.01550 | 2460954.02053 ± 0.01241 | 2460953.95291 ± 0.01860 | 2460954.03107 ± 0.00621 |
| 2460962.53698 ± 0.04976 | 2460962.49376 ± 0.01555 | 2460962.48374 ± 0.01245 | 2460962.41603 ± 0.01866 | 2460962.49433 ± 0.00623 |
| 2460970.99987 ± 0.04992 | 2460970.95715 ± 0.01560 | 2460970.94706 ± 0.01249 | 2460970.87976 ± 0.01872 | 2460970.95765 ± 0.00625 |
| 2460979.46290 ± 0.05008 | 2460979.42066 ± 0.01565 | 2460979.41031 ± 0.01253 | 2460979.34272 ± 0.01878 | 2460979.42091 ± 0.00627 |
| 2460987.92586 ± 0.05024 | 2460987.88411 ± 0.01570 | 2460987.87348 ± 0.01257 | 2460987.80584 ± 0.01884 | 2460987.88414 ± 0.00629 |
| 2460996.38929 ± 0.05040 | 2460996.34754 ± 0.01575 | 2460996.33675 ± 0.01261 | 2460996.26948 ± 0.01890 | 2460996.34721 ± 0.00631 |
| 2461004.85287 ± 0.05056 | 2461004.81128 ± 0.01580 | 2461004.79995 ± 0.01265 | 2461004.73249 ± 0.01896 | 2461004.81053 ± 0.00633 |
| 2461013.31520 ± 0.05072 | 2461013.27459 ± 0.01585 | 2461013.26307 ± 0.01269 | 2461013.19552 ± 0.01902 | 2461013.27371 ± 0.00635 |
| 2461021.77810 ± 0.05088 | 2461021.73799 ± 0.01590 | 2461021.72630 ± 0.01273 | 2461021.65914 ± 0.01908 | 2461021.73704 ± 0.00637 |
| 2461030.24085 ± 0.05104 | 2461030.20129 ± 0.01595 | 2461030.18944 ± 0.01277 | 2461030.12209 ± 0.01914 | 2461030.20006 ± 0.00639 |
| 2461038.70360 ± 0.05120 | 2461038.66465 ± 0.01600 | 2461038.65252 ± 0.01281 | 2461038.58500 ± 0.01920 | 2461038.66313 ± 0.00641 |
| 2461047.16640 ± 0.05136 | 2461047.12799 ± 0.01605 | 2461047.11571 ± 0.01285 | 2461047.04861 ± 0.01926 | 2461047.12626 ± 0.00643 |
| 2461055.62901 ± 0.05152 | 2461055.59132 ± 0.01610 | 2461055.57879 ± 0.01289 | 2461055.51146 ± 0.01932 | 2461055.58939 ± 0.00645 |
| 2461064.09182 ± 0.05168 | 2461064.05491 ± 0.01615 | 2461064.04184 ± 0.01293 | 2461063.97438 ± 0.01938 | 2461064.05263 ± 0.00647 |
| 2461072.55449 ± 0.05184 | 2461072.51814 ± 0.01620 | 2461072.50500 ± 0.01297 | 2461072.43793 ± 0.01944 | 2461072.51557 ± 0.00649 |
| 2461081.01716 ± 0.05200 | 2461080.98144 ± 0.01625 | 2461080.96804 ± 0.01301 | 2461080.90077 ± 0.01950 | 2461080.97866 ± 0.00651 |
| 2461089.47990 ± 0.05216 | 2461089.44462 ± 0.01630 | 2461089.43107 ± 0.01305 | 2461089.36364 ± 0.01956 | 2461089.44173 ± 0.00653 |
| 2461097.94255 ± 0.05232 | 2461097.90785 ± 0.01635 | 2461097.89418 ± 0.01309 | 2461097.82711 ± 0.01962 | 2461097.90493 ± 0.00655 |
| 2461106.40585 ± 0.05248 | 2461106.37107 ± 0.01640 | 2461106.35719 ± 0.01313 | 2461106.28993 ± 0.01968 | 2461106.36801 ± 0.00657 |
| 2461114.86921 ± 0.05264 | 2461114.83426 ± 0.01645 | 2461114.82018 ± 0.01317 | 2461114.75269 ± 0.01974 | 2461114.83102 ± 0.00659 |
| 2461123.33160 ± 0.05280 | 2461123.29777 ± 0.01650 | 2461123.28327 ± 0.01321 | 2461123.21611 ± 0.01980 | 2461123.29390 ± 0.00661 |
| 2461131.79419 ± 0.05296 | 2461131.76089 ± 0.01655 | 2461131.74624 ± 0.01325 | 2461131.67887 ± 0.01986 | 2461131.75694 ± 0.00663 |
| 2461140.25667 ± 0.05312 | 2461140.22407 ± 0.01660 | 2461140.20922 ± 0.01329 | 2461140.14158 ± 0.01992 | 2461140.22005 ± 0.00665 |
| 2461148.71921 ± 0.05328 | 2461148.68713 ± 0.01665 | 2461148.67228 ± 0.01333 | 2461148.60500 ± 0.01998 | 2461148.68307 ± 0.00667 |
| 2461157.18188 ± 0.05344 | 2461157.15023 ± 0.01670 | 2461157.13523 ± 0.01337 | 2461157.06772 ± 0.02004 | 2461157.14606 ± 0.00669 |
| 2461165.64434 ± 0.05360 | 2461165.61334 ± 0.01675 | 2461165.59821 ± 0.01341 | 2461165.53044 ± 0.02010 | 2461165.60892 ± 0.00671 |
| 2461174.10701 ± 0.05376 | 2461174.07643 ± 0.01680 | 2461174.06125 ± 0.01345 | 2461173.99378 ± 0.02016 | 2461174.07206 ± 0.00673 |
| 2461182.56948 ± 0.05392 | 2461182.53987 ± 0.01685 | 2461182.52418 ± 0.01349 | 2461182.45648 ± 0.02022 | 2461182.53503 ± 0.00675 |
| 2461191.03200 ± 0.05408 | 2461191.00286 ± 0.01690 | 2461190.98716 ± 0.01353 | 2461190.91915 ± 0.02028 | 2461190.99817 ± 0.00677 |
| 2461199.49456 ± 0.05424 | 2461199.46592 ± 0.01695 | 2461199.45018 ± 0.01357 | 2461199.38238 ± 0.02034 | 2461199.46100 ± 0.00679 |
| 2461207.95684 ± 0.05440 | 2461207.92889 ± 0.01700 | 2461207.91309 ± 0.01361 | 2461207.84507 ± 0.02040 | 2461207.92387 ± 0.00681 |
| 2461216.42012 ± 0.05456 | 2461216.39186 ± 0.01705 | 2461216.37607 ± 0.01365 | 2461216.30762 ± 0.02046 | 2461216.38691 ± 0.00683 |
| 2461224.88339 ± 0.05472 | 2461224.85489 ± 0.01710 | 2461224.83909 ± 0.01369 | 2461224.77088 ± 0.02052 | 2461224.84988 ± 0.00685 |
| 2461233.34610 ± 0.05488 | 2461233.31789 ± 0.01715 | 2461233.30200 ± 0.01373 | 2461233.23354 ± 0.02058 | 2461233.31298 ± 0.00687 |
| 2461241.80881 ± 0.05504 | 2461241.78120 ± 0.01720 | 2461241.76500 ± 0.01377 | 2461241.69614 ± 0.02064 | 2461241.77581 ± 0.00689 |
| 2461250.27142 ± 0.05520 | 2461250.24414 ± 0.01725 | 2461250.22803 ± 0.01381 | 2461250.15938 ± 0.02070 | 2461250.23877 ± 0.00691 |
| 2461258.73411 ± 0.05536 | 2461258.70713 ± 0.01730 | 2461258.69093 ± 0.01385 | 2461258.62200 ± 0.02076 | 2461258.70177 ± 0.00693 |
| 2461267.19692 ± 0.05552 | 2461267.17002 ± 0.01735 | 2461267.15396 ± 0.01389 | 2461267.08460 ± 0.02082 | 2461267.16489 ± 0.00695 |
| 2461275.65950 ± 0.05568 | 2461275.63291 ± 0.01740 | 2461275.61697 ± 0.01393 | 2461275.54770 ± 0.02088 | 2461275.62786 ± 0.00697 |

**Table A11**
(Continued)

| $P_d = 6.47$ days | $P_d = 11.9$ days | $P_d = 12.6$ days | $P_d = 12.7$ days | $P_d = 14.1$ days |
|---|---|---|---|---|
| 2461284.12226 ± 0.05584 | 2461284.09587 ± 0.01745 | 2461284.07987 ± 0.01397 | 2461284.01035 ± 0.02094 | 2461284.09079 ± 0.00699 |
| 2461292.58481 ± 0.05600 | 2461292.55878 ± 0.01750 | 2461292.54293 ± 0.01401 | 2461292.47286 ± 0.02100 | 2461292.55364 ± 0.00701 |
| 2461301.04749 ± 0.05616 | 2461301.02204 ± 0.01755 | 2461301.00595 ± 0.01405 | 2461300.93593 ± 0.02106 | 2461301.01667 ± 0.00703 |
| 2461309.51024 ± 0.05632 | 2461309.48494 ± 0.01760 | 2461309.46888 ± 0.01409 | 2461309.39859 ± 0.02112 | 2461309.47978 ± 0.00705 |
| 2461317.97243 ± 0.05648 | 2461317.94788 ± 0.01765 | 2461317.93197 ± 0.01413 | 2461317.86109 ± 0.02118 | 2461317.94276 ± 0.00707 |
| 2461326.43594 ± 0.05664 | 2461326.41073 ± 0.01770 | 2461326.39500 ± 0.01417 | 2461326.32421 ± 0.02124 | 2461326.40577 ± 0.00709 |
| 2461334.89936 ± 0.05680 | 2461334.87358 ± 0.01775 | 2461334.85795 ± 0.01421 | 2461334.78685 ± 0.02130 | 2461334.86867 ± 0.00711 |
| 2461343.36244 ± 0.05696 | 2461343.33650 ± 0.01780 | 2461343.32108 ± 0.01425 | 2461343.24941 ± 0.02136 | 2461343.33187 ± 0.00713 |
| 2461351.82545 ± 0.05712 | 2461351.79938 ± 0.01785 | 2461351.78414 ± 0.01429 | 2461351.71243 ± 0.02142 | 2461351.79490 ± 0.00715 |
| 2461360.28832 ± 0.05728 | 2461360.26264 ± 0.01790 | 2461360.24709 ± 0.01433 | 2461360.17508 ± 0.02148 | 2461360.25806 ± 0.00717 |
| 2461368.75131 ± 0.05744 | 2461368.72551 ± 0.01795 | 2461368.71027 ± 0.01437 | 2461368.63759 ± 0.02154 | 2461368.72097 ± 0.00719 |
| 2461377.21433 ± 0.05760 | 2461377.18842 ± 0.01800 | 2461377.17334 ± 0.01441 | 2461377.10054 ± 0.02160 | 2461377.18395 ± 0.00721 |
| 2461385.67718 ± 0.05776 | 2461385.65128 ± 0.01805 | 2461385.63632 ± 0.01445 | 2461385.56321 ± 0.02166 | 2461385.64715 ± 0.00723 |
| 2461394.14020 ± 0.05792 | 2461394.11412 ± 0.01810 | 2461394.09956 ± 0.01449 | 2461394.02570 ± 0.02172 | 2461394.11024 ± 0.00725 |
| 2461402.60310 ± 0.05808 | 2461402.57706 ± 0.01815 | 2461402.56265 ± 0.01453 | 2461402.48869 ± 0.02178 | 2461402.57345 ± 0.00727 |

**Note.**The columns are for each three-planet configuration.

**Table A12**
List of Predicted Midpoint Times in BJD for AU Mic c (After Accounting for TTVs) Over the Next Three Years (Part I)

| $P_d = 5.08$ days | $P_d = 5.39$ days | $P_d = 5.64$ days | $P_d = 5.86$ days | $P_d = 6.20$ days |
|---|---|---|---|---|
| 2460322.63096 ± 0.03046 | 2460322.47156 ± 0.11235 | 2460322.58173 ± 0.06196 | 2460322.44772 ± 0.03781 | 2460322.57336 ± 0.00430 |
| 2460341.49211 ± 0.03075 | 2460341.33078 ± 0.11342 | 2460341.44194 ± 0.06255 | 2460341.30710 ± 0.03817 | 2460341.43354 ± 0.00434 |
| 2460360.35401 ± 0.03104 | 2460360.19004 ± 0.11449 | 2460360.30267 ± 0.06314 | 2460360.16643 ± 0.03853 | 2460360.29392 ± 0.00438 |
| 2460379.21496 ± 0.03133 | 2460379.04925 ± 0.11556 | 2460379.16335 ± 0.06373 | 2460379.02565 ± 0.03889 | 2460379.15426 ± 0.00442 |
| 2460398.07527 ± 0.03162 | 2460397.90847 ± 0.11663 | 2460398.02398 ± 0.06432 | 2460397.88484 ± 0.03925 | 2460398.01477 ± 0.00446 |
| 2460416.93603 ± 0.03191 | 2460416.76769 ± 0.11770 | 2460416.88424 ± 0.06491 | 2460416.74416 ± 0.03961 | 2460416.87513 ± 0.00450 |
| 2460435.79777 ± 0.03220 | 2460435.62695 ± 0.11877 | 2460435.74478 ± 0.06550 | 2460435.60353 ± 0.03997 | 2460435.73562 ± 0.00454 |
| 2460454.65919 ± 0.03249 | 2460454.48616 ± 0.11984 | 2460454.60551 ± 0.06609 | 2460454.46282 ± 0.04033 | 2460454.59619 ± 0.00458 |
| 2460473.51959 ± 0.03278 | 2460473.34540 ± 0.12091 | 2460473.46615 ± 0.06668 | 2460473.32202 ± 0.04069 | 2460473.45678 ± 0.00461 |
| 2460492.38011 ± 0.03307 | 2460492.20456 ± 0.12198 | 2460492.32658 ± 0.06727 | 2460492.18124 ± 0.04105 | 2460492.31741 ± 0.00465 |
| 2460511.24151 ± 0.03336 | 2460511.06379 ± 0.12305 | 2460511.18692 ± 0.06786 | 2460511.04060 ± 0.04141 | 2460511.17797 ± 0.00469 |
| 2460530.10326 ± 0.03365 | 2460529.92297 ± 0.12412 | 2460530.04767 ± 0.06845 | 2460529.89995 ± 0.04177 | 2460530.03866 ± 0.00473 |
| 2460548.96396 ± 0.03394 | 2460548.78219 ± 0.12519 | 2460548.90830 ± 0.06904 | 2460548.75920 ± 0.04213 | 2460548.89928 ± 0.00477 |
| 2460567.82431 ± 0.03423 | 2460567.64130 ± 0.12626 | 2460567.76891 ± 0.06963 | 2460567.61837 ± 0.04249 | 2460567.76003 ± 0.00481 |
| 2460586.68528 ± 0.03452 | 2460586.50054 ± 0.12733 | 2460586.62915 ± 0.07022 | 2460586.47766 ± 0.04285 | 2460586.62053 ± 0.00485 |
| 2460605.54716 ± 0.03481 | 2460605.35970 ± 0.12840 | 2460605.48979 ± 0.07081 | 2460605.33703 ± 0.04321 | 2460605.48116 ± 0.00489 |
| 2460624.40832 ± 0.03510 | 2460624.21893 ± 0.12947 | 2460624.35048 ± 0.07140 | 2460624.19635 ± 0.04357 | 2460624.34170 ± 0.00493 |
| 2460643.26861 ± 0.03539 | 2460643.07807 ± 0.13054 | 2460643.21115 ± 0.07199 | 2460643.05555 ± 0.04393 | 2460643.20230 ± 0.00497 |
| 2460662.12924 ± 0.03568 | 2460661.93728 ± 0.13161 | 2460662.07145 ± 0.07258 | 2460661.91476 ± 0.04429 | 2460662.06271 ± 0.00501 |
| 2460680.99090 ± 0.03597 | 2460680.79644 ± 0.13268 | 2460680.93191 ± 0.07317 | 2460680.77409 ± 0.04465 | 2460680.92310 ± 0.00505 |
| 2460699.85248 ± 0.03626 | 2460699.65565 ± 0.13375 | 2460699.79266 ± 0.07376 | 2460699.63346 ± 0.04501 | 2460699.78351 ± 0.00509 |
| 2460718.71294 ± 0.03655 | 2460718.51480 ± 0.13482 | 2460718.65327 ± 0.07435 | 2460718.49273 ± 0.04537 | 2460718.64384 ± 0.00513 |
| 2460737.57340 ± 0.03684 | 2460737.37395 ± 0.13589 | 2460737.51379 ± 0.07494 | 2460737.35192 ± 0.04573 | 2460737.50421 ± 0.00516 |
| 2460756.43466 ± 0.03713 | 2460756.23310 ± 0.13696 | 2460756.37410 ± 0.07553 | 2460756.21117 ± 0.04609 | 2460756.36439 ± 0.00520 |
| 2460775.29646 ± 0.03742 | 2460775.09228 ± 0.13803 | 2460775.23479 ± 0.07612 | 2460775.07053 ± 0.04645 | 2460775.22471 ± 0.00524 |
| 2460794.15730 ± 0.03771 | 2460793.95140 ± 0.13910 | 2460794.09544 ± 0.07671 | 2460793.92987 ± 0.04681 | 2460794.08494 ± 0.00528 |
| 2460813.01766 ± 0.03800 | 2460812.81055 ± 0.14017 | 2460812.95610 ± 0.07730 | 2460812.78909 ± 0.04717 | 2460812.94532 ± 0.00532 |
| 2460831.87850 ± 0.03829 | 2460831.66970 ± 0.14124 | 2460831.81633 ± 0.07789 | 2460831.64829 ± 0.04753 | 2460831.80552 ± 0.00536 |
| 2460850.74029 ± 0.03858 | 2460850.52889 ± 0.14231 | 2460850.67691 ± 0.07848 | 2460850.50759 ± 0.04789 | 2460850.66587 ± 0.00540 |
| 2460869.60163 ± 0.03887 | 2460869.38803 ± 0.14338 | 2460869.53764 ± 0.07907 | 2460869.36697 ± 0.04825 | 2460869.52626 ± 0.00544 |
| 2460888.46196 ± 0.03916 | 2460888.24721 ± 0.14445 | 2460888.39828 ± 0.07966 | 2460888.22627 ± 0.04861 | 2460888.38672 ± 0.00548 |
| 2460907.32249 ± 0.03945 | 2460907.10630 ± 0.14552 | 2460907.25865 ± 0.08025 | 2460907.08546 ± 0.04897 | 2460907.24718 ± 0.00552 |
| 2460926.18402 ± 0.03974 | 2460925.96549 ± 0.14659 | 2460926.11906 ± 0.08084 | 2460925.94469 ± 0.04933 | 2460926.10764 ± 0.00556 |
| 2460945.04575 ± 0.04003 | 2460944.82460 ± 0.14766 | 2460944.97979 ± 0.08143 | 2460944.80403 ± 0.04969 | 2460944.96825 ± 0.00560 |
| 2460963.90632 ± 0.04032 | 2460963.68377 ± 0.14873 | 2460963.84042 ± 0.08202 | 2460963.66339 ± 0.05005 | 2460963.82882 ± 0.00564 |
| 2460982.76670 ± 0.04061 | 2460982.54282 ± 0.14980 | 2460982.70100 ± 0.08261 | 2460982.52263 ± 0.05041 | 2460982.68955 ± 0.00568 |
| 2461001.62781 ± 0.04090 | 2461001.40200 ± 0.15087 | 2461001.56125 ± 0.08320 | 2461001.38183 ± 0.05077 | 2461001.55009 ± 0.00572 |
| 2461020.48965 ± 0.04119 | 2461020.26110 ± 0.15194 | 2461020.42192 ± 0.08379 | 2461020.24110 ± 0.05113 | 2461020.41080 ± 0.00576 |

**Table A12**
(Continued)

| $P_d = 5.08$ days | $P_d = 5.39$ days | $P_d = 5.64$ days | $P_d = 5.86$ days | $P_d = 6.20$ days |
|---|---|---|---|---|
| 2461039.35065 ± 0.04148 | 2461039.12026 ± 0.15301 | 2461039.28260 ± 0.08438 | 2461039.10047 ± 0.05149 | 2461039.27144 ± 0.00580 |
| 2461058.21099 ± 0.04177 | 2461057.97934 ± 0.15408 | 2461058.14325 ± 0.08497 | 2461057.95978 ± 0.05185 | 2461058.13218 ± 0.00583 |
| 2461077.07172 ± 0.04206 | 2461076.83851 ± 0.15515 | 2461077.00352 ± 0.08556 | 2461076.81900 ± 0.05221 | 2461076.99274 ± 0.00587 |
| 2461095.93343 ± 0.04235 | 2461095.69763 ± 0.15622 | 2461095.86406 ± 0.08615 | 2461095.67821 ± 0.05257 | 2461095.85333 ± 0.00591 |
| 2461114.79490 ± 0.04264 | 2461114.55680 ± 0.15729 | 2461114.72476 ± 0.08673 | 2461114.53753 ± 0.05293 | 2461114.71392 ± 0.00595 |
| 2461133.65530 ± 0.04293 | 2461133.41590 ± 0.15836 | 2461133.58542 ± 0.08732 | 2461133.39690 ± 0.05329 | 2461133.57444 ± 0.00599 |
| 2461152.51578 ± 0.04322 | 2461152.27502 ± 0.15943 | 2461152.44587 ± 0.08791 | 2461152.25617 ± 0.05365 | 2461152.43496 ± 0.00603 |
| 2461171.37716 ± 0.04351 | 2461171.13412 ± 0.16050 | 2461171.30617 ± 0.08850 | 2461171.11536 ± 0.05401 | 2461171.29529 ± 0.00607 |
| 2461190.23897 ± 0.04380 | 2461189.99327 ± 0.16157 | 2461190.16692 ± 0.08909 | 2461189.97461 ± 0.05437 | 2461190.15573 ± 0.00611 |
| 2461209.09968 ± 0.04409 | 2461208.85235 ± 0.16264 | 2461209.02757 ± 0.08968 | 2461208.83397 ± 0.05473 | 2461209.01603 ± 0.00615 |
| 2461227.96003 ± 0.04438 | 2461227.71145 ± 0.16371 | 2461227.88819 ± 0.09027 | 2461227.69331 ± 0.05509 | 2461227.87644 ± 0.00619 |
| 2461246.82097 ± 0.04467 | 2461246.57056 ± 0.16478 | 2461246.74842 ± 0.09086 | 2461246.55254 ± 0.05545 | 2461246.73660 ± 0.00623 |
| 2461265.68281 ± 0.04496 | 2461265.42972 ± 0.16585 | 2461265.60905 ± 0.09145 | 2461265.41173 ± 0.05581 | 2461265.59689 ± 0.00627 |
| 2461284.54399 ± 0.04525 | 2461284.28882 ± 0.16692 | 2461284.46973 ± 0.09204 | 2461284.27104 ± 0.05617 | 2461284.45715 ± 0.00631 |
| 2461303.40433 ± 0.04554 | 2461303.14796 ± 0.16799 | 2461303.33042 ± 0.09263 | 2461303.13040 ± 0.05653 | 2461303.31748 ± 0.00635 |
| 2461322.26496 ± 0.04583 | 2461322.00705 ± 0.16906 | 2461322.19073 ± 0.09322 | 2461321.98970 ± 0.05689 | 2461322.17774 ± 0.00639 |
| 2461341.12657 ± 0.04612 | 2461340.86621 ± 0.17013 | 2461341.05116 ± 0.09381 | 2461340.84890 ± 0.05725 | 2461341.03802 ± 0.00643 |
| 2461359.98817 ± 0.04641 | 2461359.72530 ± 0.17120 | 2461359.91190 ± 0.09440 | 2461359.70813 ± 0.05761 | 2461359.89843 ± 0.00647 |
| 2461378.84865 ± 0.04670 | 2461378.58445 ± 0.17227 | 2461378.77255 ± 0.09499 | 2461378.56748 ± 0.05797 | 2461378.75881 ± 0.00651 |
| 2461397.70909 ± 0.04699 | 2461397.44349 ± 0.17334 | 2461397.63308 ± 0.09558 | 2461397.42683 ± 0.05833 | 2461397.61934 ± 0.00655 |

**Note.** The columns are for each three-planet configuration..

**Table A13**
List of Predicted Midpoint Times in BJD for AU Mic c (After Accounting for TTVs) Over the Next Three Years (Part II)

| $P_d = 6.47$ days | $P_d = 11.9$ days | $P_d = 12.6$ days | $P_d = 12.7$ days | $P_d = 14.1$ days |
|---|---|---|---|---|
| 2460322.58254 ± 0.03466 | 2460322.52001 ± 0.04516 | 2460322.40457 ± 0.00950 | 2460322.48933 ± 0.00845 | 2460322.35068 ± 0.01368 |
| 2460341.44311 ± 0.03499 | 2460341.38002 ± 0.04559 | 2460341.26429 ± 0.00959 | 2460341.34919 ± 0.00853 | 2460341.20880 ± 0.01381 |
| 2460360.30406 ± 0.03532 | 2460360.23997 ± 0.04602 | 2460360.12350 ± 0.00967 | 2460360.20886 ± 0.00861 | 2460360.06637 ± 0.01394 |
| 2460379.16458 ± 0.03565 | 2460379.09968 ± 0.04645 | 2460378.98336 ± 0.00976 | 2460379.06903 ± 0.00869 | 2460378.92560 ± 0.01407 |
| 2460398.02486 ± 0.03598 | 2460397.95978 ± 0.04688 | 2460397.84285 ± 0.00985 | 2460397.92928 ± 0.00877 | 2460397.78454 ± 0.01420 |
| 2460416.88527 ± 0.03631 | 2460416.81973 ± 0.04731 | 2460416.70288 ± 0.00994 | 2460416.78973 ± 0.00885 | 2460416.64275 ± 0.01433 |
| 2460435.74612 ± 0.03664 | 2460435.67976 ± 0.04774 | 2460435.56255 ± 0.01003 | 2460435.65028 ± 0.00893 | 2460435.50253 ± 0.01446 |
| 2460454.60686 ± 0.03697 | 2460454.53974 ± 0.04817 | 2460454.42273 ± 0.01012 | 2460454.51091 ± 0.00901 | 2460454.36224 ± 0.01459 |
| 2460473.46716 ± 0.03730 | 2460473.39956 ± 0.04860 | 2460473.28264 ± 0.01021 | 2460473.37153 ± 0.00909 | 2460473.22079 ± 0.01472 |
| 2460492.32752 ± 0.03763 | 2460492.25962 ± 0.04903 | 2460492.14302 ± 0.01030 | 2460492.23213 ± 0.00917 | 2460492.08034 ± 0.01485 |
| 2460511.18822 ± 0.03796 | 2460511.11941 ± 0.04946 | 2460511.00312 ± 0.01039 | 2460511.09259 ± 0.00925 | 2460510.94007 ± 0.01498 |
| 2460530.04912 ± 0.03829 | 2460529.97943 ± 0.04989 | 2460529.86361 ± 0.01048 | 2460529.95282 ± 0.00933 | 2460529.79857 ± 0.01511 |
| 2460548.90954 ± 0.03862 | 2460548.83949 ± 0.05032 | 2460548.72391 ± 0.01057 | 2460548.81303 ± 0.00941 | 2460548.65767 ± 0.01524 |
| 2460567.76986 ± 0.03895 | 2460567.69947 ± 0.05075 | 2460567.58458 ± 0.01066 | 2460567.67272 ± 0.00949 | 2460567.51685 ± 0.01537 |
| 2460586.63036 ± 0.03928 | 2460586.55944 ± 0.05118 | 2460586.44505 ± 0.01075 | 2460586.53264 ± 0.00957 | 2460586.37442 ± 0.01550 |
| 2460605.49129 ± 0.03961 | 2460605.41916 ± 0.05161 | 2460605.30575 ± 0.01084 | 2460605.39167 ± 0.00964 | 2460605.23284 ± 0.01563 |
| 2460624.35189 ± 0.03994 | 2460624.27915 ± 0.05204 | 2460624.16637 ± 0.01093 | 2460624.25136 ± 0.00972 | 2460624.09145 ± 0.01576 |
| 2460643.21215 ± 0.04027 | 2460643.13932 ± 0.05247 | 2460643.02717 ± 0.01102 | 2460643.10988 ± 0.00980 | 2460642.94823 ± 0.01589 |
| 2460662.07253 ± 0.04060 | 2460661.99935 ± 0.05290 | 2460661.88792 ± 0.01111 | 2460661.96939 ± 0.00988 | 2460661.80565 ± 0.01602 |
| 2460680.93334 ± 0.04093 | 2460680.85928 ± 0.05333 | 2460680.74871 ± 0.01120 | 2460680.82762 ± 0.00996 | 2460680.66359 ± 0.01615 |
| 2460699.79415 ± 0.04126 | 2460699.71899 ± 0.05376 | 2460699.60952 ± 0.01129 | 2460699.68702 ± 0.01004 | 2460699.52062 ± 0.01628 |
| 2460718.65448 ± 0.04159 | 2460718.57901 ± 0.05419 | 2460718.47031 ± 0.01138 | 2460718.54524 ± 0.01012 | 2460718.37790 ± 0.01641 |
| 2460737.51484 ± 0.04192 | 2460737.43911 ± 0.05462 | 2460737.33118 ± 0.01147 | 2460737.40466 ± 0.01020 | 2460737.23557 ± 0.01654 |
| 2460756.37547 ± 0.04225 | 2460756.29915 ± 0.05505 | 2460756.19195 ± 0.01156 | 2460756.26311 ± 0.01028 | 2460756.09332 ± 0.01667 |
| 2460775.23639 ± 0.04258 | 2460775.15910 ± 0.05548 | 2460775.05276 ± 0.01165 | 2460775.12264 ± 0.01036 | 2460774.95136 ± 0.01680 |
| 2460794.09687 ± 0.04291 | 2460794.01884 ± 0.05591 | 2460793.91349 ± 0.01174 | 2460793.98152 ± 0.01044 | 2460793.80975 ± 0.01693 |
| 2460812.95717 ± 0.04324 | 2460812.87893 ± 0.05634 | 2460812.77429 ± 0.01183 | 2460812.84130 ± 0.01052 | 2460812.66844 ± 0.01706 |
| 2460831.81761 ± 0.04357 | 2460831.73882 ± 0.05677 | 2460831.63496 ± 0.01192 | 2460831.70073 ± 0.01060 | 2460831.52707 ± 0.01719 |
| 2460850.67849 ± 0.04390 | 2460850.59884 ± 0.05720 | 2460850.49564 ± 0.01201 | 2460850.56076 ± 0.01068 | 2460850.38639 ± 0.01731 |
| 2460869.53918 ± 0.04423 | 2460869.45885 ± 0.05763 | 2460869.35624 ± 0.01210 | 2460869.42075 ± 0.01076 | 2460869.24605 ± 0.01744 |
| 2460888.39945 ± 0.04456 | 2460888.31870 ± 0.05806 | 2460888.21685 ± 0.01219 | 2460888.28106 ± 0.01084 | 2460888.10515 ± 0.01757 |
| 2460907.25981 ± 0.04489 | 2460907.17876 ± 0.05849 | 2460907.07737 ± 0.01228 | 2460907.14147 ± 0.01092 | 2460906.96478 ± 0.01770 |
| 2460926.12057 ± 0.04522 | 2460926.03851 ± 0.05892 | 2460925.93786 ± 0.01237 | 2460926.00196 ± 0.01100 | 2460925.82463 ± 0.01783 |

**Table A13**
(Continued)

| $P_d = 6.47$ days | $P_d = 11.9$ days | $P_d = 12.6$ days | $P_d = 12.7$ days | $P_d = 14.1$ days |
|---|---|---|---|---|
| 2460944.98145 ± 0.04555 | 2460944.89852 ± 0.05935 | 2460944.79827 ± 0.01245 | 2460944.86252 ± 0.01108 | 2460944.68405 ± 0.01796 |
| 2460963.84182 ± 0.04588 | 2460963.75860 ± 0.05978 | 2460963.65866 ± 0.01254 | 2460963.72308 ± 0.01116 | 2460963.54371 ± 0.01809 |
| 2460982.70216 ± 0.04621 | 2460982.61863 ± 0.06021 | 2460982.51900 ± 0.01263 | 2460982.58358 ± 0.01124 | 2460982.40300 ± 0.01822 |
| 2461001.56271 ± 0.04654 | 2461001.47858 ± 0.06064 | 2461001.37932 ± 0.01272 | 2461001.44397 ± 0.01132 | 2461001.26188 ± 0.01835 |
| 2461020.42363 ± 0.04687 | 2461020.33830 ± 0.06107 | 2461020.23952 ± 0.01281 | 2461020.30426 ± 0.01140 | 2461020.12112 ± 0.01848 |
| 2461039.28417 ± 0.04720 | 2461039.19829 ± 0.06150 | 2461039.09978 ± 0.01290 | 2461039.16423 ± 0.01148 | 2461038.97974 ± 0.01861 |
| 2461058.14446 ± 0.04753 | 2461058.05844 ± 0.06193 | 2461057.95990 ± 0.01299 | 2461058.02429 ± 0.01156 | 2461057.83773 ± 0.01874 |
| 2461077.00487 ± 0.04786 | 2461076.91849 ± 0.06236 | 2461076.82014 ± 0.01308 | 2461076.88370 ± 0.01164 | 2461076.69570 ± 0.01887 |
| 2461095.86571 ± 0.04819 | 2461095.77842 ± 0.06279 | 2461095.68014 ± 0.01317 | 2461095.74351 ± 0.01172 | 2461095.55354 ± 0.01900 |
| 2461114.72647 ± 0.04852 | 2461114.63813 ± 0.06322 | 2461114.54039 ± 0.01326 | 2461114.60236 ± 0.01180 | 2461114.41089 ± 0.01913 |
| 2461133.58677 ± 0.04885 | 2461133.49817 ± 0.06365 | 2461133.40031 ± 0.01335 | 2461133.46200 ± 0.01188 | 2461133.26774 ± 0.01926 |
| 2461152.44712 ± 0.04918 | 2461152.35820 ± 0.06408 | 2461152.26063 ± 0.01344 | 2461152.32040 ± 0.01196 | 2461152.12497 ± 0.01939 |
| 2461171.30781 ± 0.04951 | 2461171.21824 ± 0.06451 | 2461171.12049 ± 0.01353 | 2461171.17995 ± 0.01204 | 2461170.98195 ± 0.01952 |
| 2461190.16874 ± 0.04984 | 2461190.07822 ± 0.06494 | 2461189.98086 ± 0.01362 | 2461190.03811 ± 0.01212 | 2461189.83846 ± 0.01965 |
| 2461209.02915 ± 0.05017 | 2461208.93796 ± 0.06537 | 2461208.84070 ± 0.01371 | 2461208.89761 ± 0.01220 | 2461208.69618 ± 0.01978 |
| 2461227.88946 ± 0.05050 | 2461227.79808 ± 0.06580 | 2461227.70118 ± 0.01380 | 2461227.75589 ± 0.01228 | 2461227.55347 ± 0.01991 |
| 2461246.74995 ± 0.05083 | 2461246.65789 ± 0.06623 | 2461246.56109 ± 0.01389 | 2461246.61538 ± 0.01236 | 2461246.41023 ± 0.02004 |
| 2461265.61085 ± 0.05116 | 2461265.51790 ± 0.06666 | 2461265.42162 ± 0.01398 | 2461265.47400 ± 0.01243 | 2461265.26893 ± 0.02017 |
| 2461284.47147 ± 0.05149 | 2461284.37793 ± 0.06709 | 2461284.28161 ± 0.01407 | 2461284.33360 ± 0.01251 | 2461284.12733 ± 0.02030 |
| 2461303.33175 ± 0.05182 | 2461303.23788 ± 0.06752 | 2461303.14227 ± 0.01416 | 2461303.19274 ± 0.01259 | 2461302.98495 ± 0.02043 |
| 2461322.19214 ± 0.05215 | 2461322.09790 ± 0.06795 | 2461322.00242 ± 0.01425 | 2461322.05256 ± 0.01267 | 2461321.84420 ± 0.02056 |
| 2461341.05294 ± 0.05248 | 2461340.95763 ± 0.06838 | 2461340.86320 ± 0.01434 | 2461340.91223 ± 0.01275 | 2461340.70353 ± 0.02069 |
| 2461359.91376 ± 0.05281 | 2461359.81762 ± 0.06881 | 2461359.72348 ± 0.01443 | 2461359.77234 ± 0.01283 | 2461359.56210 ± 0.02082 |
| 2461378.77410 ± 0.05314 | 2461378.67771 ± 0.06924 | 2461378.58442 ± 0.01452 | 2461378.63253 ± 0.01291 | 2461378.42180 ± 0.02095 |
| 2461397.63445 ± 0.05347 | 2461397.53782 ± 0.06967 | 2461397.44494 ± 0.01461 | 2461397.49293 ± 0.01299 | 2461397.28144 ± 0.02108 |

**Note.** The columns are for each three-planet configuration.

## ORCID iDs

Justin M. Wittrock https://orcid.org/0000-0002-7424-9891
Peter P. Plavchan https://orcid.org/0000-0002-8864-1667
Bryson L. Cale https://orcid.org/0000-0002-2078-6536
Thomas Barclay https://orcid.org/0000-0001-7139-2724
Mathis R. Ludwig https://orcid.org/0000-0002-8382-0236
Richard P. Schwarz https://orcid.org/0000-0001-8227-1020
Djamel Mékarnia https://orcid.org/0000-0001-5000-7292
Amaury H. M. J. Triaud https://orcid.org/0000-0002-5510-8751
Lyu Abe https://orcid.org/0000-0002-0856-4527
Olga Suarez https://orcid.org/0000-0002-3503-3617
Tristan Guillot https://orcid.org/0000-0002-7188-8428
Dennis M. Conti https://orcid.org/0000-0003-2239-0567
Karen A. Collins https://orcid.org/0000-0001-6588-9574
Ian A. Waite https://orcid.org/0000-0002-3249-3538
John F. Kielkopf https://orcid.org/0000-0003-0497-2651
Kevin I. Collins https://orcid.org/0000-0003-2781-3207
Stefan Dreizler https://orcid.org/0000-0001-6187-5941
Mohammed El Mufti https://orcid.org/0000-0001-8364-2903
Dax L. Feliz https://orcid.org/0000-0002-2457-7889
Eric Gaidos https://orcid.org/0000-0002-5258-6846
Claire S. Geneser https://orcid.org/0000-0001-9596-8820
Keith D. Horne https://orcid.org/0000-0003-1728-0304
Stephen R. Kane https://orcid.org/0000-0002-7084-0529
Patrick J. Lowrance https://orcid.org/0000-0001-8014-0270
Eder Martioli https://orcid.org/0000-0002-5084-168X
Don J. Radford https://orcid.org/0000-0002-3940-2360
Michael A. Reefe https://orcid.org/0000-0003-4701-8497
Veronica Roccatagliata https://orcid.org/0000-0002-4650-594X
Avi Shporer https://orcid.org/0000-0002-1836-3120
Keivan G. Stassun https://orcid.org/0000-0002-3481-9052
Christopher Stockdale https://orcid.org/0000-0003-2163-1437
Thiam-Guan Tan https://orcid.org/0000-0001-5603-6895
Angelle M. Tanner https://orcid.org/0000-0002-2903-2140
Laura D. Vega https://orcid.org/0000-0002-5928-2685

## References

Abe, L., Gonçalves, I., Agabi, A., et al. 2013, A&A, 553, A49
Addison, B. C., Horner, J., Wittenmyer, R. A., et al. 2021, AJ, 162, 137
Akeson, R. L., Chen, X., Ciardi, D., et al. 2013, PASP, 125, 989
Arnold, J. A., Weinberger, A. J., Videen, G., & Zubko, E. S. 2022, ApJ, 930, 123
Astropy Collaboration, Price-Whelan, A. M., Sipőcz, B. M., et al. 2018, AJ, 156, 123
Astropy Collaboration, Robitaille, T. P., Tollerud, E. J., et al. 2013, A&A, 558, A33
Ballard, S., Fabrycky, D., Fressin, F., et al. 2011, ApJ, 743, 200
Benz, W., Broeg, C., Fortier, A., et al. 2021, ExA, 51, 109
Bertini, L., Roccatagliata, V., & Kim, M. 2023, A&A, 671, L2
Bolmont, E., Selsis, F., Raymond, S. N., et al. 2013, A&A, 556, A17
Borucki, W. J., & Summers, A. L. 1984, Icar, 58, 121
Brown, T. M., Baliber, N., Bianco, F. B., et al. 2013, PASP, 125, 1031
Buchhave, L. A., Dressing, C. D., Dumusque, X., et al. 2016, AJ, 152, 160
Butler, C. J., Byrne, P. B., Andrews, A. D., & Doyle, J. G. 1981, MNRAS, 197, 815
Cale, B. L., Reefe, M., Plavchan, P., et al. 2021, AJ, 162, 295
Cavanaugh, J. E. 1997, Stat. Probab. Lett., 33, 201
Chen, J., & Kipping, D. 2017, ApJ, 834, 17
Choi, J., Dotter, A., Conroy, C., et al. 2016, ApJ, 823, 102

Christiansen, J. L., Vanderburg, A., Burt, J., et al. 2017, AJ, 154, 122
Cincotta, P. M., Giordano, C. M., & Simó, C. 2003, PhyD, 182, 151
Cincotta, P. M., & Simó, C. 2000, A&AS, 147, 205
Claret, A., & Bloemen, S. 2011, A&A, 529, A75
Collins, K. A., Kielkopf, J. F., Stassun, K. G., & Hessman, F. V. 2017, AJ, 153, 77
Cully, S. L., Siegmund, O. H. W., Vedder, P. W., & Vallerga, J. V. 1993, ApJL, 414, L49
Cumming, A., Marcy, G. W., & Butler, R. P. 1999, ApJ, 526, 890
David, T. J., Petigura, E. A., Luger, R., et al. 2019a, ApJL, 885, L12
David, T. J., Cody, A. M., Hedges, C. L., et al. 2019b, AJ, 158, 79
Donati, J. F., Cristofari, P. I., Finociety, B., et al. 2023, MNRAS, 525, 455
Dotter, A. 2016, ApJS, 222, 8
Eastman, J., Gaudi, B. S., & Agol, E. 2013, PASP, 125, 83
Eastman, J., Siverd, R., & Gaudi, B. S. 2010, PASP, 122, 935
Eastman, J. D., Rodriguez, J. E., Agol, E., et al. 2019, arXiv:1907.09480
Fabrycky, D. C., Lissauer, J. J., Ragozzine, D., et al. 2014, ApJ, 790, 146
Fajardo-Acosta, S. B., Beichman, C. A., & Cutri, R. M. 2000, ApJL, 538, L155
Fang, J., & Margot, J.-L. 2012, ApJ, 761, 92
Feinstein, A. D., France, K., Youngblood, A., et al. 2022, AJ, 164, 110
Foreman-Mackey, D. 2018, RNAAS, 2, 31
Foreman-Mackey, D., Agol, E., Ambikasaran, S., & Angus, R. 2017, AJ, 154, 220
Foreman-Mackey, D., Hogg, D. W., Lang, D., & Goodman, J. 2013, PASP, 125, 306
Foreman-Mackey, D., Luger, R., Agol, E., et al. 2021, JOSS, 6, 3285
Freudenthal, J., von Essen, C., Ofir, A., et al. 2019, A&A, 628, A108
Gaia Collaboration, Brown, A. G. A., Vallenari, A., et al. 2021, A&A, 649, A1
Gallenne, A., Desgrange, C., Milli, J., et al. 2022, A&A, 665, A41
Gelman, A., & Rubin, D. B. 1992, StaSc, 7, 457
Gilbert, E. A., Barclay, T., Quintana, E. V., et al. 2022, AJ, 163, 147
Gillon, M., Jehin, E., Lederer, S. M., et al. 2016, Natur, 533, 221
Gillon, M., Triaud, A. H. M. J., Demory, B.-O., et al. 2017, Natur, 542, 456
Goodman, J., & Weare, J. 2010, Comm. App. Math. Comp. Sci., 5, 65
Grady, C. A., Wisniewski, J. P., Schneider, G., et al. 2020, ApJL, 889, L21
Guillot, T., Abe, L., Agabi, A., et al. 2015, AN, 336, 638
Hara, N. C., Bouchy, F., Stalport, M., et al. 2020, A&A, 636, L6
Harris, C. R., Millman, K. J., van der Walt, S. J., et al. 2020, Natur, 585, 357
Heller, R., Hippke, M., Freudenthal, J., et al. 2020, A&A, 638, A10
Huber, D., White, T. R., Metcalfe, T. S., et al. 2022, AJ, 163, 79
Hunter, J. D. 2007, CSE, 9, 90
Hurvich, C. M., & Tsai, C.-L. 1989, Biometrika, 76, 297
Ilin, E., & Poppenhaeger, K. 2022, MNRAS, 513, 4579
Jensen, E., 2013 Tapir: A web interface for transit/eclipse observability, Astrophysics Source Code Library, ascl:1306.007
Kalas, P., Liu, M. C., & Matthews, B. C. 2004, Sci, 303, 1990
Kane, S. R., Foley, B. J., Hill, M. L., et al. 2022, AJ, 163, 20
Kreidberg, L. 2015, PASP, 127, 1161
Kundu, M. R., Jackson, P. D., White, S. M., & Melozzi, M. 1987, ApJ, 312, 822
Laskar, J. 1997, A&A, 317, L75
Laskar, J. 2000, PhRvL, 84, 3240
Laskar, J., & Petit, A. C. 2017, A&A, 605, A72
Lissauer, J. J., Ragozzine, D., Fabrycky, D. C., et al. 2011, ApJS, 197, 8
Lithwick, Y., Xie, J., & Wu, Y. 2012, ApJ, 761, 122
Liu, M. C., Matthews, B. C., Williams, J. P., & Kalas, P. G. 2004, ApJ, 608, 526
Lightkurve Collaboration, Cardoso, J. V. d. M., Hedges, C., et al., 2018 Lightkurve: Kepler and TESS time series analysis in Python, Astrophysics Source Code Library, ascl:1812.013
Luger, R., Sestovic, M., Kruse, E., et al. 2017, NatAs, 1, 0129
MacGregor, M. A., Wilner, D. J., Rosenfeld, K. A., et al. 2013, ApJL, 762, L21
Mamajek, E. E., & Bell, C. P. M. 2014, MNRAS, 445, 2169
Mancini, L., Lillo-Box, J., Southworth, J., et al. 2016, A&A, 590, A112
Martioli, E., Hébrard, G., Correia, A. C. M., Laskar, J., & Lecavelier des Etangs, A. 2021, A&A, 649, A177
Martioli, E., Hébrard, G., Moutou, C., et al. 2020, A&A, 641, L1
Masuda, K. 2017, AJ, 154, 64
Mékarnia, D., Guillot, T., Rivet, J. P., et al. 2016, MNRAS, 463, 45
Olofsson, J., Thébault, P., Kral, Q., et al. 2022, MNRAS, 513, 713
Osborn, A., Armstrong, D. J., Cale, B., et al. 2021, MNRAS, 507, 2782
Palle, E., Oshagh, M., Casasayas-Barris, N., et al. 2020, A&A, 643, A25
Perez, F., & Granger, B. E. 2007, CSE, 9, 21
Picogna, G., & Marzari, F. 2014, A&A, 564, A28
Plavchan, P., Barclay, T., Gagné, J., et al. 2020, Natur, 582, 497
Plavchan, P., Jura, M., & Lipscy, S. J. 2005, ApJ, 631, 1161
Plavchan, P., Werner, M. W., Chen, C. H., et al. 2009, ApJ, 698, 1068
Rando, N., Asquier, J., Corral Van Damme, C., et al. 2020, Proc. SPIE, 11443, 1144314
Rein, H., & Liu, S. F. 2012, A&A, 537, A128
Rein, H., & Spiegel, D. S. 2015, MNRAS, 446, 1424
Sackett, P. D. 1999, in NATO Advanced Study Institute (ASI) Series C, Planets Outside the Solar System: Theory and Observations, ed. J. M. Mariotti & D. Alloin, Vol. 532 (Dordrecht: Kluwer), 189
Schwarz, G. 1978, AnSta, 6, 461
Song, I., Weinberger, A. J., Becklin, E. E., Zuckerman, B., & Chen, C. 2002, AJ, 124, 514
Steffen, J. H., Fabrycky, D. C., Agol, E., et al. 2013, MNRAS, 428, 1077
Strubbe, L. E., & Chiang, E. I. 2006, ApJ, 648, 652
Sugiura, N. 1978, Commun. Stat.—Theory and Methods, 7, 13
Sun, L., Ioannidis, P., Gu, S., et al. 2019, A&A, 624, A15
Sun, L., Ioannidis, P., Gu, S., et al. 2022, MNRAS, 512, 4604
Szabó, G. M., Gandolfi, D., Brandeker, A., et al. 2021, A&A, 654, A159
Szabó, G. M., Garai, Z., Brandeker, A., et al. 2022, A&A, 659, L7
Tamayo, D., Cranmer, M., Hadden, S., et al. 2020, PNAS, 117, 18194
Tamayo, D., Gilbertson, C., & Foreman-Mackey, D. 2021, MNRAS, 501, 4798
Tejada Arevalo, R., Tamayo, D., & Cranmer, M. 2022, ApJL, 932, L12
Ter Braak, C. J. F. 2006, Stat. Comput., 16, 239
Trifonov, T., 2019 The Exo-Striker: Transit and radial velocity interactive fitting tool for orbital analysis and N-body simulations, Astrophysics Source Code Library, ascl:1906.004
Tsikoudi, V., & Kellett, B. J. 2000, MNRAS, 319, 1147
Van Laerhoven, C., Barnes, R., & Greenberg, R. 2014, MNRAS, 441, 1888
Virtanen, P., Gommers, R., Oliphant, T. E., et al. 2020, NatMe, 17, 261
Vizgan, D., Hughes, A. M., Carter, E. S., et al. 2022, ApJ, 935, 131
White, R., Schaefer, G., Boyajian, T., et al. 2019, AAS Meeting Abstracts, 233, 259.41
Wit, E., Heuvel, E. v. d., & Romeijn, J.-W. 2012, Statistica Neerlandica, 66, 217
Wittrock, J. M., Dreizler, S., Reefe, M. A., et al. 2022, AJ, 164, 27
Zechmeister, M., Reiners, A., Amado, P. J., et al. 2018, A&A, 609, A12
Zicher, N., Barragán, O., Klein, B., et al. 2022, MNRAS, 512, 3060
Zuckerman, B. 2001, ARA&A, 39, 549